Instituto Tecnológico y de Estudios Superiores de Monterrey

Campus Monterrey

School of Engineering and Sciences


# BIORESORBABLE MATERIALS AND ADDITIVE MANUFACTURING PROCESSES FOR MEDICAL IMPLANTS

A dissertation presented by

Raquel Tejeda Alejandre

Submitted to the

School of Engineering and Sciences

in partial fulfillment of the requirements for the degree of

Doctor of Philosophy

In

Engineering Science

Major in Mechatronics

Monterrey Nuevo León, December 9th, 2019.

# Dedication

To my family and my Tulio.

# Acknowledgments

First, I would like thank to my advisor Dr. Ciro Rodríguez for the support during my Ph.D and related research, for his patience, motivation, and great knowledge. More than an advisor, he has been a mentor on my career.

My honest thanks to Dr. David Dean who gave me the opportunity to join his research group at The Ohio State University, with access to the laboratory and research facilities. I appreciate the opportunity to work on this university.

In addition to my tutors, I would like to express my gratitude to Dr. Erika García for her support during my stay in the laboratories in Monterrey, for her support, advice, patience and guidance.

Thank you to the rest of my thesis committee for their comments and encouragement: Dra. Aída Rodríguez, Dra. Elisa Vázquez, Dr. Víctor Segura, specially I would like to express my gratitude to Dr. Erika García for her support during my stay in the laboratories in Monterrey, for her support, advice, patience and guidance.

I appreciate the support that I received from my family for encourage me to continue throughout my life in general. I am blessed for having them.

My sincere gratitude to Tecnológico de Monterrey support on tuition and CONACyT with the support for living.

**“Bioresorbable materials and additive manufacturing processes for medical implants”**

By

Raquel Tejeda-Alejandre

**Abstract**

The application of additive manufacturing technologies in tissue engineering has been growing in recent years. Among different technology options, 3D printing is becoming popular due to the ability to directly print scaffolds with designed shape and has a great potential like manufacturing method in the production of scaffolds for tissue engineering. Applications of additive manufacturing in regenerative medicine and tissue engineering are restricted for the available materials for each technology. Great part of research has focused on the development of new materials to be used to create complex geometries, culture different kind of cells from different type of tissues and applications.

In this work, recent developed additive manufacturing techniques and biomaterials for vascular and bone tissue are studied. The objective of tissue engineering is to produce functional and viable structures and multiple biomaterials and fabrication methods need to be researched. To achieve this purpose, the fabrication of bifurcated vascular grafts using the combination of electrospinning and 3D printing, and the characterization of a new biomaterial for bone regeneration applications, were explored. Polycaprolactone (PCL) was used to electrospun a mandrel obtaining a bifurcated construct that was morphological and mechanical characterized. For bone regeneration applications, a new resorbable biomaterial was investigated. Process parameters and materials properties, such as separation force and green strength were studied in order to probe the printability of this material, compositional changes, or defects during the 3D printing process, of porous structures using Continuous Digital Light Processing (cDLP) and Isosorbide.

# Scientific production of this thesis

## Publications in scientific journals

***From chapter 3***

**Tejeda-Alejandre, R**.; Lammel-Lindemann, J.A.; Lara-Padilla, H.; Dean, D.; Rodriguez, C.A. "Influence of Electrical Field Collector Positioning and Motion Scheme on Electrospun Bifurcated Vascular Graft Membranes*"*. *Materials* 2019, *12*, 2123.

**Tejeda-Alejandre, R.**; Lara-Padilla, H.; Mendoza-Buenrostro, C.; Rodriguez, C.A.; Dean, D. "Electrospinning Complexly-shaped, Resorbable, Bifurcated Vascular Grafts". *Procedia CIRP*, *65*, 207–212.

***From chapter 4***

**Tejeda-Alejandre, R**.; Lammel-Lindemann, J.A.; Dourado, I.; Charles, R.; Pattel, P.; Catalani, H.; Rodriguez, C.A; Dean, D. "Continuous Digital Light Processing of unsaturated polyesters from Isosorbide for Bone Tissue Engineering". *In prep.*

Lara-Padilla, H.; **Tejeda-Alejandre, R**.; Rodriguez, C.A; Dean, D. "Reliability in Additive Manufacturing Processes: a Case Study using Continuous Digital Light Processing of Poly(Propylene Fumarate)". *In prep.*

## Oral presentations in conferences

***From chapter 3***

**Tejeda-Alejandre, R.**; Lara-Padilla, H.; Mendoza-Buenrostro, C.; Rodriguez, C.A.; Dean, D. "Electrospinning Complexly-shaped, Resorbable, Bifurcated Vascular Grafts". *Procedia CIRP 2017*. Chicago, IL. USA.

## Poster presentations in conferences

***From chapter 3***

**Tejeda-Alejandre, R.**; Lara-Padilla, H.; Lammel-Lindemann, J.A.; Rodriguez, C.A. ; Dean, D. "Electrospinning Methods for the Production of Resorbable Bifurcated Vascular Grafts: Influence of process parameters on mandrel adherence and mechanical properties". *International Conference on Biofabrication 2019*. Columbus, OH.

**Tejeda-Alejandre, R.**; Lammel-Lindemann, J.A.; Lara-Padilla, H.; Dean, D.; Rodriguez,C.A. “Development and characterization of Electrospun Bifurcated Scaffolds (EBS) for medical applications”. *Annual OSUWMC Trainee research day 2019*. Columbus, OH. USA.

**Tejeda-Alejandre, R.**; Lara-Padilla, H.; Lammel-Lindemann, J.A.; Rodriguez, C.A. ; Dean, D. “Progress in Development of Bifurcated Stents: Influence of Process Parameters on Mechanical Properties”. *International Conference on Biofabrication 2018*. Würzburg, Germany.

Rodriguez, C.A., **Tejeda-Alejandre, R.**, Lara-Padilla, H., Mendoza-Buenrostro, C., Dean, D. “Electrospinning for Resorbable Vascular Scaffolds with Complex Shape and Bifurcation”*. 2017 TERMIS-AM Annual Conference and Exhibition*. Charlotte, NC. USA.

***From chapter 4***

**Tejeda-Alejandre, R**.; Charles, R.; Patel, P.; Lammel-Lindemann, J.A.; Dourado, I.A; Catalani, L.H; Rodriguez, C.A.; Dean, D. “Mechanical Reliability Approach of Continuous Digital Light Processing (cDLP) of Isosorbide Scaffolds: A New Material for Resorbable Medical Devices”. *International Conference on Biofabrication 2019*. Columbus, OH.

## Patents

**Tejeda-Alejandre, R.;** Lara-Padilla, H.; Rodriguez, C.A.; Dean, D. “Three-dimensional printing modality combining fused deposition modeling and electrospinning”. International Patent Application No. WO/2018/170328

# Contents

# List of Figures

# List of Tables

# Chapter 1 . Introduction

## 1.1 Background

The methodology of supportive tissue regeneration is often denoted to as tissue engineering (TE) or regenerative medicine (RM). Exterior reinforces are frequently called scaffolds, which generate the platform for cells to migrate to the site they are needed and forms new tissue. Hence, scaffolds perform a significant role in TE and regenerative medicine. These scaffolds are often loaded with growth factors to accelerate cell differentiation to generate new tissue formation. Due to the cell viability and proliferation, chemical and physical compositions of scaffolds are crucial. The selection of biomaterial and technique of construction to create a scaffold, are significant factors that shape the use of scaffolds. Much investigation has been done on adapting and generating new biomaterials. Biomaterials are described as any materials that interface with biological systems [1].

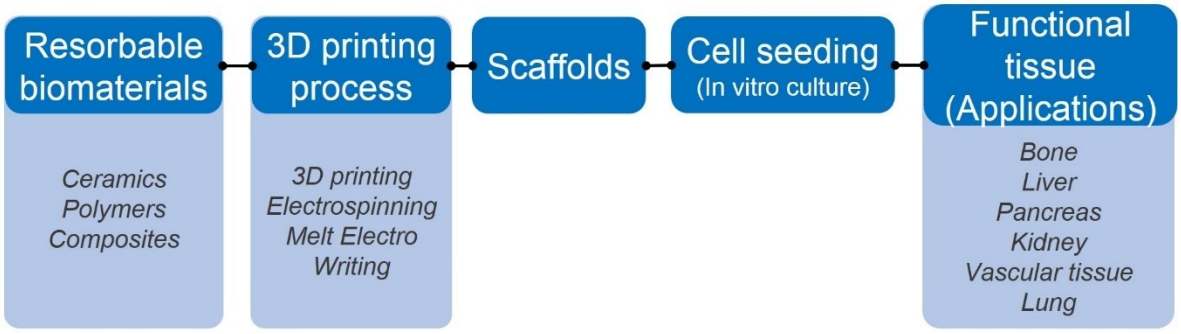


**Figure 1.1** Diagram to describe the creation process for functional tissues from biomaterials. [1]

Through the last years, the concept of regeneration has become feasible and has been recently introduced in medicine. Tissue engineering and regenerative medicine are terms for the field in biomedicine that deal with the transformation of these fundamental ideas to practical approaches.

The use of biomaterials is a common treatment option in clinical practice. One reason for the priority of tissue grafts over nonliving biomaterials is that they contain cells and tissue-inducing substances, thereby possessing biological plasticity Research is currently in progress to develop cell-containing hybrid materials and to create replacements for bone tissue that are bioactive after implantation, imparting physiological functions as well as structure to the tissue or organ damaged by disease or trauma [2].

## 1.2 Thesis outline

In the present research document, it is recommended that the relationships between fabrication methods and the materials should be defined by their specific characteristics. In this understanding, the following objectives of this thesis are investigated:

In **Chapter 2**, the main concepts of additive manufacturing for vascular grafts and bone tissue engineering are discussed. Moreover, different strategies for the design and optimization of scaffold are reviewed. Some of the advantages of each manufacturing processes and the results nowadays.

In **Chapter 3**, the combination of additive manufacturing and electrospinning techniques to create bifurcated vascular membranes. This work is focused on the construction of bifurcated vascular grafts combining 3D printing techniques and electrospinning creating polycaprolactone (PCL) electrospun fibers. This combination offers the possibility to construct bifurcated structures using a positioning system and the addition of an electrical field collector to get the mat of fibers. The technologies of digital light processing (DLP) and electrospinning were combined to create bifurcated constructs.

In **Chapter 4**, the printability of photocurable resin made with Isosorbide was studied. In the case of continuous digital light processing (cDLP) printing technology, detaching a cured photopolymer model from a basement is a challenging process. Forces, which appear during removing of cured photopolymer layer formed in cDLP printer, can destroy the built model. In this chapter, the relationship between the material and process is evaluated in order to improve the reliability of printing

process. The separation force produced during the printing process and green strength of the cured polymer were measured, obtained results are statistically analyzed, and a relation between separation force, exposure time and percentage of photoattenuator are verified. The separation force and green strength were studied in solid and porous structures and compared with polymers well reported.

In **Chapter 5**, key conclusions and limitations are provided, and prospects for the application of this thesis research are presented.

# Chapter 2 . Background

## 2.1 Introduction

Additive manufacturing is an advanced fabrication method building three-dimensional components (usually designed using computer-aided design (CAD) models) by deposition of materials layer by layer. The benefit of this technology is the chance to manufacture highly complex structures with narrowed geometries, which cannot be generated by the subtractive process. This technology is usually used for rapid prototype modelling. It simplifies the prompt and efficient evaluation of a concept through rapid fabrication. The rapid prototyping process may be repeated several times until the element meets a variety of demands, included and user needs. As a consequence, numerous cutting edge research studies have focused on the fabrication of end-use products based on AM technology [3].

Tissue engineering (TE) is continuously developing adapting inputs from nearby areas of science and their technological advances, counting nanotechnology progresses that have been producing the available options for the manipulation and cellcontrol and cellular settings. Consecutively, TE has a rising and evident impact in other fields, such as cancer and other diseases research, enabling tri-dimensional (3D) tumor/tissue models of increased complexity that more closely resemble living tissue dynamics, playing a decisive role in the development of new and improved therapies. However, TE is still fighting with translational issues. On this concern, the beginning of tailored and precision medicine has opened new outlooks, particularly with the outstanding evolution supported by 3D bioprinting technologies [4].

## 2.2 Scaffolds and Tissue Engineering

### 2.2.1 Vascular grafts

Additive manufacturing (AM) techniques are widely used to fabricate tissue-engineered scaffolds due to their unique capability in constructing controllable

macro/microarchitectures. Nevertheless, it is a challenge to create flexible assemblies with mechanical properties comparable to those of native soft tissues by utilizing AM techniques and clinically available biodegradable polymers. To get the mechanical constraints of aimed soft tissues, massive studies have been conducted changing biopolymer constituents or the macro/microporosity of the scaffolds [5].

Vascular graft biomechanical reliability, both initially and over time if tissue is to form, involves a durable structure with burst strength (i.e., biomechanical properties) like those of native vessels. This structural integrity is usually achieved by a robust, but non-resorbable, outer layer, most often formed from ePTFE (i.e., Gore-Tex®) and polyethylene terephthalate (PET, or Dacron®) and Polyurethane (PU) [6,7]. Thus, these grafts do not have growth capacity [8,9]. Thus, the ideal Tissue Engineering Vascular Grafts (TEVG) would be fully biodegradable, thereby obviating the need for risky serial reoperation to upsize the graft due to somatic overgrowth [10]. In addition to pediatric congenital anomalies, there is a need for small-diameter vascular grafts for patients with vasospasm, limited length, poor quality, and prior use [11,12].

Angiogenesis and vasculogenesis are critical processes that are used to recapitulate most tissues and organs.41–44 The efficient oxygen transfer, delivery of nutrients, and transport and clearance of metabolic waste beyond the characteristic diffusional limit (typically 100–200 mm) 45 are vital for homeostasis and functionality, and failed vascularization results in necrosis. Due to its ability for positioning different types of cells in discrete 3D spaces and for designing controlled multiple length-scale structures, 3D bioprinting is emerging as a powerful biofabrication approach to generate functional, high-resolution, and hierarchical vascular networks. However, engineering vessel networks to ensure normal cellular metabolism and promote the host tissue integration48 is a complex process that should enable remodeling while maintaining an open-vessel lumen, be permeable, and allow extravasation of cells. However, vascularization per se can be associated with pathological conditions such as pre-eclampsia, in which blood vessels are abnormally developed and the placenta is characterized by poor trophoblastic invasion [4].

### 2.2.2 Bone regeneration

The destruction of bone tissue due to disease (osteonecrosis, tumors, osteoporosis) or inefficient healing posttraumatic injury is a problem affecting the world population. The repair of small defect may be mediated by the osteoblast and osteoclast activity which ensures a balanced control of bone resorption and formation, allowing the bone repair, renewal, and growth. However, when the defect reaches a crucial size, it is necessary to appeal to the promising field of tissue engineering in order to develop a new methodology of bone regeneration [13].

In general, the bone is regarded as a tough matrix that is mineralized that gives it its strength. The matrix is about 30% of the bone and over 90% is based on collagen fibers, the rest is a gel-like substance in the extracellular space that comprises of all components of the extracellular matrix. The remaining 70% of the bone is comprised of minerals and salts that provide strength. Minerals in bone are mostly calcium phosphate in the form of hydroxyapatite. All these are created by bone-forming cells, known as osteoblasts that produce mostly type 1 collagen. Osteoblasts secretes these collagen fibers all around themselves and then they deposit calcium phosphate. This new bone is called osteoid. Once the Osteoblast is trapped, it is known as an Osteocyte. Osteoclasts are large cells that resorb the bone, in a never ending remodeling that is balanced by osteoblasts, and that are also play an important role in calcium homeostasis. The key regulator of osteoblast and osteoclast activity is mechanical strain, such as when there's increased load, the bone will adapt and add new bone in response to it or remove in response to unloading [14].

## 2.3 Scaffold Fabrication Methods

There are numerous approaches for scaffold fabrication. The manufacturing process is the phase after biomaterials are converted into scaffolds. These construction methods are physical and/or chemical procedures that are completed on biomaterials to make them usable for tissue engineering. Not all biomaterials are appropriate for a given manufacture method. Hence, biomaterials are continuously adapted to allow their use in each fabrication method. Conventional manufacturing

methods include electrospinning, phase separation, freeze drying, self-assembly, solvent casting, textile technologies, material injections, and additive manufacturing [15,16]. Each fabrication method has its own advantages and disadvantages. To overcome certain disadvantages, these fabrication methods may be used in combination with other methods.

In electrospinning, a polymer solution is ejected through a needle by the action of high voltage. Due to the potential difference, the polymer solution is deposited like fibers while the solvent evaporates, with a resultant polymeric scaffold. While a numerous diversity of polymers can be used in this process, fabricating scaffolds with complex geometries and structures is still a restraint [17].

In textile-based fabrication methods, fibers form polymers and composites are knitted, woven, and braided to create scaffolds. This manufacturing technique has many benefits, including the capability to create porous, pre-vascularized, and permeable scaffolds. Some inconveniences for this scaffold production technique are its incompetence to capture within the scaffolds and the critical manufacturing process [1].

## 2.4 Challenges for tissue engineering

The challenges faced by tissue engineering can be seen in two categories, one category being the research and development of novel biomaterials for different tissues or one universal biomaterial for all tissues, and other category being regulatory. Ideally, a universal biomaterial should be a blend of biomaterials that support native tissue viability, chemical cues, and growth factors for angiogenesis and channels for nerve innervation. These challenges can be addressed with availability of new technologies, such as additive manufacturing, that enables fabrication of complex tissues [1].

Vascularization is one of the most critical challenges about generating feasible approaches to encourage angiogenesis, comprising the addition of angiogenic growth factors (vascular endothelial growth factor—VEGF), the addition of platelets, bone marrow clots, and utilizing bioreactors. Owing the capability of bioprinters to

use manifold print-heads loaded with different cell types, presenting vasculature to a 3D printed device was made possible [18].

Some scaffold constraints have been acknowledged. The first is geometrical in nature. Bone scaffolds are mandatory to have optimally sized and interconnected porous spaces to house the appropriate cells and allow the transportation of nutrients and metabolic wastes to and from the cells. A suitable gradient of pore architecture is additionally at early stages of exploration. While the outside contours of the defect site are a good design criterion to follow, it is not clear if mimicking the original pore structure of the bone is the right approach, since regenerative events may not be optimal with the final architecture of the mature tissue. The second requirement is related to properties of the material the scaffolds are derived. These materials must be osteoconductive, biocompatible, and biodegradable that plays a vital role in initial cell attachment and subsequent cellular penetration and mineralization stages.

The third requirement is related to the mechanical properties of the scaffold to match the load-carrying characteristic of the implant site. While some degree of mechanical support is desirable, certain sites are not as demanding and healing has been achieved in the past using particulate implants that lack a cohesive macroscopic mechanical integrity (hence strength). Finally, scaffolds are expected to bear bioactive molecules capable of modulating cellular activity within and at the proximity of the implant site. While incorporating sensitive bioactive factors is an additional hurdle for any large-scale manufacturing, the demand for accelerated and complete healing is likely to necessitate such an approach [19].

The last group of challenge is transformation of this research to next level, i.e., releasing these progressions accessible to patients. This area is more interesting due to the supervisory aspects that need to be unblocked. The Food and Drug Administration (FDA) has guidelines and many other prerequisites that need to be encountered before success the patient. Formerly, the 3D-printed tissues and scaffolds are used for showing resolutions and evaluation in animal models.

# Chapter 3 . Influence of Electrical Field Collector Positioning and Motion Scheme on Electrospun Bifurcated Vascular Graft Membranes

## 3.1 Introduction

### 3.1.1 Justification

The generation of tubular membranes for vascular applications commonly uses electrospinning as the basic manufacturing process for a resorbable or an inert inner membrane. However, producing vascular graft devices with complex geometries is challenging. The use of resorbable materials for a curving, bifurcated grafts is potentially beneficial to pediatric patients with congenital heart defects and pancreatitis patients undergoing resection of the pancreaticoduodenal junction.

Congenital cardiac anomalies are the most common birth defect, affecting nearly 1% of all live births, with approximately 25% of patients with congenital heart disease having critical defects. The most common critical congenital heart defects are ventricular and atrial septal defects, which are two of a limited number of defects which may be monitored in certain patients [10,20]. With or without monitoring, congenital heart defects are the most common cause of newborn death. These defects require surgical or transcatheter intervention before one year of age. Technology and science have contributed to produce new solutions and improve patient outcomes [21].

A significant percent of the morbidity and mortality of pediatric cardiac surgery arises from the fact that the inert synthetic conduits and patches frequently used to repair congenital defects are susceptible to thromboembolism, stenosis, ectopic calcification, and infection [20]. Tissue engineering provides a potential solution to this problem using a biodegradable vascular graft membrane which is implanted and degrades over time, replaced with autologous vascular tissue that can repair,

remodel, and even grow with the patient. The most important obstacle to performing bypass grafts in infants and children is the small caliber of corresponding vessels [8]. In the Fontan surgical procedure (see **Figure 3.1**) used for children with univentricular hearts, is to oversize the graft thereby allowing a child to “grow into” it. An ideal tissue-engineered vascular graft would be antithrombotic, nonimmunogenic, and the internal surface rapidly endothelialized. Rapid endothelialization is the best way to ensure thrombosis does not occur at the graft/host junction or on the graft itself.

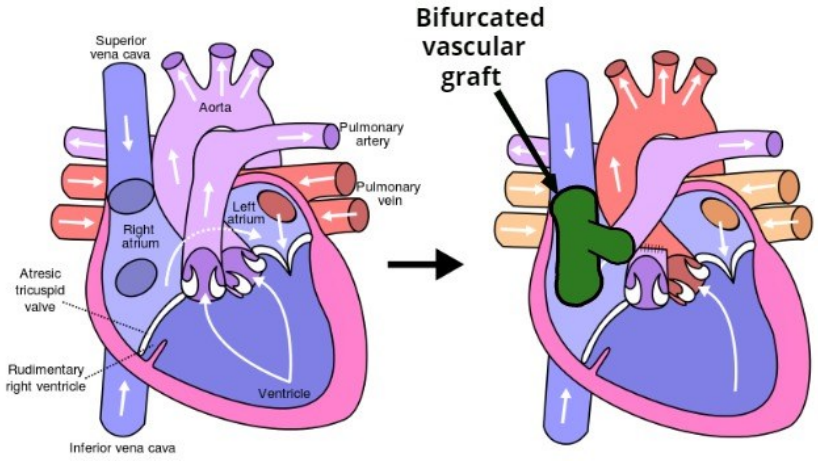


**Figure 3.1** The Fontan procedure consists on reallocate the inferior vena cava and superior vena cava to the pulmonary arteries avoiding going through right ventricle.

Vascular graft biomechanical integrity, both initially and over time if tissue is to form, requires a durable structure with burst strength (i.e., biomechanical properties) akin to those of native vessels. This structural integrity is usually accomplished by a strong, but non-resorbable, outer layer, most often formed from ePTFE (i.e., Gore-Tex®) and polyethylene terephthalate (PET, or Dacron®) and Polyurethane (PU) [6,7]. Thus, these grafts do not have growth capacity [8,9]. Thus, the ideal Tissue Engineering Vascular Grafts (TEVG) would be fully biodegradable, thereby obviating the need for risky serial reoperation to upsize the graft due to somatic overgrowth [10]. In addition to pediatric congenital anomalies, there is need for small-diameter vascular grafts for patients with vasospasm, limited length, poor quality, and prior use. The problems encountered in the design of vascular grafts are commonly

encountered in pancreaticoduodenectomy (PD) procedures, the most common of which is the Whipple procedure (see **Figure 3.2**). While previously associated with morbidity and mortality rates that were considered prohibitive, the Whipple procedure is currently associated with postoperative mortality as low as 1% in high-volume medical centers. Several studies have reported the use of PD stents to decrease postoperative pancreatic leak and fistula from the cut surface of the distal pancreas [8].

The use of metal stents for drainage of pancreatic fluid collections is associated with improved clinical success, fewer adverse events and reduced bleeding compared to plastic stents. Plastic stents have substantially smaller lumens than metal stents leaving them more susceptible to blockage or occlusion [22]. In many cases, after healing the stent is removed.

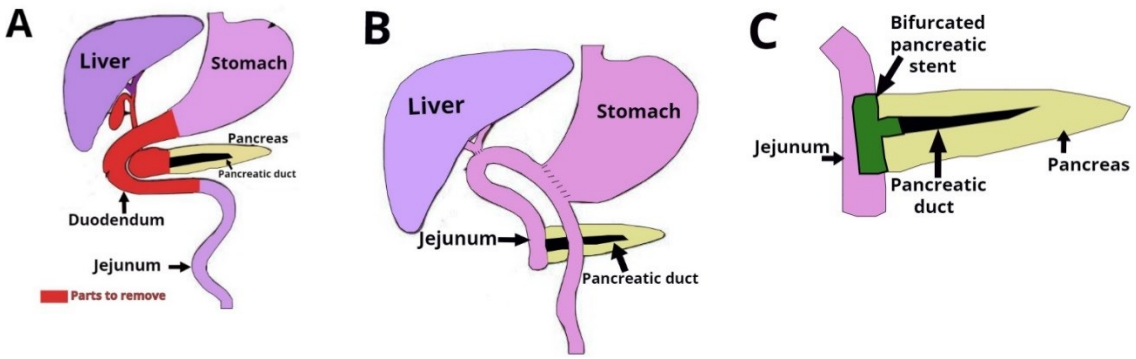


**Figure 3.2** Pancreaticoduodenectomy (PD) or Whipple is a surgical procedure performed to remove cancerous tumors from the pancreas. The technique consists of: A) The extirpation of antrum and pylorus, the first and second portions of duodenum, the head of the pancreas, the common bile duct and the gallbladder; B) The stomach is anastomosed to the small intestines and Pancreatic duct and biliary duct to the jejunum; C) The bifurcated pancreatic stent is inserted halfway into the main pancreatic duct and halfway into the jejunum.

Bifurcated, complex-shaped grafts based on resorbable materials, with tunable resorption rate and appropriate mechanical properties, would be extremely useful in surgical operations such as the Fontan procedure for heart and the Whipple procedure for pancreas. This study focuses on the development of this kind of next generation vascular grafts.

### 3.1.2 Related work

Synthetic materials, such as poly(ε-caprolactone) (PCL), have been extensively employed in the research of vascular graft tissue engineering [6,21] because of its excellent biocompatibility, bioactivity, non-toxicity and, in some configurations, high elasticity and degradability. However, the long degradation of pure PCL, usually more than 18 months in vivo, could act as a barrier to tissue regeneration if the healing window is missed. PCL is resistant to degradation because of its hydrophobic nature and the high level of crystallinity [10,21]. Additionally, if it fails mechanically before it resorbs, small, broken-up pieces can become distributed throughout the site where regeneration is needed, further preventing adequate tissue regeneration.

One of the ideal tissue engineered vascular graft perquisites is similar mechanical properties to the native tissue at placement, before tissue regeneration and remodeling has taken place. A mechanical mismatch is acknowledged as a key determinant in the loss of long-term patency, resulting in aneurysm formation and implant failure [6]. Different approaches and techniques have been explored to produce a clinically viable vascular graft. These can be classified into different categories: vascular graft membrane-based, self-assembly processes [7], 3D printing, solvent casting, phase separation spinning, and electrospinning [23]. However, electrospinning is the most widely studied and applied to fabricate vascular grafts.

The electrospinning process uses an electric field to direct a jet of polymer solution from a syringe's capillary tip toward a target for deposition [24,25]. Under the influence of a strong electrostatic field, charges are induced in the solution and the charged polymer is accelerated towards the grounded metal collector. At low electrostatic field strength, the pendant drop emerging from the tip of the pipette is prevented from dripping due to the surface tension of the solution. It is therefore critical to control a syringe pump's speed to release polymer in the speed window between insufficient material to form a thread to dripping material that overtakes the surface tension needed to engage the electrical field. As the intensity of the electric field is increased, the induced charges on the liquid surface repel each other and

create shear stresses [26]. In the electrospinning of vascular graft membranes, fiber diameter, orientation, alignment (if any—mandrels increase the possibility of alignment), and pore size incur a significant impact on the final functionality of the vascular conduit [27]. According to the standard procedures for setting up a basic electrospinning process [28], once the polymer is selected, the literature recommends two principles to select the solvent: a) the polymer should be completely soluble and b) the boiling point of the solvent should be moderate in order to allow evaporation during the trajectory of the solution between the needle tip and the collector. Some of the most common solvents used in combination with PCL are hexafluoropropanol (HFP), chloroform, acetone and dimethylformamide (DMF) [29]. The most important point in vascular tissue engineering is simulating the native tri-layered structure and recovering vascular function on placement and throughout the regenerative process.

As previously noted, electrospinning methods have been primarily used to generate the internal membrane. The diameter and orientation of fibers and the pore geometry and permeability are essential to rapid cell attachment and endothelialization. It is equally important to develop a mechanically long-lasting and functionally sustainable tissue-engineered vascular graft for clinical application in the outer layers [30]. Reports of earlier relevant studies (see **Table 3.1** Summary of morphology and mechanical properties for electrospun vascular grafts based on PCL and related materials.) show workers carefully considering vascular graft morphology and mechanical characteristics. Techniques like electrospinning allow the construction of tubular vascular graft membranes through a rotating mandrel, acting as an internal collector to attract the fibers. Efforts trying to emulate complex geometries such as bifurcations date back to 1970's where the graft, made out of Dacron fiber, was used as an arterial bypass graft in 135 patients [31]. Later, a Y-graft tailored from a bovine pericardium was formed from two tubes of pericardium [32]. These bovine grafts were closer in size to the human aorta and common iliac arteries than other available standard bifurcated grafts.

Most progress in tissue engineered vascular grafts has been concentrated on tubular shapes (see **Table 3.1** Summary of morphology and mechanical properties for

electrospun vascular grafts based on PCL and related materials.). More recently, tissue engineering approaches have used different materials to create customizable bifurcated grafts or the combination of different technologies, such as 3D printing, electrospinning and custom-designed mandrels with the cardiovascular magnetic resonance imaging (MRI) datasets from different patients [33], aiming to emulate the original tissue, in terms of mechanical and morphological characteristics. Despite all this progress, there is still need for a bifurcated vascular graft based on resorbable materials and with appropriate mechanical properties. This study, on these types of complex shapes and mechanical properties for high performance.

**Table 3.1** Summary of morphology and mechanical properties for electrospun vascular grafts based on PCL and related materials.

| | **Morphology** | | **Mechanical properties** | | **Reference** |
|---|---|---|---|---|---|
| | **Vascular graft membrane shape** | **Membrane thickness [Fiber diameter]** | **Suture retention strength** | **Burst pressure** | |
| PCL | Tubular | 1.18 ± 0.08mm [150 ± 62 nm] | N/A | 2,925 ± 600 mmHg | [34] |
| PCL (12 % PCL, 10 mL/h) | Tubular | 0.72 ± 0.07 mm [1.5 ± 0.2 µm] | 20 N | N/A | [35] |
| PCL (10 % PCL, 3.5 mL/h) | | 0.91 ± 0.05 mm [1.0 ± 0.1 µm] | | | |
| PU | Tubular | 295 ± 42 µm [300-600 nm] | 7.1 ± 1.2 N | 985 ± 75 mmHg | [36] |
| PCL-PU-LT | | 615 ± 35 µm | 36.2 ± 2.0 N | 3,580 ± 125 mmHg | |
| PCL-PU-HT | | 910 ± 25 µm | 45.4 ± 2.6 N | 4,320 ± 115 mmHg | |
| PCL | Tubular | [<1µm] | N/A | 1,550 ± 7.5 mmHg | [37] |
| PCL/Heparin | | [3.5µm] | | 1,560 ± 15 mmHg | |
| PCL | Tubular | 0.4 µm [300 - 500 nm] | N/A | N/A | [38] |
| PLA/PCL | Tubular | 600 µm [600 ± 400 nm] | N/A | N/A | [39] |
| PCL-collagen | Tubular | N/A [520 ± 14 nm] | 3.0 ± 1.1 N | 4,915 ± 155 mmHg | [40] |
| PLA / PLCL | Tubular | 0.33 ± 0.03 mm | 20 N | 15,000-22,500 | [41] |

| | | |
|---|---|---|
| | [N/A] | mmHg |

### 3.1.3 Objective

In this study we propose to test bifurcated vascular graft membranes that we fabricated via electrospinning. Through several iterations of design-prototyping-testing we have refined a manufacturing system with custom-made positioning mechanism and custom collector for this purpose (patent pending [42]). In this study the objective is to explore the influence of collector placement and motion scheme on graft membrane external shape, fiber diameter, and mechanical properties. The collector is connected both inside and outside the mandrel on different configurations. The motion schemes used include: a) rotation vs. b) the combination of rotation & longitudinal movement. Bifurcated vascular grafts are characterized via both morphology measurements and mechanical testing.

## 3.2 Materials and methods

### 3.2.1. Fabrication Process

*3.2.1.1 Positioning the Mechanism*

The proof-of-concept for the type of positioning mechanism used in this study was reported by [12] (see **Figure 3.3**). It was based on two degrees of freedom (2-DOF) with a rotational and longitudinal motion that tilted the mandrel in order to create different relative angles between the mandrel and the electrospinning needle.

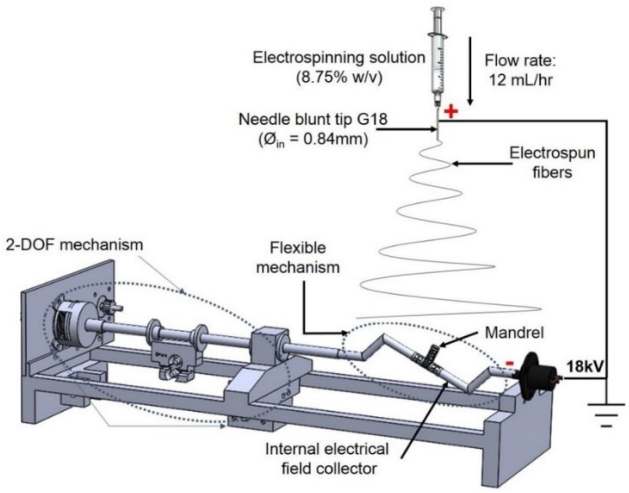


**Figure 3.3** Two degrees of freedom (2-DOF) mechanism used for bifurcated vascular graft membrane.

### *3.2.1.2. Mandrel and Electrical Field Collector*

The mandrel design was created as a parametric model using SolidWorks 2018 (Dassault Systèmes, Waltham, MA, USA), with a bifurcated tubular shape, as shown in **Figure 3.4** Dimensions of 3D printed bifurcating vascular graft mandrel. To facilitate the deposition of fibers that fully coat the mandrel, an internal collector was designed (see **Figure 3.5**). The aim was to transform the flexible mechanism where the mandrel is mounted into a collector that fills its internal space entirely, and evenly, with a layer of conductive material.

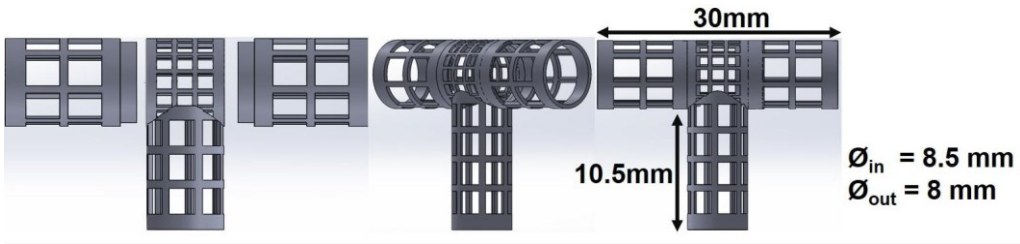


**Figure 3.4** Dimensions of 3D printed bifurcating vascular graft mandrel.

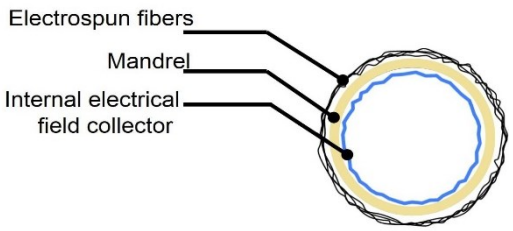

**Figure 3.5** Vascular graft membrane cross-section during electrospinning process, showing location of internal electrical field collector.

The mandrels were fabricated via continuous digital light processing (cDLP) with a 3D printing projector system, which created solid objects by photopolymerization of a liquid polymer resin [43]. A high-resolution EnvisionTec Perfactory 3 Multilens machine cDLP was used to 3D print, with E-Shell 300 polymer resin (EnvisionTEC, Dearborn, MI, USA), the mandrels used in this study.

Electrospinning was done under four different sets of process conditions (see **Table 3.2**), including external vs. internal electrical field collector and two types of motion schemes for the mandrel positioning relative to the source of fibers (needle). The collector configuration and motion scheme are illustrated in **Figure 3.6**. A total of 6 replications were used for each combination of process parameters.

*3.2.1.3. Electrospinning Process*

Polycaprolactone (PCL) pellets (Polysciences Inc, Warrington, PA, USA) with a molecular number (Mn) of 80,000 $g \cdot mol^{-1}$ were used. Acetone was selected as the solvent and was a non-variable parameter. A PCL solution was prepared by dissolving 8.75 wt % of PCL and acetone. The electrospinning was conducted at 18 kV (voltage source model ESP20P-5W, Gamma High Voltage Research Inc., Ormond Beach, FL, USA) with a flow rate of 12 $mL \cdot h^{-1}$ using a syringe pump, Harvard model PHD2000 (Harvard Apparatus, Holliston, MA, USA), and a distance of 7–10 cm between the collector and the tip of the needle. The influence of this factor was not evaluated in this study. This approach was used to form a mat of fibers on the mandrel's surface (see **Figure 3.6** Schematic illustration of electrical field collector configuration and mandrel motion scheme.).

**Table 3.2** Characteristics used for the electrospinning experiments

| Factors | | Experimental Group Name |
|---|---|---|
| **Collector** | **Motion Scheme** | |

| | | |
|---|---|---|
| External | Rotational | BLSP_SC_R |
| External | Rotational and Longitudinal | BLSP_SC_RL |
| Internal | Rotational | BLSP_CC_R |
| Internal | Rotational and Longitudinal | BLSP_CC_RL |

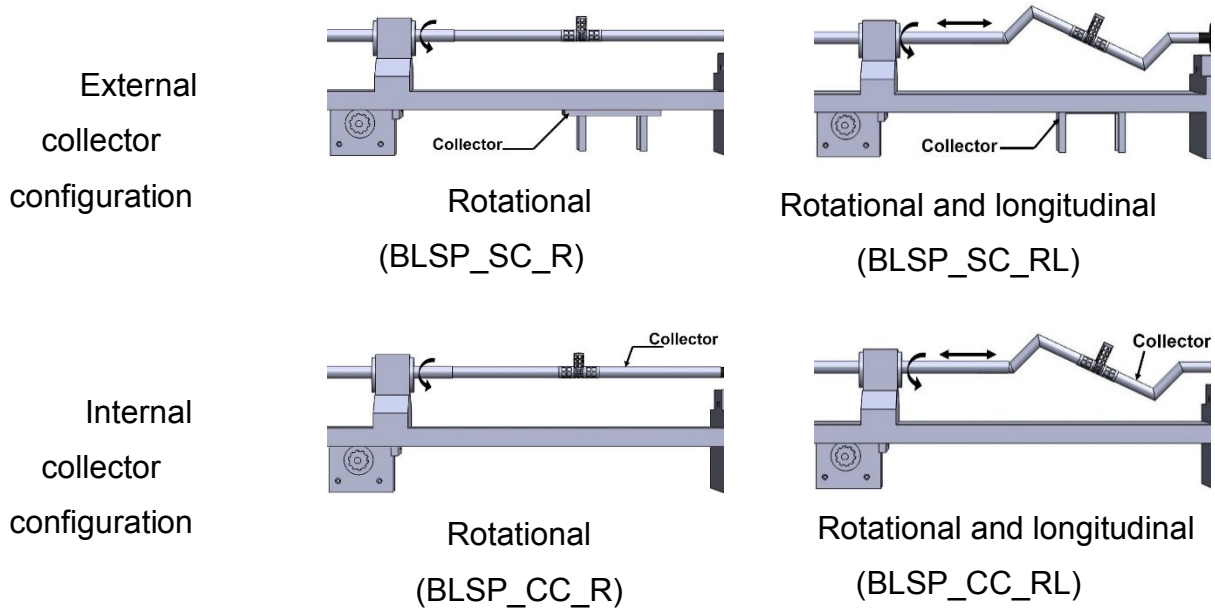


**Figure 3.6** Schematic illustration of electrical field collector configuration and mandrel motion scheme.

### 3.2.2. Characterization of Vascular Graft Membrane Morphology

The following measurements were used to characterize the samples: a) fiber diameter, b) corner profile fidelity ($F_{CP}$ [%]) to determine how the electrospun fibers adhered to the shape of mandrel, c) membrane thickness (t[μm]) of the resultant vascular graft membrane, and d) burst pressure reached by the bifurcated vascular graft membrane. The vascular graft membrane was divided into regions to analyze

how the electrospun fibers were distributed over the mandrel. The procedures are detailed next.

*3.2.2.1. Fiber Diameter and Alignment*

A scanning electron microscope (SEM) EVOMA25 (Carl Zeiss, Oberkochen, Germany) was used to characterize the vascular graft membrane morphology. The coating procedure was conducted using gold. Images were acquired using conventional SEM operating at an accelerated voltage of 5 kV with a working distance of 9 mm. The images were analyzed using ImageJ software (version 1.44p, U.S. National Institutes of Health, Bethesda, MD, USA) to determine the diameter of fibers and alignment. Fiber diameter measurements were conducted at 200 random positions. Distribution and average diameter were computed and reported. The alignment analysis was achieved using ImageJ software.

*3.2.2.2. Corner Profile Fidelity*

In order to characterize how closely the vascular graft membrane followed (adhered to) the surface of the mandrel, we defined the following indicator: corner profile fidelity ($F_{CP}$). This indicator was defined as the percentage of projected area without fibers, relative to the total area in a picture taken from a fixed angle on regions R5 and R6, as defined in **Figure 3.7**. Therefore, a higher $F_{CP}$ indicated a better vascular graft membrane that fits more closely to the surface of the mandrel shape, and this translated to a bifurcated shape of better quality.

An optical microscope USB2-MICRO-250X (Plugable Technologies, Redmond, WA, USA), with 0x–250x magnification range, was used to visualize the corner profile's fidelity to the mandrel surface, $F_{CP}$ [%]. Images were then measured in ImageJ. The samples were photographed in the same position they were in when extracted from the positioning mechanism (see **Figure 3.8**). Based on the "measurement area" tool available on ImageJ, $F_{CP}$ [%] was determined. The results are expressed as the mean ± standard error. The corner profile fidelity was measured while the mandrel was still inside. The procedure was as follows: a) draw

a square around region R5 with “rectangle” tool on ImageJ to measure the resulting area to establish the reference total area ($A_s$); b) delineate the area free of fibers, inside the previously drawn rectangle, and register the measurement ($A_i$) with “polygon selections” tool; and c) compute $F_{CP}$ [%] on R5 as $F_{CP}[\%] = \left(\frac{A_i}{A_s}\right) * 100$. The same process was repeated for region R6. The whole measurement protocol is summarized in **Figure 3.9**.

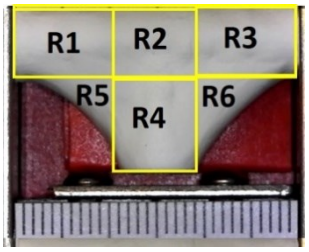


**Figure 3.7** Definition of measurement regions for corner profile fidelity (each mark on the scale is 1 mm)

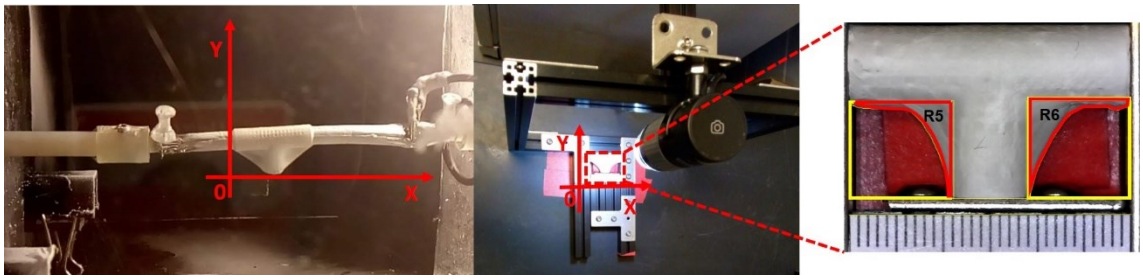


**Figure 3.8.** The position to observe the sample and analyze $F_{CP}$ (%) related to the direction it was electrospun to characterize how the electrospun material was deposited over the mandrel.

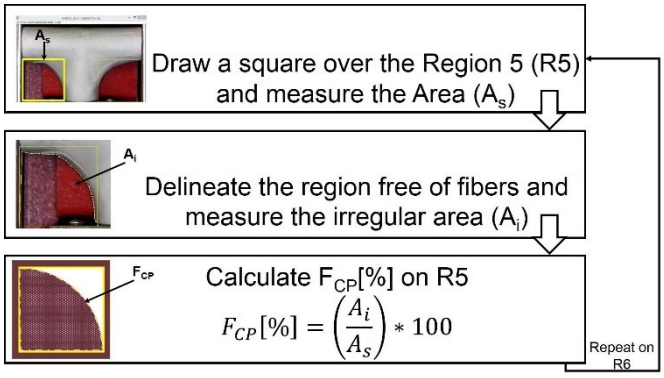


**Figure 3.9.** Measuring process to calculate corner profile fidelity $F_{CP}$ (%) on regions R5 and R6 of the vascular graft membrane with ImageJ software.

*3.2.2.3. Thickness Measurement*

After removal of the mandrel, membrane thickness (t) in each region was measured with a digital micrometer (IP65 coolant proof, Mitutoyo, Aurora, IL, USA) with a resolution of ±1 μm (see **Figure 3.10**). For consistency of these measurements, a fixture was constructed to hold the micrometer and great care was taken to not break the vascular graft membranes.

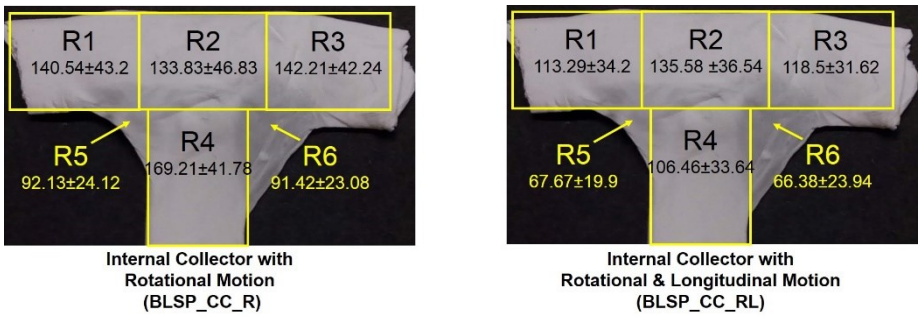


**Figure 3.10** Regions for membrane thickness measurement

### 3.2.3. Characterization of Mechanical Properties

*3.2.3.1. Burst Pressure Test*

Using the bifurcated electrospun vascular graft membranes and an angioplasty balloon, pressurization to burst was achieved and the pressure at bursting was measured (see **Figure 3.11**). The measurements were conducted on all electrospun bifurcated vascular graft membranes (30 mm length). The burst set-up began with an angioplasty balloon (Cordis, Co., Hialeah, FL, USA) being inserted into the vascular graft membrane. The membrane had been hydrated for 6 h with phosphate buffered saline (PBS) at ambient temperature prior to this test. An Encore™ 20 Inflator (Boston Scientific, Marlborough, MA, USA) was used to expand the balloon. Pressure was registered by a digital pressure meter (Wide Range Pressure Meter 840065, Sper Scientific, Scottsdale, AZ, USA), together with a LabVEW.vi system. The inflator, with the mounted vascular graft membrane, was filled with distilled water

at room temperature, while the LabView routine recorded the pressure. The burst pressure was defined as the highest pressure reached before failure.

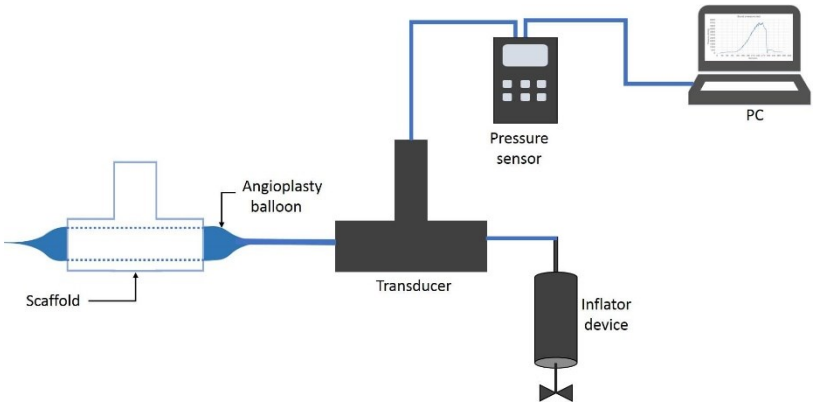


**Figure 3.11** Burst pressure test system.

*3.2.3.2. Suture Retention Strength*

For this test, samples were cut out of the bifurcated membrane to generate a flat rectangular shape. Therefore, the thickness of these samples corresponded to the average thickness in regions R1, R2 and R3. Characterization, to determine the force necessary to pull a suture from the vascular graft membrane, was carried out using a universal testing machine Instron 3365 (Norwood, Massachusetts, USA), according to the International ISO 7198:2016 for Cardiovascular implants and extracorporeal systems -- Vascular prostheses -- Tubular vascular grafts and vascular patches, with a 5 N load cell under physiological conditions [44] and a temperature controlled bath in PBS at 37 °C (BioPuls Temperature Controlled Bath 3130-100), as shown in **Figure 3.12**. A Prolene 5–0 (Ethicon, Inc, Bridgewater, NJ, USA) suture was pierced through the wall of the vascular graft membrane 2.0 mm away from the edge and tied to form a loop. The thread was passed through the vascular graft membrane by means of the needle provided. The non-sutured end of the vascular graft membrane and the suture loop were each attached to separate clamps in the universal testing machine and the suture was pulled at 5 mm per minute. The suture point was centered with respect to the specimen width and its distance from the clamp [45].

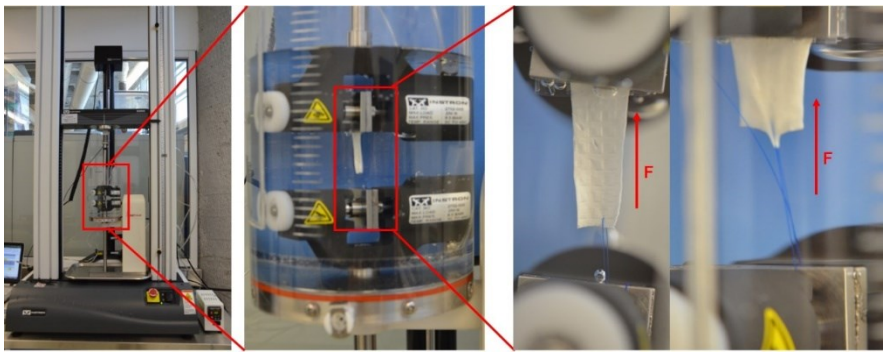


**Figure 3.12** Set up used for mechanical characterization.

### 3.2.4 Cytotoxicity Assay

To assess the in vitro cytotoxicity of the produced mats, the International ISO 10993-5 for Biological evaluation of medical devices was followed. Samples of PCL mats were soaked in 70% ethanol for 30 min, followed by washing, twice, in sterile PBS. Then, the samples were exposed to UV light for 15 min, 30 min prior to cell seeding.

Human fibroblasts (Detroit 548 ATCC, CCL-116, American Type Culture Collection, Rockville, MD, USA) were placed into sterile of 96-well plates with low glucose Dulbecco's Modified Eagle's Medium (DMEM, GIBCO, Invitrogen, Grand Island, NY, USA) supplemented with 10% FBS (Laboratorios Microlab, Mexico City, Mexico) and 1% penicillin–streptomycin (Sigma, St. Louis, MO, USA). The cultures were kept at 37 °C and 5% $CO_2$ in an incubator (Sanyo, MCO-19AIC, (UV), Moriguchi, Japan) for 24 h to allow attachment. The culture medium was replaced every day and the cells were trypsinized upon reaching a confluence of 50%. Cell proliferation was assessed using MTT assay.

This method was based on the conversion of MTT (3-(4,5-Dimethylthiazol-2-yl)-2,5-diphenyltetrazolium bromide) into formazan, which determined the mitochondrial activity. Fibroblasts were seeded, in triplicate, in 96-well culture microtiter plates at a density of $3 \times 10^3$. Next, 100 µL of medium without cells and 100 µL of 1% Triton X-100 in PBS were added to the wells and were used as negative and positive controls, respectively. The microtiter plates were incubated for 96 h in an incubator with 5% CO2 at 37 °C. After incubation, 20 µL of MTT were

added to the test wells and allowed to react for 6 h at 37 °C and 5% $CO_2$. Afterwards, the medium was discarded and replaced with 150 µL of dimethyl sulfoxide. After gently shaking for 10min, the optical density (OD) was determined by reading the absorbance at 500 nm on a Biotek Synergy 2 microplate reader (Winooski, VT, USA).

### 3.2.5. Statistical Analysis

GraphPad Prism Software Version 8.0 (San Diego, CA, USA) was used for statistical analysis. Data were expressed as mean ± standard deviation (SD). Univariate statistical comparisons were made with a Student's t-test. Multivariate statistical analysis was carried out using ANOVA and Tukey's tests. A p-value of $p < 0.05$ was considered statistically significant.

## 3.3 Results

### 3.3.1. Fabrication Process

Four groups of mandrels were electrospun under different conditions, as indicated in **Table 3.2**. **Figure 3.13a,b** shows that bifurcated vascular graft membranes were not viable when the electrical field collector was outside the mandrel. When the collector was placed inside the mandrel, it attracted a significant amount of fibers, as shown in **Figure 3.13c,d.**

### 3.3.2. Characterization of Vascular Graft Membrane Morphology

*3.3.2.1. Fiber Diameter and Alignment*

After imaging and analysis, the mean observed fiber diameter for single axis rotation-only average fiber diameter was 290.2 ± 104.6 nm and 60° alignment fiber around 3000 measured fibers, while a motion scheme that involved rotational and

longitudinal motion resulted in an average fiber diameter of 276.8 ± 78.5 nm and around –90°. Almost 6000 fibers were measured, as shown in **Figure 3.14**.

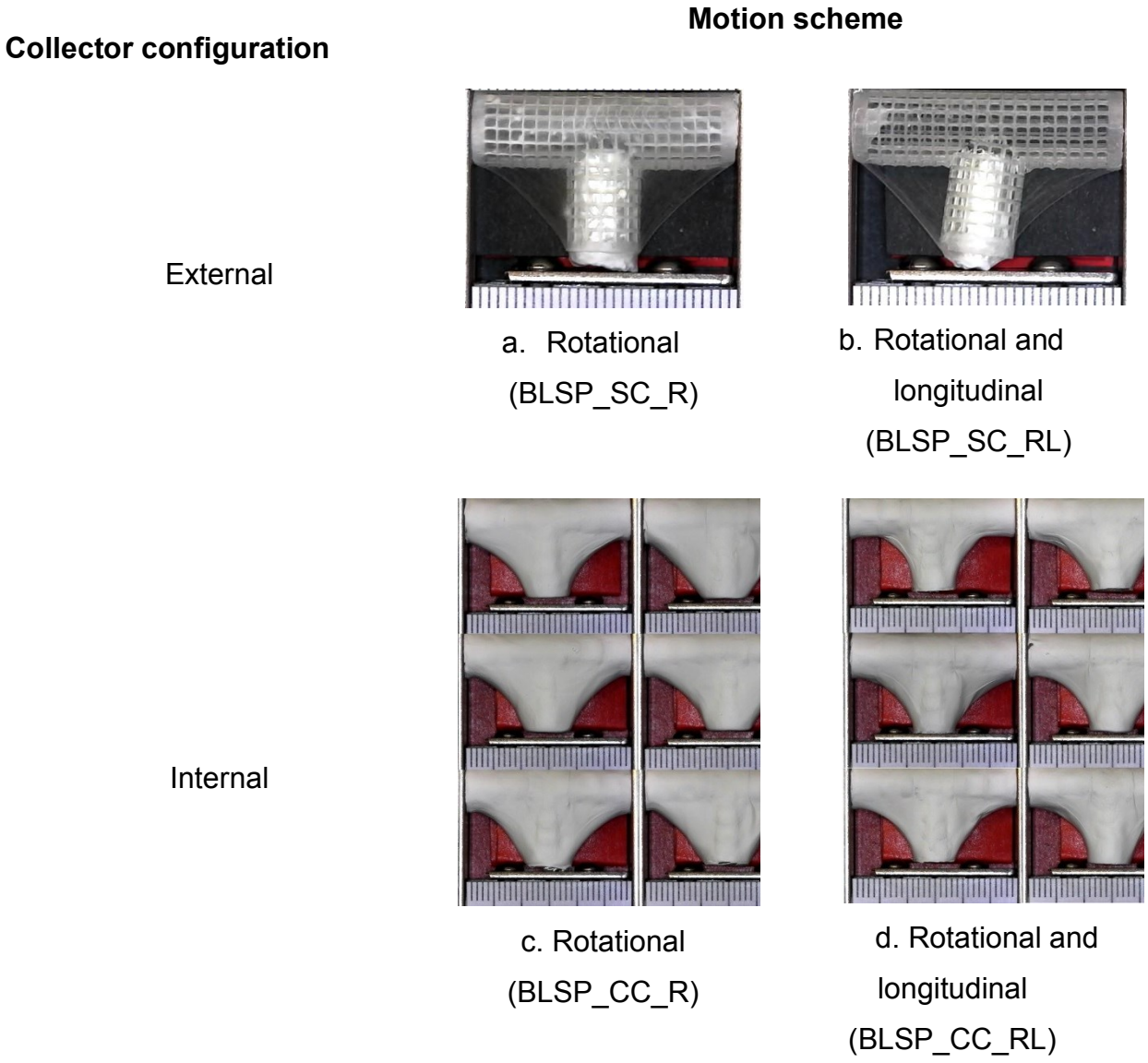


**Figure 3.13** Overview of bifurcated vascular grafts obtained under different sets of process parameters.

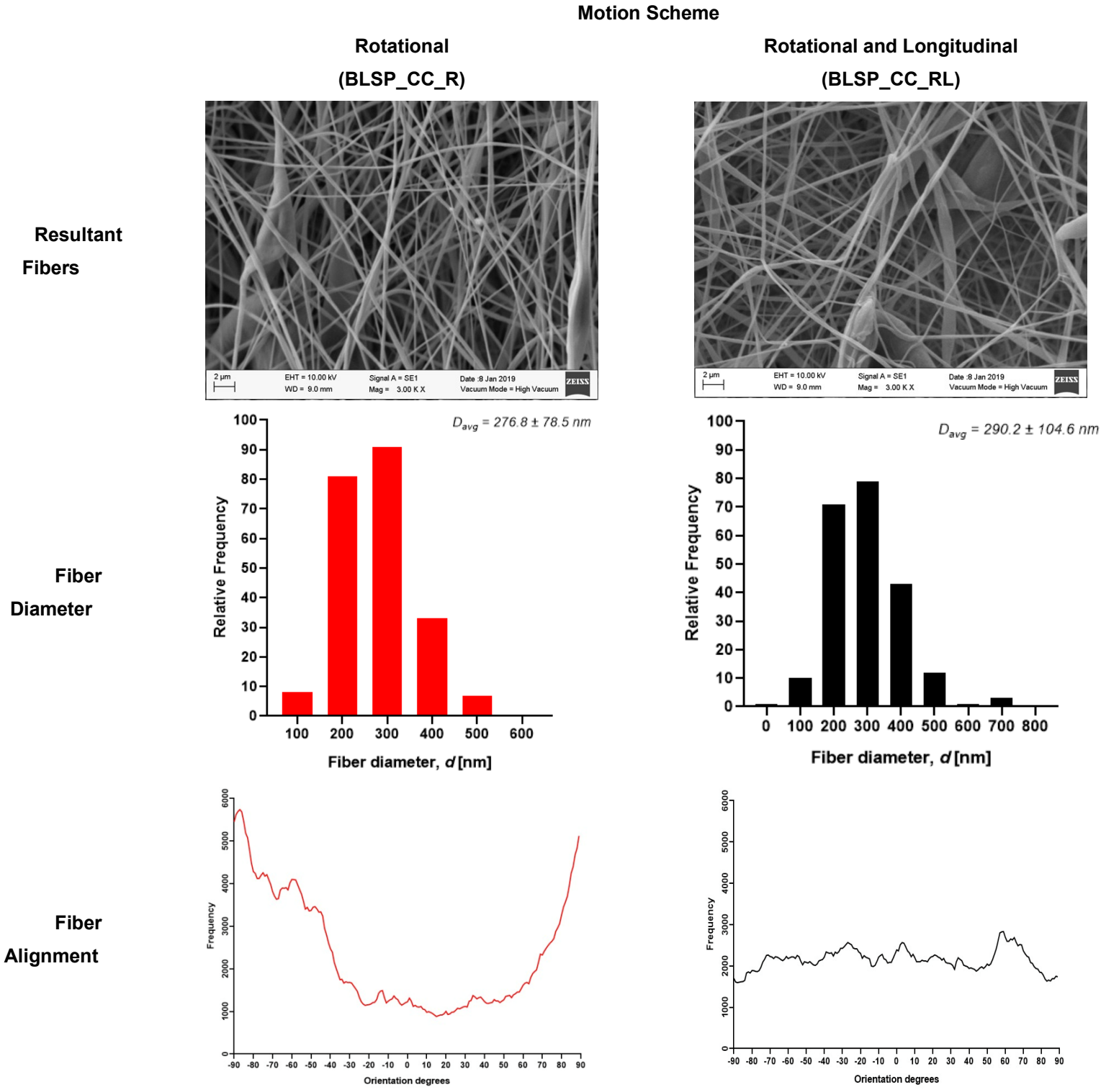


**Figure 3.14** Electrospun fibers of the outer layer from bifurcated vascular graft membranes (SEM imaging).

### *3.3.2.2. Corner Profile Fidelity ($F_{CP}$)*

The goal was to obtain the highest $F_{CP}$ to show that the electrospun membrane properly fit the given shape of the mandrel. There was no significant difference between region R5 and R6 (see **Figure 3.15**). However, it was clear that the combination of rotational and longitudinal motion on the mandrel produced a better fit of the membrane.

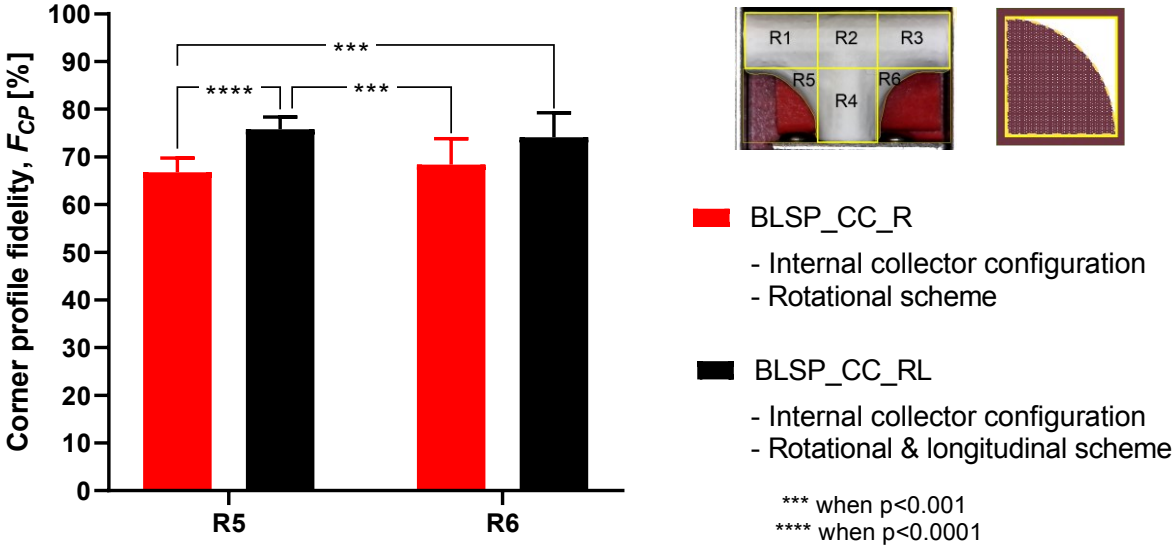


**Figure 3.15.** Average corner profile fidelity at regions R5 and R6. (A two-way ANOVA showed that the motion scheme with rotational and longitudinal approach increased the corner profile fidelity).

### *3.3.2.3. Membrane Thickness Distribution*

The vascular graft membrane thickness of 6 different regions was measured. **Table 3.3** and **Figure 3.16** show the membrane thickness per region. **Figure 3.17** shows the average membrane thickness considering all regions.

The motion scheme for mandrel positioning influenced the average membrane thickness, where the rotational and longitudinal approach produced a thinner membrane. The motion scheme also clearly generated a different membrane thickness distribution among the different regions. Under rotational motion, R4 tended to have the thickest membrane (although not statistically significant when compared to R1 and R2). Under both motion schemes there was a statistically

significant difference between R5 and R6 compared to at least one of the other regions. The fact that R5 and R6 had thinner membranes was thought to be due to their location at the corner of the mandrel, where deposition of electrospun fibers tended to be more difficult.

**Table 3.3** Average membrane thickness at different regions.

| Experimental Group | Average Thickness per Region [$t_R$] (μm) | | | | | |
|---|---|---|---|---|---|---|
| | $t_{R1}$ | $t_{R2}$ | $t_{R3}$ | $t_{R4}$ | $t_{R5}$ | $t_{R6}$ |
| Internal Collector with Rotational Motion (BLSP_CC_R) | 140.54 ± 43.2 | 133.83 ± 46.83 | 142.21 ± 42.24 | 169.21 ± 41.78 | 92.13 ± 24.12 | 91.42 ± 23.08 |
| Internal Collector with Rotational and Longitudinal Motion (BLSP_CC_RL) | 113.29 ± 34.2 | 135.58 ± 36.54 | 118.5 ± 31.62 | 106.46 ± 33.64 | 67.67 ± 19.9 | 66.38 ± 23.94 |

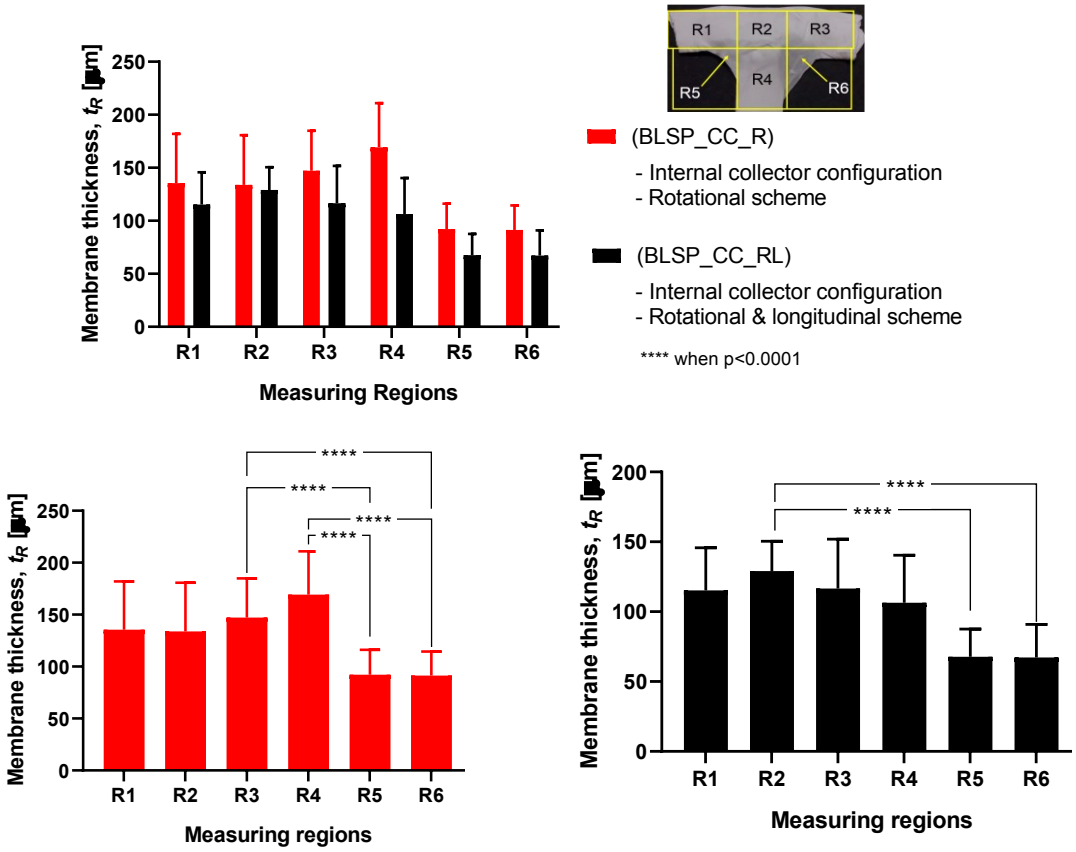


**Figure 3.16** Membrane thickness distribution along the vascular graft membrane surface. (A two-way ANOVA was performed to determine any statistically significant differences between experiments.).

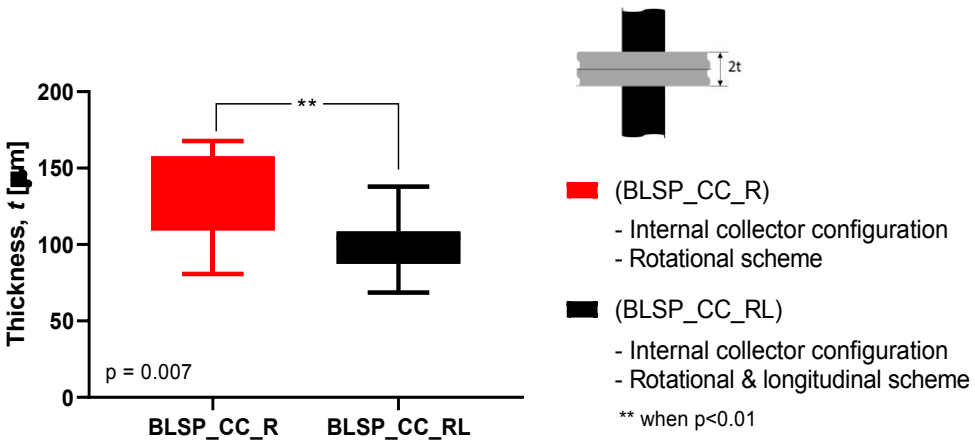


**Figure 3.17** Average membrane thickness of the whole vascular graft considering all regions. (A Student's t-test was performed to determine any statistically significant differences between experiments. All tests were carried out at a 95% confidence interval).

### 3.3.3. Characterization of Mechanical Properties

#### 3.3.3.1. Burst Pressure Strength

**Figure 3.18** shows the observed results of the burst pressure test for both groups. Both met or exceeded the goal (4000 mmHg) according to [46]. These results suggested that burst pressure was not related to any difference in thickness of the two vascular graft membranes. In addition, the motion approach based on rotational and longitudinal motion produced a statistically significant increase in bust pressure strength, with an average of 5126 mmHg.

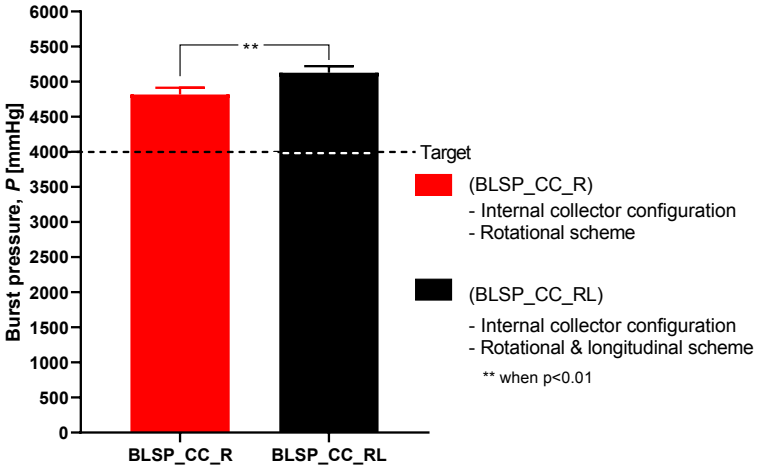


**Figure 3.18** Burst pressure strength.

*3.3.3.2. Suture Retention Strength (SRS)*

**Figure 3.19** shows that the motion scheme did not influence the suture retention strength. There was no statistical difference between these conditions (rotational vs. rotational and longitudinal motion). The vascular graft membrane with the highest SRS was on the experiment BSLP_CC_R at 1.44 N, which meant 75% of the minimum clinical requirement [41,45,47]. More importantly, neither graft obtained the target strength. In addition, **Figure 3.20** shows that while member thickness changed with motion scheme, thicker membranes did not produce an increase in suture retention strength.

### 3.3.4. Cytotoxicity Assay

Our data revealed that all bifurcated scaffolds showed viability higher than 86%, which confirmed that PCL bifurcated scaffolds presented cytocompatibility (cell viability higher than 50%).

### 3.3.5. Summary of Results

**Table 3.4** shows a summary of the experimental results. The motion scheme, by comparing only the rotation of the mandrel relative to the fiber source vs. rotation and tilting produced by the longitudinal movement, produced different effects on the response variables of interest. The application of rotational and longitudinal motion by the positioning mechanism produced statistically significant effects on the corner profile fidelity, burst pressure strength, and suture retention strength.

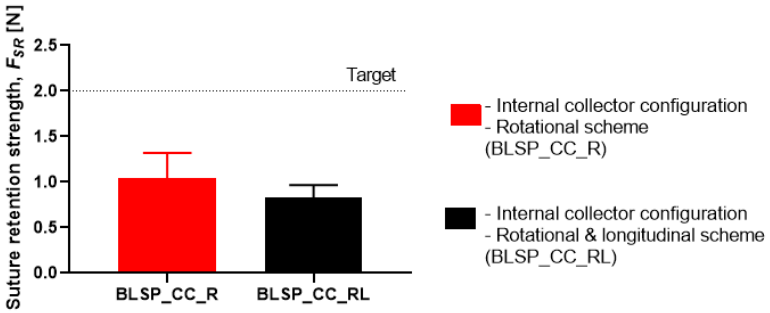


**Figure 3.19** Suture retention strength. (A Student's t-test was performed to determine any statistically significant differences between experiments. All tests were carried out at a 95% confidence interval and the results did not show statistically significant differences.)

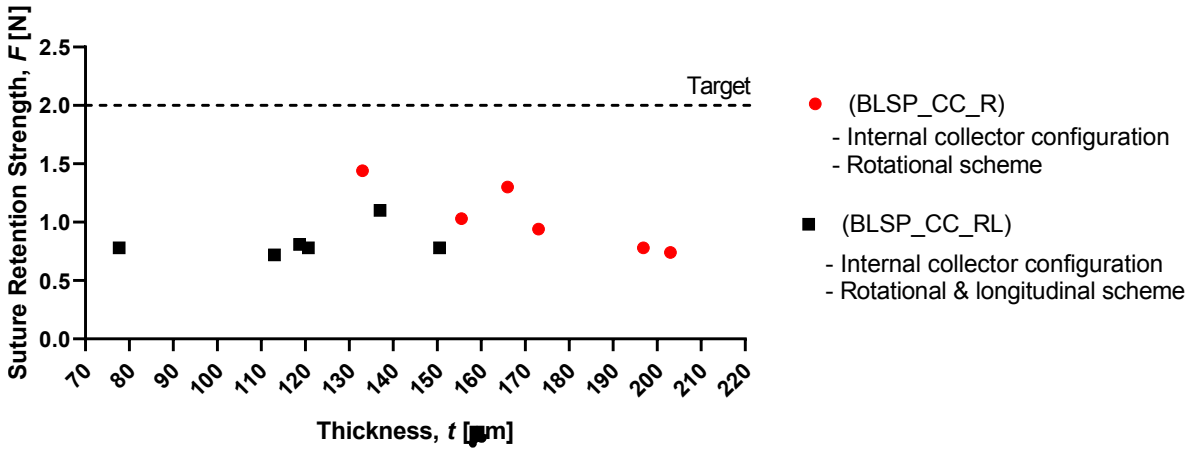


**Figure 3.20** Membrane thickness vs. graft suture retention strength.

**Table 3.4** Summary of morphology and mechanical properties.

| Motion Scheme | Corner Profile Fidelity $F_{CP}$ [%] +++ | | Fiber Diameter *d* [nm] | Membrane Thickness *t* [μm] +++ | Burst Pressure Strength *P* [mmHg] +++ | Suture Retention Strength $F_{SR}$ [N] |
|---|---|---|---|---|---|---|
| | R5 | R6 | | | | |
| Internal Collector with Rotational Motion (BLSP_CC_R) | 33.22 ± 0.03 | 31.6 ± 0.05 | 276.8 ± 78.5 | 171.22 ± 26.09 | 4388.3 ± 1,027.2 | 1.04 ± 0.3 |
| Internal Collector with Rot. and Long. Motion (BLSP_CC_RL) | 24.23 ± 0.03 | 25.89 ± 0.05 | 290.2 ± 104.6 | 119.58 ± 24.74 | 5126.6 ± 1074.6 | 0.83 ± 0.1 |

NOTE: +++ indicates response variables with statistically significant difference due to motion scheme.

## 3.4 Discussion

The work presented here demonstrates that bifurcated vascular grafts can be constructed via electrospinning by combining an internal electrical field collector design and a 2-DOF positioning mechanism, for the mandrel. The addition of a second longitudinal axis for tilting of the mandrel improved the corner profile fidelity of the vascular graft membrane. However, it was not closely adherent in either case,

suggesting that a more direct, perhaps robotically-assisted, approach to controlling needle tip orientation and mandrel surface was needed to ensure closer apposition. Alternatively, ejection pressure, mandrel speed, and/or needle tip distance to the mandrel may also improve apposition.

### 3.4.1. Characterization of Vascular Graft Membrane Morphology

Vascular graft membrane morphology was evaluated through fiber diameter, corner profile fidelity ($F_{CP}$), and membrane thickness. The average fiber diameter obtained in these experiments was 276.8 and 290.2 nm. These diameters were thinner but comparable to the low end of those previously reported, as shown in **Table 3.1**, where membrane thickness ranged between 0.4 and 900 μm. According to the literature, the diameter range of the self-expandable metal stents (SEMS) used as pancreatic stents is about 8–10 mm [48]. The bifurcated graft that we produced was within this range (internal diameter of 8 mm). The alignment obtained can be attributed to the motion scheme reported in the literature [49]. When high-speed profiles and rotational collectors were used, fiber orientation between –90° and +90° was expected. Based on the corner profile fidelity ($F_{CP}$) indicator there was a clear benefit to having a combination of rotational and longitudinal motion. In the case of region R6, this benefit was not statistically significance. The need for better apposition of the vascular graft membrane to the mandrel, especially in regions R5 and R6, suggested that the relationship of speed, fiber alignment, and mechanical properties could be further explored, as suggested by [34]. The study of membrane thickness showed that the rotational and longitudinal motion tended to lower this value (although no statistical significance was observed with the current data).

Previous studies demonstrated that PCL was a promising candidate for vascular grafts due to its bioactivity and nontoxicity [40,49]. In this study, the cytotoxicity assessment using MTT assay showed that the produced mats based on 3D printed mandrels provided a suitable surface to maintain adhesion of the seeded cells. The assay did not reveal whether fibroblasts penetrated the porous mats (see **Figure 3.14**). However it was assumed that the cells could infiltrate this type of fiber. The scope of the reported study was to obtain the necessary bifurcated morphology

and mechanical properties for the proposed applications. Therefore, further studies are required to validate the proliferation of the seeded cells into the bifurcated grafts.

This study focused on T-shaped bifurcated vascular grafts. Using the same approach as that based on the 2-DOF positioning system and internal electrical field collector design, it was possible to generate Y-shaped bifurcated vascular grafts, as shown in **Figure 3.21**. This kind of Y-graft was similar to those reported in related studies [33]. An improvement could be to construct a mandrel based on patient image studies and, therefore, generate patient-specific bifurcated vascular grafts with varying cross-sections and complex overall geometries. In this process $F_{CP}$ was a relevant quantitative measurement of the quality of the constructed bifurcation structure. The objective continues to be to obtain an $F_{CP}$ closer to 100%, to achieve patient-specific bifurcated shapes.

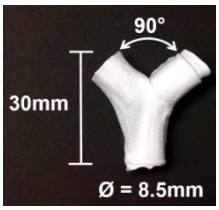


**Figure 3.21** Vascular Y-graft produced by electrospinning, with a the 2-DOF positioning system and an internal electrical field collector approach.

### 3.4.2. Characterization of Mechanical Properties

The burst pressure strength (BPS) tests showed that the proposed approach yielded acceptable results. For the rotational and longitudinal motion approach, an average BPS of 5126.6 ± 1074.57 mmHg was obtained for the bifurcated vascular grafts. This may have correlated with other measured characteristics such as fiber diameter. However, that variable was not studied. These levels of strength were comparable to those reported for straight tubular electrospun vascular graft membranes that did not change diameter (see **Table 3.1**). These values ranged between 985 and 4915 mmHg (except for the case of Kim et al. where an extremely thick membrane of 0.33 mm was tested [31]). Previously reported results for SRS suggest that this parameter was determined mostly by membrane thickness [50]. However, in the range of test conditions covered in this study, we did not find such

a correlation. The SRS values for the bifurcated vascular graft membranes observed in the two groups in this study (1.04 N and 0.83 N) were not satisfactory according to the established target value (2 N based on [41,45,47]) and those shown in **Table 3.1**. Further process parameter optimization for apposition to the mandrel, increasing membrane thickness, or a change in materials could improve SRS, for potential vascular applications. In the case of the Whipple procedure, SRS was not as critical when compared to vascular applications. In that context, we expect that degradation kinetics under the influence of bile will be a challenge.

### 3.4.3. Relationship between Process Parameters and Vascular Functional Specifications.

In the context of Y-grafts, we identified the following major functional specifications: a) corner profile fidelity, b) burst pressure strength, and c) suture retention strength. These functional specifications correlated to the basic properties of the electrospun fibers and their corresponding membranes, which were from the complete array of process parameters. **Figure 3.22** shows a schematic relationship between the process parameters, basic properties (fibers and membranes) and graft functional specifications. This study reported the significant influence of the internal electrical field collector design and the motion scheme. As we continue to refine this complex fabrication method, a more detailed study of process parameters will be needed (for example: solution viscosity, mandrel design, positioning angles and speed). We also expect to explore variants of this process, such as melt electrospinning and melt electrowriting.

## 3.5 Conclusions and future work

This study aimed to characterize the basic impact of spinning one versus two long axes of vascular graft membrane thickness and the resulting properties of the electrospun vascular graft membranes (see **Table 3.4**). These vascular graft membranes were generated by electrospinning PCL solution onto mandrels with bifurcated shapes prepared by 3D printing with E-Shell® 200 (EnvisionTEC, Dearborn, MI) photocurable resin. The values obtained for bifurcated vascular graft

membrane thickness and fiber diameter with rotational scheme motion (BLSP_CC_R), 171.22 ± 26.09μm and 276.8 ± 78.5nm respectively, and rotational and longitudinal scheme motion (BLSP_CC_RL), 119.58 ± 24.74 μm and 290.2 ± 104.6nm respectively, were comparable to similar studies with tubular vascular graft membranes (see **Table 3.1**). In terms of mechanical properties, the burst pressure strength obtained with rotational scheme motion and rotational and longitudinal scheme motion, 4,388.3 ± 1,027.2 mmHg and 5,126.6 ± 1,074.6 mmHg respectively, were also comparable to tubular vascular graft membranes. The only limitation we have found so far was in terms of suture retention strength, in which the target was set to 2 N and approximately 50% of the expected yield was obtained. Further investigation is required to improve the mechanical performance of bifurcated vascular graft membranes based on refinement of the positioning mechanism kinematics and optimization of process parameters. The first refinement in positioning will be to better ensure orthogonality of the mandrel surface and polymer-exuding needle, followed by control of the rate of spinning. Once membrane apposition to the mandrel is improved, we will be able to study the effect of membrane biomaterials.

In this study we identified the potential applications of bifurcated constructs such as vascular grafts for use in the Fontan procedure (see **Figure 3.1**), or pancreatic stents to be used in pancreaticoduodenectomy (PD) procedures (see **Figure 3.2**). The scope of this work was limited to successfully obtaining the basic requirements: appropriate morphology and suitable mechanical properties. In the next phase, we expect to continue the development of these devices with additional in vivo and in vitro testing.

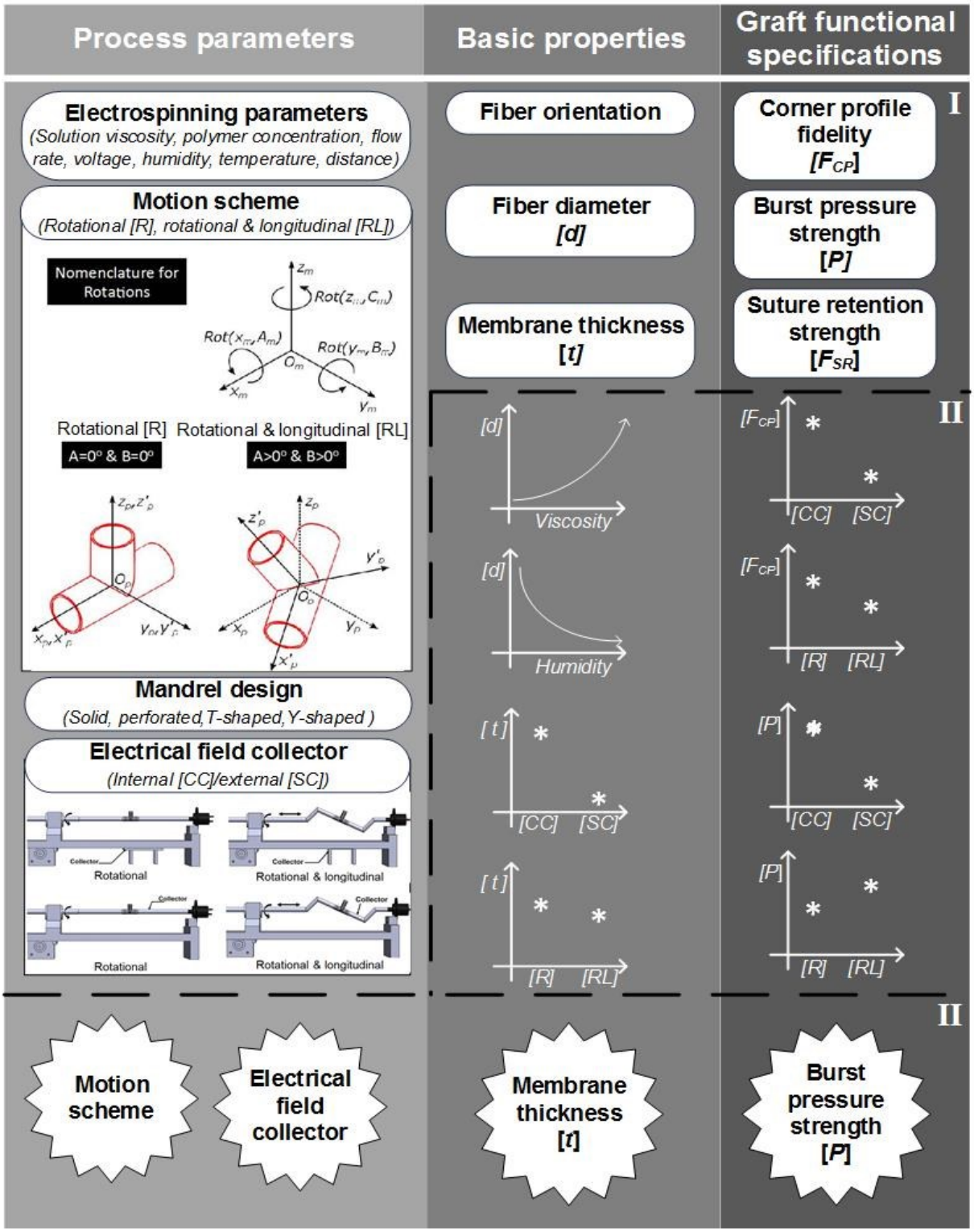


**Figure 3.22** Schematic description of the construction process of bifurcated vascular grafts proposed in this work. (I) Process parameters and properties involved on the construction process' (II) influence of some process parameters on the basic properties of the graft; III) classification of the most influencing parameters and properties into the graft functional specifications.

# Chapter 4 . Continuous Digital Light Processing of unsaturated polyesters from Isosorbide for Bone Tissue Engineering

## 4.1 Introduction

In recent years, additive manufacturing techniques have become fundamental methods in the use of new biomaterials. Stereolithography enables the printing of scaffolds for cellular support of highly complex architectures if the materials have photocrosslinking potential. Nonetheless, there is a small group of resins (see **Table 4.1**) that can be printed, since they must meet such characteristics as biocompatibility, biodegradability, and in some printing techniques, photocrosslinking potential.

Scaffold characteristics that can be modified, improved, or changed to make a scaffold suitable for bone tissue engineering applications can be grouped into four main categories: biological requirements, structural features, biomaterial composition, and types of fabrication process [51]. Scaffolds that are currently used for bone tissue engineering applications are polymers, bioactive ceramics (glasses) and hybrids (composites).

Bone is a key component of the musculoskeletal system, providing structure for ambulatory and environmental manipulating functions, storing nutrients, protecting vital organs, and playing a key role in hematopoietic and immunological functions. Although bone possesses an extraordinary regenerative capacity, it can fail to heal under unstable and large deficit conditions [52].

The most reported printable photopolymers for tissue scaffolds, poly(propylene fumarate) (PPF), show excellent biocompatibility and demonstrates promise for its use in scaffolds for hard tissue replacement. Besides, other polymers reported include poly(ε-caprolactone), poly(ethylene glycol) diacrylate, trimethylene

carbonate, and poly (D,L-lactide). These polymers are limited about the range of mechanical and chemical properties making them appropriate to construct scaffolds for certain types of tissue replacement [53]. The most common additive manufacturing technologies developed within the last years are Stereolithography (SL), Fused Deposition Modeling (FDM), Selective Laser Sintering (SLS), Digital Light Processing (DLP), and Bioprinting [51].

Digital Light Processing (DLP) utilizes visible blue light. It was based on lithography-based additive manufacturing technologies, for building ceramic or glass parts. In the DLP method, dynamic masks are employed to cure a whole layer at a time. Therefore, this method suggests a higher building speed. Additional improvements of DLP consist of a high lateral resolution of 40 lm (*50 lm of conventional SLA), an effective method for filling a large volume of ceramic particles (*40–60 % solid loading), and no need for expensive specific apparatus such as a laser or a heating chamber [54].

**Table 4.1** Polymer scaffolds fabricated using 3D printing for use in bone tissue regeneration.

| Material | 3D Printing Process | DYE package | Ref. |
|---|---|---|---|
| Poly(tri(ethylene glycol)adipate) dimethacrylate (PTEGA-DMA) | Microstereolitography (MPμSL) | Avobenzone (Light attenuator) | [53] |
| Poly (propylene fumarate) (PPF) | Continuous Digital Light processing (cDLP) | TiO2 and bis (2,4,6-trimethylbenzoyl) phenylphosphine oxide | [55] |
| Poly (propylene fumarate) (PPF) | Continuous Digital Light processing (cDLP) | Titanium dioxide (TiO2) as a dye, Irgacure® 819 as photoinitiator Diethyl fumarate as a solvent | [56] |
| Vinylester, vinylcarbonate | DLP | IrgacureVR 819 as photoinitiator CGL 097 as UV-absorber | [57] |
| Nanocrystalline HA, PLGA | Stereolithography | Bis(2,4,6-trimethylbenzoyl)-phenylphosphineoxide (BAPO) as photoinitiator | [58] |

| | | | |
|---|---|---|---|
| Water-based polyurethane based photosensitive materials with hyaluronic acid (HA) | DLP | 2,4,6-trimethylbenzoyl-diphenyl-phosphineoxide (TPO) as photoinitiator<br><br>2-Hydroxylethyl methacrylate (HEMA) as a solvent | [59] |
| Hydroxyapatite (HA) and Tricalcium phosphate (TCP) powder with a photocurable resin (FA1260T; SKCytec) | Projection-based microstereolithography (pMSTL) | NA | [60] |
| trimethylene carbonate/trimethylolpropane (TMC/TMP) | Microstereolithography | NA | [61] |
| Poly (propylene fumarate) (PPF) | Microstereolithography | Dimethoxy phenyl acetophenone (DMPA) as photoinitiator | [62] |
| Poly(ethylene glycol) diacrylate (PEGda) | Two-photon polymerization microfabrication (TPPM) | 1,4-bis(4-(N,N-bis(6-(N,N,Ntrimethylammonium)hexyl)amino)-styryl)-2,5- dimethoxybenzene tetraiodide as photoinitiator | [63] |

In the research reported here, a new biomaterial is being studied to analyze its capability to be used in cDLP technology. The differences between PPF were studied from the perspective of morphology and mechanical properties, due to PPF is one of the most characterized biopolymers for bone scaffolding.

The previous work shown in **Table 4.1** includes a wide range of resin formulations and manufacturing parameters. Given these variations, comparison of mechanical properties and other features is difficult among different studies. In order to validate the proposed approach, using Isosorbide and cDLP, gyroids with PPF resin printed using cDLP technology were used as reference in the study reported here.

## 4.2 Materials and methods

### 4.2.1 Photocurable resin formulation

#### *4.2.1.1 Isosorbide resin formulation*

A set of four resins of varying concentrations (See **Table 4.2**) of Isosorbide polymer were stirred by two hours in a sealed container without temperature, mixed with 1-vinylimidazole (VIM, Sigma-Aldrich, MO) as co-crosslinker, Irgacure 819 (BAPO, BASF, NJ) as photoinitiator, Oxybenzophenone (HMB, Sigma, St. Louis, MO) as light attenuator and dissolved in Ethyl Acetate (EA, Fischer Chemical, Pittsburgh, PA).

**Table 4.2** Resin formulation percentages

| | | (%) | (%) | (%) | (%) |
|---|---|---|---|---|---|
| Polymer | Isosorbide | 54.9 | 52.5 | 54.9 | 53 |
| Co-crosslinker | VIM | 32 | 32 | 33.5 | 33.5 |
| Photoinitiator | BAPO | 4 | 5 | 4 | 5 |
| Light attenuator | HMB | 2.1 | 3.5 | 0.7 | 1.6 |
| Solvent | EA | 7 | 7 | 6.9 | 6.9 |
| | | **ISO 1** | **ISO 2** | **ISO 3** | **ISO 4** |

#### *4.2.1.2 PPF resin formulation*

PPF resin of molecular weight 1300Da was diluted with Diethyl fumarate (DEF, Sigma-Aldrich, St. Louis, MO) in a 1:1 ratio in order to reduce the viscosity for 3D cDLP process. Photoinitiators Phenyl bis(2,4,6-trimethylbenzoyl)-phosphine oxide (BAPO, Sigma-Aldrich, St. Louis, MO) and bis[2,6-difluoro-3-(1-hydropyrrol-1-yl)phenyl]titanocene (Irgacure 784, BASF, Ludwigshafen, Germany) were added in concentration of 3 and 0.4% by mass, respectively. Finally, 0.7% of 2-Hydroxy-4-methoxybenzophenone (HMB, SigmaAldrich) was added to mitigate light scattering within layers.

### 4.2.2 Experimental setup for characterization

The set of characterization tests (see **Figure 4.1**), (i.e., curing depth tests, green strength, and 3D Gyroids printability tests) were performed according to the work of Hernan Lara-Padilla published in his thesis, employing a Micro® Printer (EnvisionTEC, Inc., Dearborn, MI). This device utilizes 405nm light and a 450 mW/cm2 intensity measured with RM 12 radiometer with a VIS-B sensor (Dr. Grobel, Ettlingen, GER).

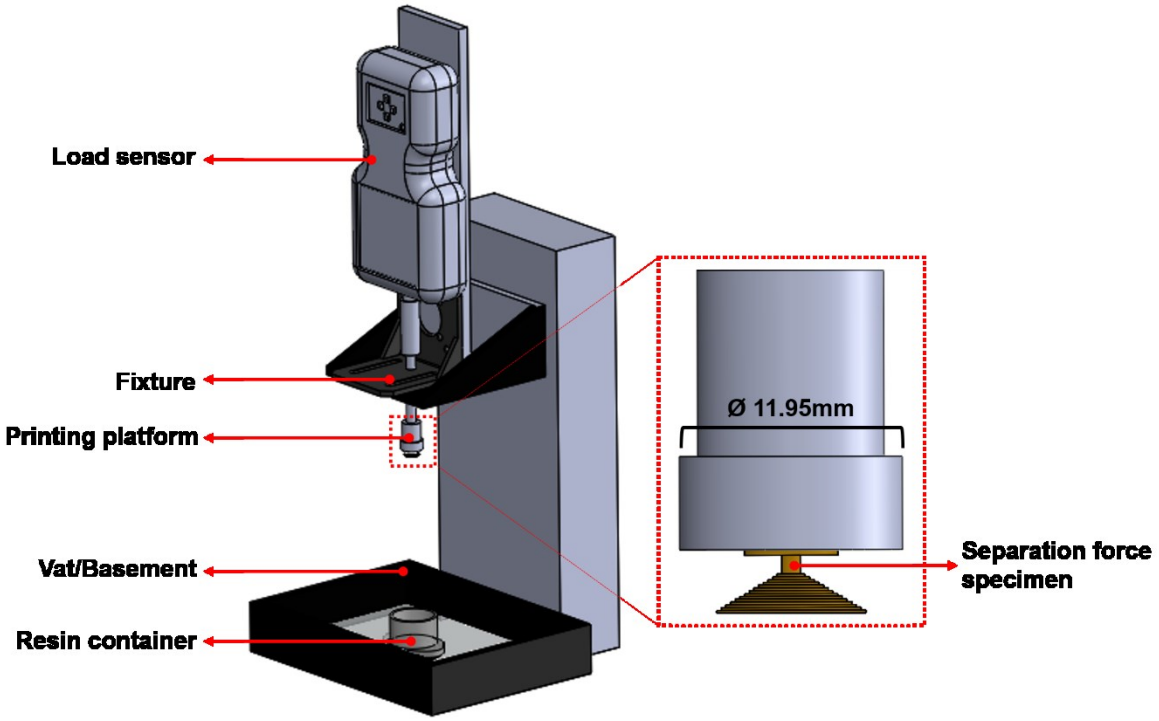


**Figure 4.1** Setup employed to accomplish the separation force and green strength using EnvisionTec 3D printer.

### 4.2.3 Mechanical characterization

#### *4.2.3.1 Cure depth test*

Due to the polymerization takes place once the energy to which the resin is exposed reaches higher values than the photo-initiator's critical energy, the measurement of the cure depth is done after the energy is delivered on the resin surface and penetrates the resin during a determined exposure time. Cure tests were

accomplished with PPF resin and Isosorbide resin, curing squares of 1cm$^2$ area at 30, 60, 90, 120 seconds [14,64].

### *4.2.3.2 Green strength test*

The green strength test consists of the measurement of the better area to print without failure. According to the method described in [14], the objective is to construct a specimen with increasing diameters and record the force at which the specimen breaks. The tests were accomplished using the setup shown in **Figure 4.1** constructing the specimen shown in **Figure 4.2**.

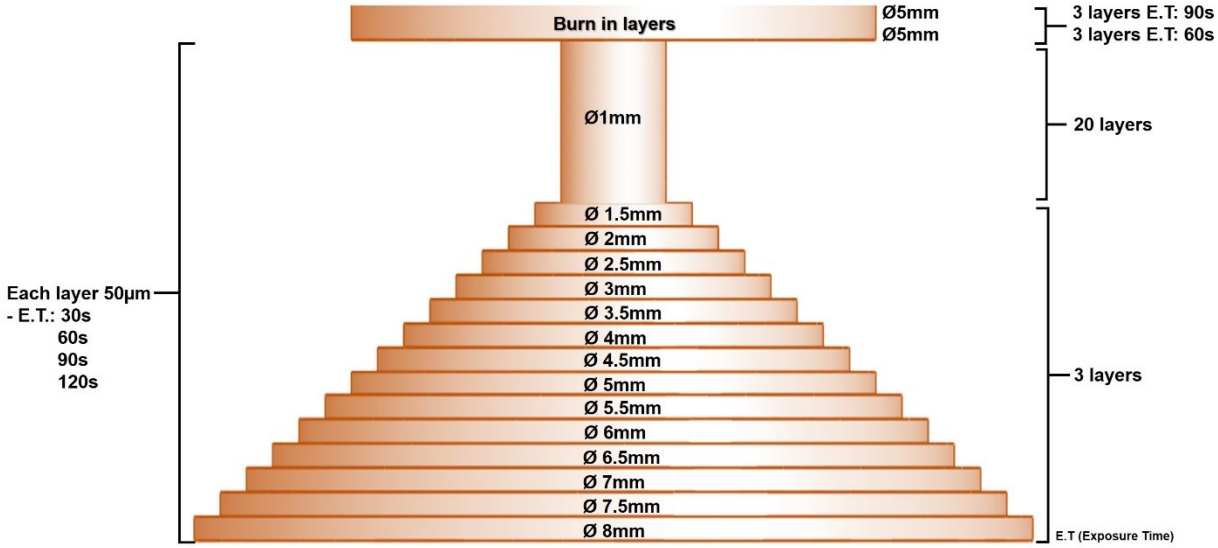


**Figure 4.2** Green strength test specimen used to measure the separation force and the interlayer strength during the printing process.

### *4.2.3.3 3D printability test*

Since scaffolds usually show a complex structure, triply periodic minimal surfaces (TPMS) represent special interest of specialists focused on the design and fabrication for bone tissue engineering applications due to the high area-volume ratio, high porosity, modulated structure, among others. Properties that improve mechanical properties, permeability, cell adhesion, degradation and resorption.

The gyroid geometry consists on 10mm by diameter with 5mm by thickness. The gyroid structure exhibits porosity and pore size and an average strut size of 44%, 800 µm and 1800 µm, respectively.

## 4.3 Results

### 4.3.1 Cure depth tests

According to the experience reported with PPF [14,56,64] a window stablished between 150µm to 250µm was set to determine the successful printing of the tested resin. Although, the data acquired from this experiment does not directly correspond with ideal 3D printing conditions, the resulting data provides important insight into potential setting of manufacturing parameters and resin chemistry that will result in successful 3D printing. A cure depth versus %HMB at four exposure times was obtained, as shown in **Figure 4.3**. As noted, $C_d$ is modified with the %HMB and for these formulations, as the percentage of HMB increases, $C_d$ decreases. The higher exposure time with ISO 1 and ISO 2, the cure depth is higher but not enough because $C_d$ reaches the higher thickness at 90sec and 120sec and cannot be higher than that. Otherwise, ISO 3 and ISO 4, reaches the “ideal” cure depth at 15sec and 30sec and then increases.

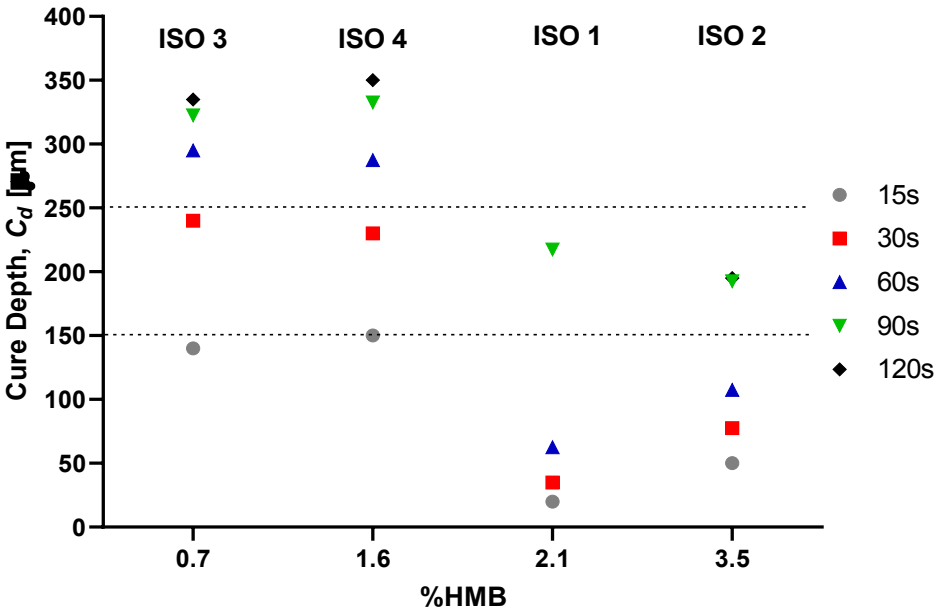


**Figure 4.3** Cure depth at different exposure times. (Average of 4 samples)

### 4.3.2 Green strength tests

This experiment considers the green strength to the relation between the breaking load and the minimal cross-sectional area. The breaking load (see **Figure 4.4**) is the load applied at some point to a component of structure which leads to fracture. **Figure 4.5** provides preliminary evidence that the green strength of the cured resin is affected by the %HMB and exposure time.

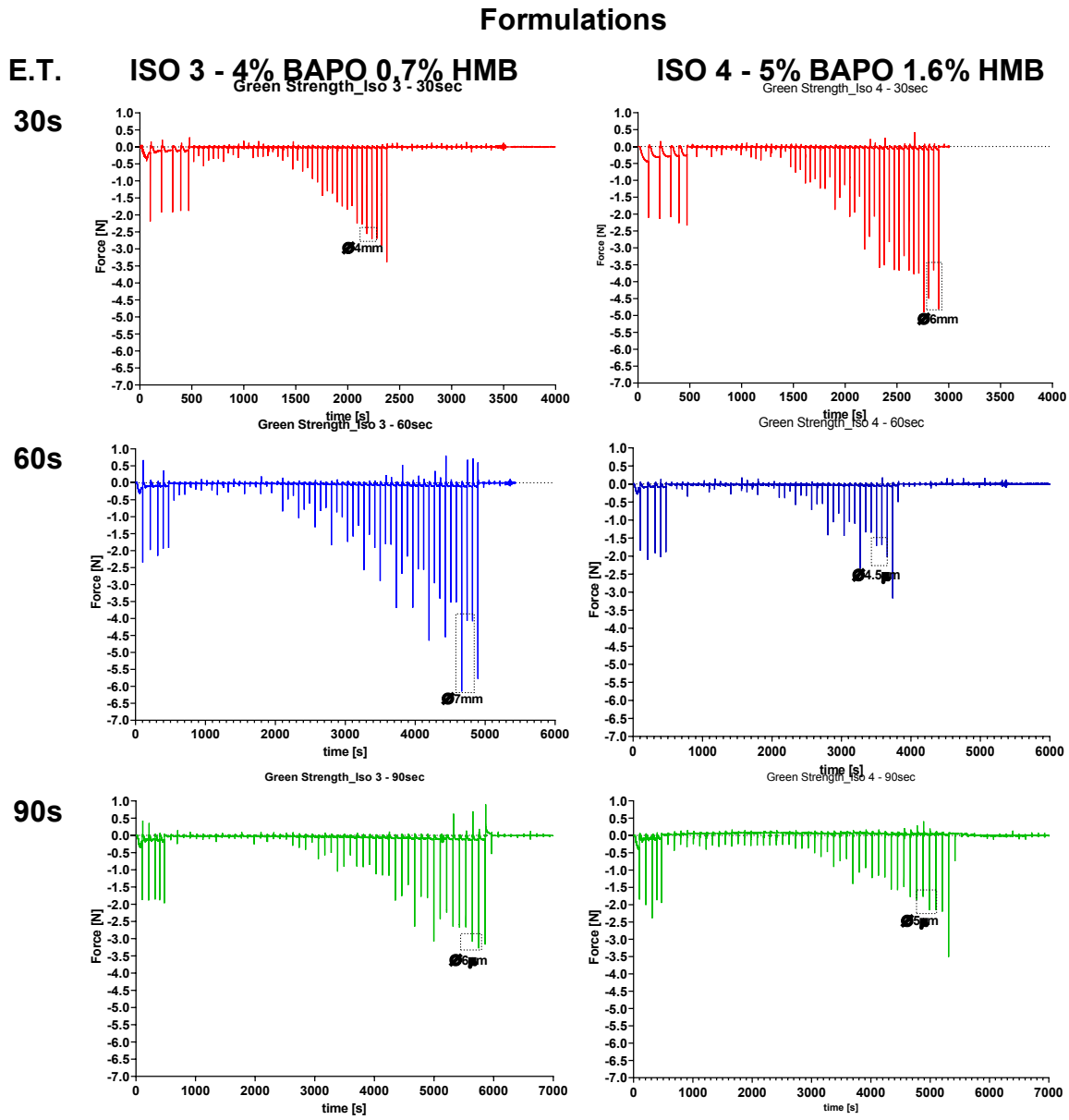


**Figure 4.4** Breaking load data collected during the cDLP printing of the tested resin formulations

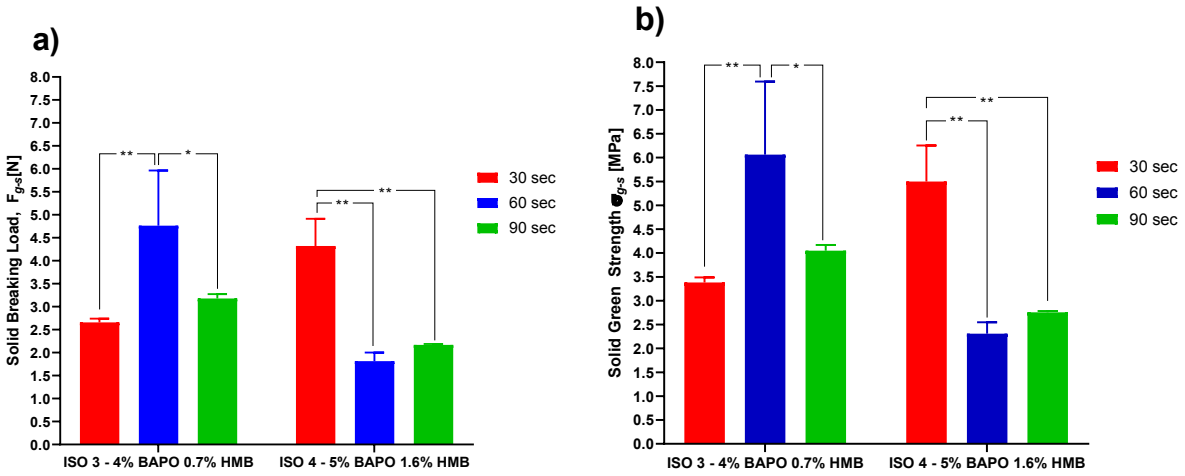


**Figure 4.5** Maximum load and stress of a solid cured part of isosorbide resin. (a) Breaking load, and (b) inter-layer green strength. (n=3) (** P ≤ 0.01, * P ≤ 0.05)

### 4.3.3 3D printability test

The Gyroid architecture will directly impact its physical properties. In the field of bone tissue engineering, it is well known that pore size and shape influence tissue regeneration while strut size dramatically affects mechanical strength and resorption kinetics. For porous structures, the influence of print geometry on separation force becomes more complicated, as the uncured resin must be removed from the pores after printing and constrained surface deformations are more complicated than when printing solid structures.

**Figure 4.6** shows the distribution of the separation force during the construction of the inverse tubular and 0°-gyroid scaffolds. It is challenging to print structures with a considerable variation between the printed layers. The distribution of the maximum stress produced by the local separation force on the minimum cross-sectional area of the porous scaffolds is shown in **Figure 4.5**.

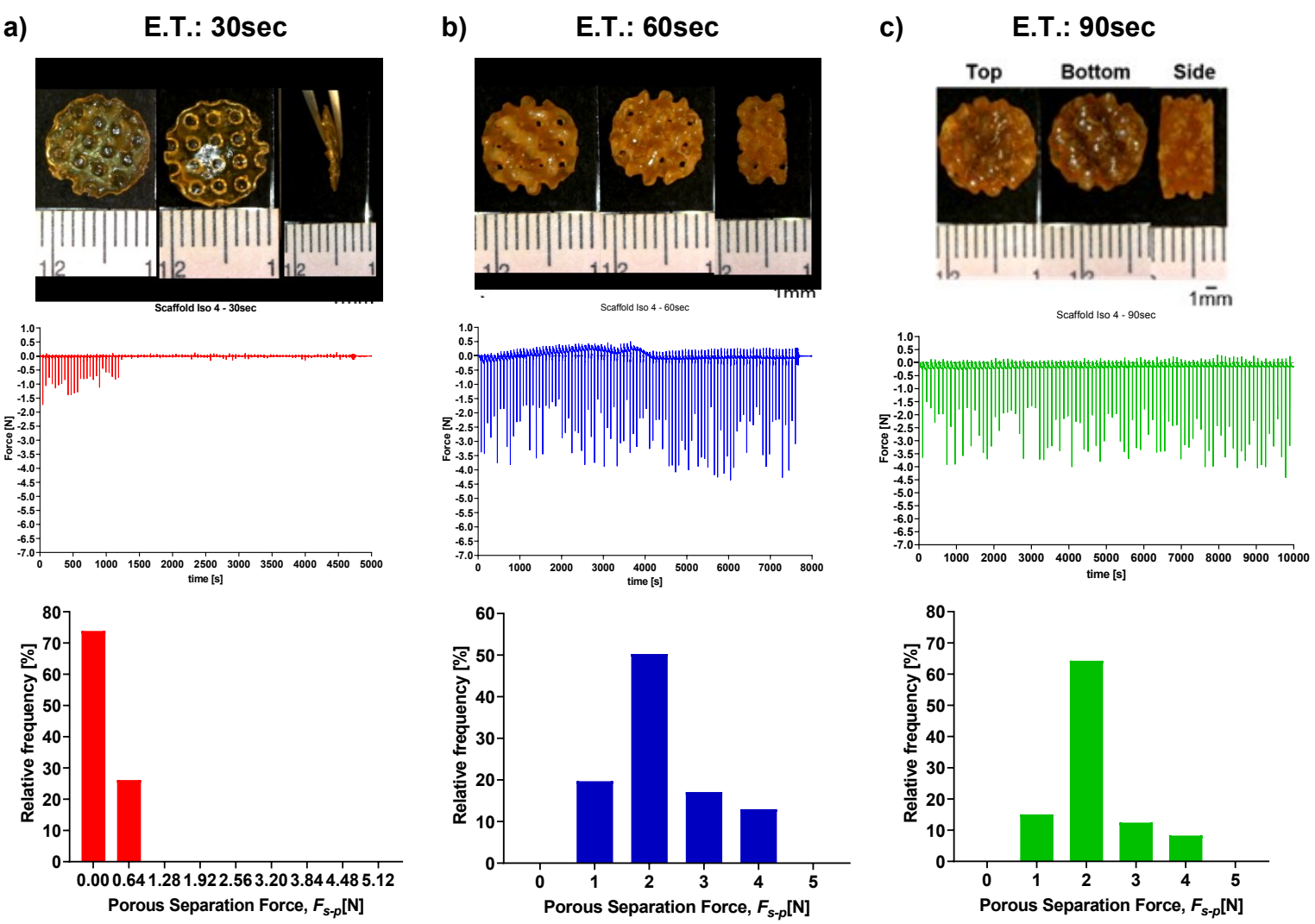


**Figure 4.6** 0°-gyroid porous scaffold printed with Isosorbide resin ISO 4 at different exposure times (30,60,90 sec). Porosity 44%, pore size 800 µm, and average strut size 1800 µm. Printed scaffolds are shown with their measured force during the printing process and the distribution of separation force

## 4.4 Discussion

This work is focused on the approach of reliability in the manufacturing of Isosorbide parts with cDLP, providing an initial point to get complicated or porous geometries are intended to be built. In terms of feasibility, this study was focused on the study of three variables: depth cure thickness, separation force and interlayer green strength related to the manufacturing process and material properties.

Previously, the influence of %HMB was identified as factor that affect the 3D printing of a complete structure [64]. First, resin formulation affects the cure depth **Figure 4.7**, as well as separation force and the interlayer green strength. Thus, working on the chemistry of the formulation and/or components is considered essential in order to reduce the inconsistency of the printing process.

**Figure 4.8** shows the variability pf the process. The model of maximum porous stress vs interlayer green strength distribution during the 3D printing of an inverted tubular scaffold (porosity 68%, pore size 700 µm, and maximum strut size 1400 µm) using PPF of 442 cP, 1600 Da with 45 s of exposure time.

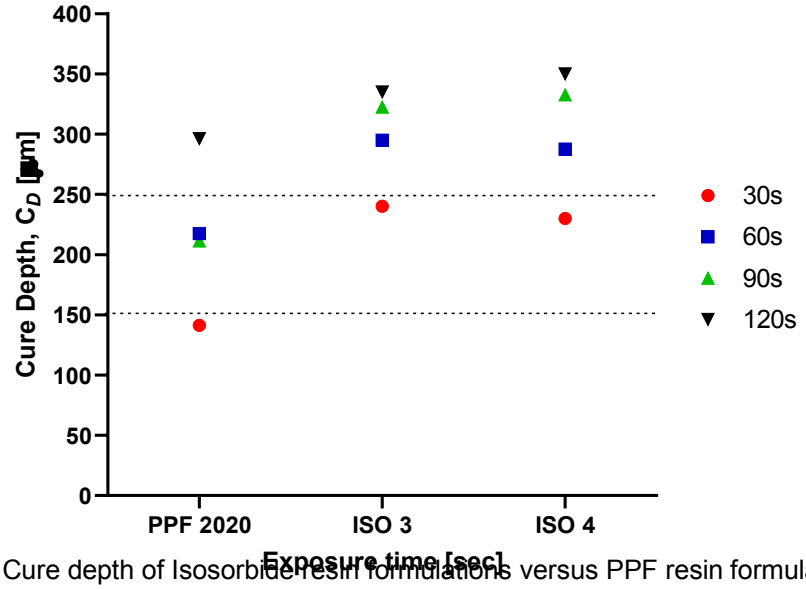


**Figure 4.7** Cure depth of Isosorbide resin formulations versus PPF resin formulation.

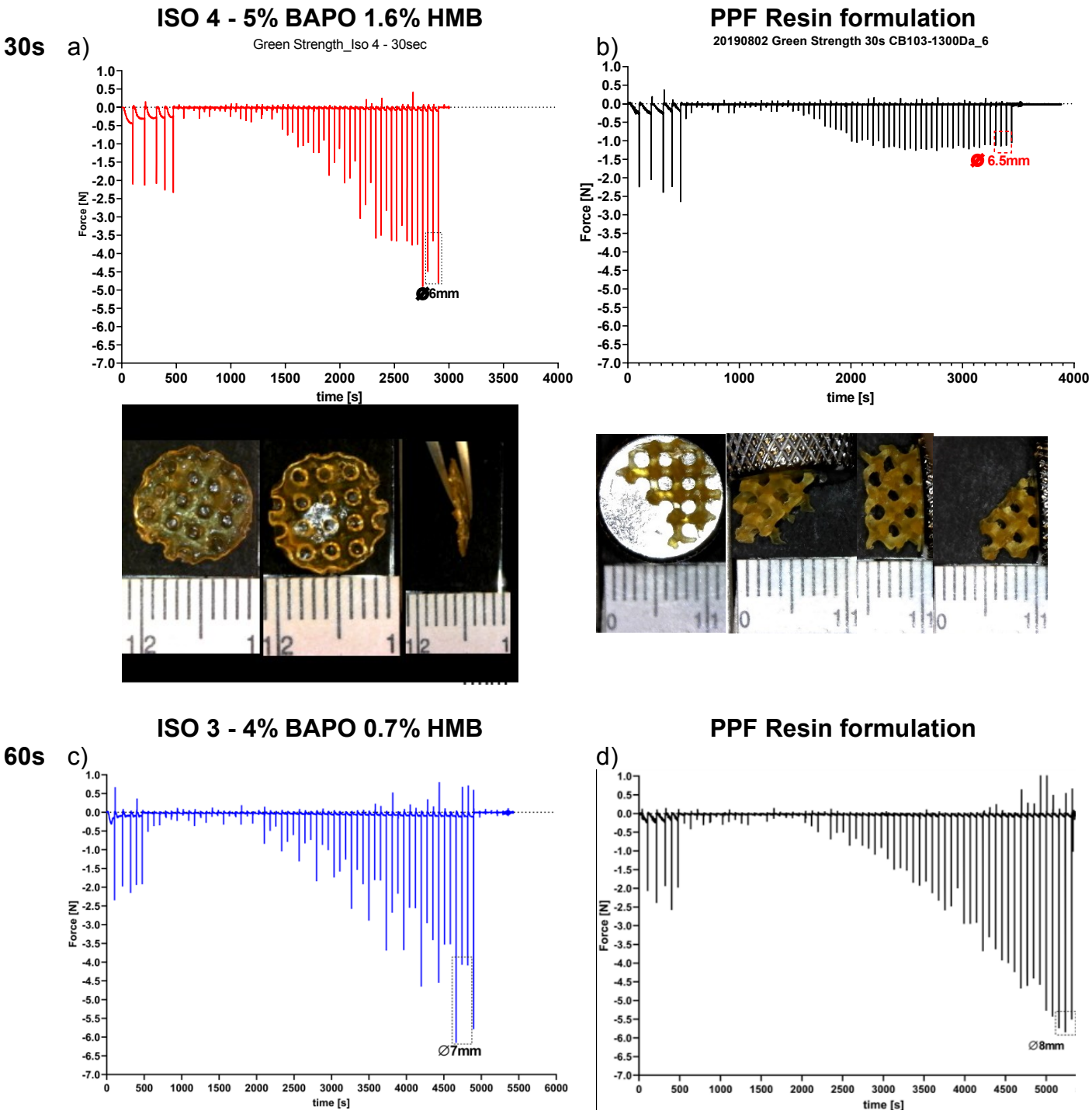


**Figure 4.8** Comparative of the Isosorbide resin formulations and PPF resin formulation already characterized. The picture shows the comparison among the resultant green strength of different Isosorbide formulations and PPF resin formulation that have been characterized before, showing a) the resultant green strength of ISO 4 and the gyroid structure that can be printed with this formulation, b) the resultant green strength of PPF resin and the gyroid structure that can be printed with this formulation. The same comparative among resultant separation force ISO 3 exhibits versus PPF resin formulation at the same exposure time.

## 4.5 Conclusions and future work

This chapter showed a method to characterize mechanical properties, cure depth thickness, separation force and inter-layer green strength of photo-curable resins made with Isosorbide. This work was focused on the feasibility of the additive manufacturing process with these formulations, based on experiments to study the influence of the % of photoattenuator on resin formulations, exposure time and geometry of the 3D printed structures. An in-line monitoring system to measure the separation force during printing was employed. Different formulations were tested to accomplish the protocol characterization analyzing the feasibility of the process.

Preliminary results show that the increase % of photoattenuator will lead to larger separation forces. Then a moderate increase of the exposure time, an Isosorbide resin formulation and a suitable printable design of the porous/solid part will be useful to improve the printability of the cDLP. Some future work includes developing a design for experiments of Isosorbide testing separation force and inter-layer green strength using resin formulations with different average molecular weight and different % of double bonds.

# Chapter 5 . Conclusions and future work

The present work focuses on the study of additive manufacturing processes for the development of scaffolds for grafting. This thesis shows the potential of additive manufacturing approaches.

In **Chapter 3**, a hybrid process combining FDM and electrospinning, bifurcated vascular grafts were fabricated. This study reported the significant influence of the internal electrical field collector design and the motion scheme. PCL was used to cover a 3D printed mandrel to produce a mat of microfibers using ESP. The influence of process parameters was evaluated. The cooling temperature was the primary factor that influences in the bonding of the different layers of the bimodal scaffold. The main contribution of this study focuses on the fabrication and characterization of bifurcated scaffolds to study how the morphology and microarchitecture affect final mechanical properties

The results of the cytotoxicity test demonstrate that electrospun scaffolds are suitable for future studies in BTE. The work presented here demonstrates that bifurcated vascular grafts can be constructed via electrospinning by combining an internal electrical field collector design and a 2-DOF positioning mechanism, for the mandrel. Several experiments showed the impact of the process parameters and material properties of the material studied.

The first refinement in positioning will be to better ensure orthogonality of the mandrel surface and polymer-exuding needle, followed by control of the rate of spinning. Once membrane apposition to the mandrel is improved, we will be able to study the effect of membrane biomaterials.

In the context of Y-grafts, we identified the following major functional specifications: a) corner profile fidelity, b) burst pressure strength, and c) suture retention strength. These functional specifications correlated to the basic properties of the electrospun fibers and their corresponding membranes, which were from the complete array of process parameters. The scope of this work was limited to successfully obtaining the basic requirements: appropriate morphology and suitable mechanical properties.

The work presented in **Chapter 4**, showed the application of a strategy to evaluate the printability of scaffolds made with Isosorbide using cDLP. The combination of different parameters and capability to manufacture at several scales open new possibilities in scaffold design for BTE applications. It was found that the influence of photo attenuator will lead to more significant printability of this new polymer. The use of Isosorbide resin with a high percentage of double bonds implies more reliable process. Then a moderate increase of the exposure time, an Isosorbide resin with high percentage of HMB, and a suitable printable design of the porous/solid part will be useful to increase the inter-layer green strength of printed parts, improving the reliability of cDLP. Future work includes developing a further study to analyze the interactions between the variables that affect the printability. These variables include viscosity, overall green strength prediction, permeability, exposure time, molecular weight, and resin components.

# References


1. Jammalamadaka, U.; Tappa, K. Recent Advances in Biomaterials for 3D Printing and Tissue Engineering. *Journal of Functional Biomaterials* 2018, *9*, 22.

2. Meyer, U. The History of Tissue Engineering and Regenerative Medicine in Perspective. In *Fundamentals of Tissue Engineering and Regenerative Medicine*; Meyer, U., Handschel, J., Wiesmann, H.P., Meyer, T., Eds.; Springer: Berlin, Heidelberg, 2009; pp. 5–12 ISBN 978-3-540-77755-7.

3. Velu, R.; Calais, T.; Jayakumar, A.; Raspall, F. A Comprehensive Review on Bio-Nanomaterials for Medical Implants and Feasibility Studies on Fabrication of Such Implants by Additive Manufacturing Technique. *Materials* 2020, *13*, 92.

4. Gomes, M.E.; Rodrigues, M.T.; Domingues, R.M.A.; Reis, R.L. Tissue Engineering and Regenerative Medicine: New Trends and Directions—A Year in Review. *Tissue Engineering Part B: Reviews* 2017, *23*, 211–224.

5. Meng, Z.; He, J.; Cai, Z.; Wang, F.; Zhang, J.; Wang, L.; Ling, R.; Li, D. Design and additive manufacturing of flexible polycaprolactone scaffolds with highly-tunable mechanical properties for soft tissue engineering. *Materials & Design* 2020, *189*, 108508.

6. Armentano, I.; Dottori, M.; Fortunati, E.; Mattioli, S.; Kenny, J.M. Biodegradable polymer matrix nanocomposites for tissue engineering: A review. *Polymer Degradation and Stability* 2010, *95*, 2126–2146.

7. Pashneh-Tala, S.; MacNeil, S.; Claeyssens, F. The Tissue-Engineered Vascular Graft—Past, Present, and Future. *Tissue Engineering Part B: Reviews* 2015, *22*, ten.teb.2015.0100.

8. Correa-Gallego, C.; Allen, P.J. Evolving Role of Drains, Tubes and Stents in Pancreatic Surgery. In *Optimizing Outcomes for Liver and Pancreas Surgery*; Rocha, F.G., Shen, P., Eds.; Springer International Publishing: Cham, 2018; pp. 153–169 ISBN 978-3-319-62624-6.

9. Onwuka, E.; King, N.; Heuer, E.; Breuer, C. The Heart and Great Vessels. *Cold Spring Harb Perspect Med* 2018, *8*.

10. Best, C.; Strouse, R.; Hor, K.; Pepper, V.; Tipton, A.; Kelly, J.; Shinoka, T.; Breuer, C. Toward a patient-specific tissue engineered vascular graft. *Journal of Tissue Engineering* 2018, *9*, 204173141876470.

11. Tejeda-Alejandre, R.; Lammel-Lindemann, J.A.; Lara-Padilla, H.; Dean, D.; Rodriguez, C.A. Influence of Electrical Field Collector Positioning and Motion Scheme on Electrospun Bifurcated Vascular Graft Membranes. *Materials* 2019, *12*, 2123.

12. Tejeda-Alejandre, R.; Lara-Padilla, H.; Mendoza-Buenrostro, C.; Rodriguez, C.A.; Dean, D. Electrospinning Complexly-shaped, Resorbable, Bifurcated Vascular Grafts. *Procedia CIRP* 2017, *65*, 207–212.

13. Cortizo, M.S.; Belluzo, M.S. Biodegradable Polymers for Bone Tissue Engineering.; 2017.

14. Lara-Padilla, H. Fabrication of porous scaffolds using additive manufacturing with potential applications in bone tissue engineering, Tecnologico de Monterrey: Monterrey, MEXICO, 2018.

15. Pedde, R.D.; Mirani, B.; Navaei, A.; Styan, T.; Wong, S.; Mehrali, M.; Thakur, A.; Mohtaram, N.K.; Bayati, A.; Dolatshahi-Pirouz, A.; et al. Emerging Biofabrication Strategies for Engineering Complex Tissue Constructs. *Advanced Materials* 2017, *29*, 1606061.

16. Ravichandran, R.; Sundarrajan, S.; Venugopal, J.R.; Mukherjee, S.; Ramakrishna, S. Advances in polymeric systems for tissue engineering and biomedical applications. *Macromol Biosci* 2012, *12*, 286–311.

17. Wang, C.; Wang, J.; Zeng, L.; Qiao, Z.; Liu, X.; Liu, H.; Zhang, J.; Ding, J. Fabrication of Electrospun Polymer Nanofibers with Diverse Morphologies. *Molecules* 2019, *24*.

18. Bourget, J.M.; Laterreur, V.; Guillemette, M.; Gauvin, R.; Miville-Godin, C.; Mounier, M.; Ruel, J.; Auger, F.A.; Veres, T.; Germain, L. Recent advances in the development of tissue-engineered vascular media made by self-assembly. *Procedia Engineering* 2013, *59*, 201–205.

19. Wubneh, A.; Tsekoura, E.K.; Ayranci, C.; Uludağ, H. Current state of fabrication technologies and materials for bone tissue engineering. *Acta Biomaterialia* 2018, *80*, 1–30.

20. Drews, J.D.; Miyachi, H.; Shinoka, T. Tissue-engineered vascular grafts for congenital cardiac disease: Clinical experience and current status. *Trends Cardiovasc Med* 2017, *27*, 521–531.

21. Ma, H.; Hu, J.; Ma, P.X. Polymer Scaffolds for Small-Diameter Vascular Tissue Engineering. *Advanced Functional Materials* 2010, *20*, 2833–2841.

22. Saunders, R.; Ramesh, J.; Cicconi, S.; Evans, J.; Yip, V.S.; Raraty, M.; Ghaneh, P.; Sutton, R.; Neoptolemos, J.P.; Halloran, C. A systematic review and meta-analysis of metal versus plastic stents for drainage of pancreatic fluid collections: metal stents are advantageous. *Surg Endosc* 2018.

23. Wu, J.; Hu, C.; Tang, Z.; Yu, Q.; Liu, X.; Chen, H. Tissue-engineered Vascular Grafts: Balance of the Four Major Requirements. *Colloids and Interface Science Communications* 2018, *23*, 34–44.

24. Ong, C.S.; Zhou, X.; Huang, C.Y.; Fukunishi, T.; Zhang, H.; Hibino, N. Tissue engineered vascular grafts: current state of the field. *Expert Review of Medical Devices* 2017, *14*, 383–392.

25. Pham, Q.P.; Sharma, U.; Mikos, A.G. Electrospinning of polymeric nanofibers for tissue engineering applications: a review. *Tissue engineering* 2006, *12*, 1197–211.

26. Baji, A.; Mai, Y.-W.; Wong, S.-C.; Abtahi, M.; Chen, P. Electrospinning of polymer nanofibers: Effects on oriented morphology, structures and tensile properties. *Composites Science and Technology* 2010, *70*, 703–718.

27. Łos, M.J.; Panigrahi, S.; Sielatycka, K.; Grillon, C. Successful Biomaterial-Based Artificial Organ—Updates on Artificial Blood Vessels. In *Stem Cells and Biomaterials for Regenerative Medicine*; Elsevier, 2019; pp. 203–222 ISBN 978-0-12-812258-7.

28. Leach, M.K.; Feng, Z.-Q.; Tuck, S.J.; Corey, J.M. Electrospinning Fundamentals: Optimizing Solution and Apparatus Parameters. *J Vis Exp* 2011.

29. Haider, A.; Haider, S.; Kang, I. A comprehensive review summarizing the effect of electrospinning parameters and potential applications of nanofibers in biomedical and biotechnology. *ARABIAN JOURNAL OF CHEMISTRY* 2015.

30. Mo, X.; Sun, B.; Wu, T.; Li, D. Electrospun Nanofibers for Tissue Engineering. In *Electrospinning: Nanofabrication and Applications*; Elsevier, 2019; pp. 719–734 ISBN 978-0-323-51270-1.

31. Buxton, B.F.; Wukasch, D.C.; Martin, C.; Liebig, W.J.; Hallman, G.L.; Cooley, D.A. Practical considerations in fabric vascular grafts introduction of a new bifurcated graft. *The American Journal of Surgery* 1973, *125*, 288–293.

32. Kohler, C.; Attigah, N.; Demirel, S.; Zientara, A.; Weber, M.; Schwegler, I. A technique for a self-made bifurcated graft with bovine pericardial patch in infectious vascular reconstruction. *Journal of Vascular Surgery Cases and Innovative Techniques* 2016, *2*, 158–160.

33. Siallagan, D.; Loke, Y.-H.; Olivieri, L.; Opfermann, J.; Ong, C.S.; de Zélicourt, D.; Petrou, A.; Daners, M.S.; Kurtcuoglu, V.; Meboldt, M.; et al. Virtual surgical planning, flow simulation, and 3-dimensional electrospinning of patient-specific grafts to optimize Fontan hemodynamics. *The Journal of Thoracic and Cardiovascular Surgery* 2018, *155*, 1734–1742.

34. Fukunishi, T.; Best, C.A.; Sugiura, T.; Shoji, T.; Yi, T.; Udelsman, B.; Ohst, D.; Ong, C.S.; Zhang, H.; Shinoka, T.; et al. Tissue-engineered small diameter arterial vascular grafts from cell-free nanofiber PCL/chitosan scaffolds in a sheep model. *PLoS ONE* 2016, *11*, 1–15.

35. Ebersole, G.C.; Buettmann, E.G.; MacEwan, M.R.; Tang, M.E.; Frisella, M.M.; Matthews, B.D.; Deeken, C.R. Development of novel electrospun absorbable polycaprolactone (PCL) scaffolds for hernia repair applications. *Surgical Endoscopy and Other Interventional Techniques* 2012, *26*, 2717–2728.

36. Abdal-hay, A.; Bartnikowski, M.; Hamlet, S.; Ivanovski, S. Electrospun biphasic tubular scaffold with enhanced mechanical properties for vascular tissue engineering. *Materials Science and Engineering C* 2018, *82*, 10–18.

37. Ye, L.; Wu, X.; Mu, Q.; Chen, B.; Duan, Y.; Geng, X.; Gu, Y.; Zhang, A.; Zhang, J.; Feng, Z. Heparin-Conjugated PCL Scaffolds Fabricated by Electrospinning and Loaded with Fibroblast Growth Factor 2. *Journal of Biomaterials Science, Polymer Edition* 2011, *22*, 389–406.

38. Wu, H.; Fan, J.; Chu, C.C.; Wu, J. Electrospinning of small diameter 3-D nanofibrous tubular scaffolds with controllable nanofiber orientations for vascular grafts. *Journal of Materials Science: Materials in Medicine* 2010, *21*, 3207–3215.

39. Vaz, C.M.; Tuijl, S.V.; Bouten, C.V.C.; Baaijens, F.P.T. Design of scaffolds for blood vessel tissue engineering using a multi-layering electrospinning technique. *Acta Biomaterialia* 2005, *1*, 575–582.

40. Jin, S.; Liu, J.; Heang, S.; Soker, S.; Atala, A.; Yoo, J.J. Development of a composite vascular scaffolding system that withstands physiological vascular conditions. *Biomaterials* 2008, *29*, 2891–2898.

41. Kim, S.; King, M.W. The Mechanical Performance of Weft- knitted / Electrospun Bilayer Small Diameter Vascular Prostheses. *Journal of the Mechanical Behavior of Biomedical Materials* 2016, *61*, 410–418.

42. Tejeda-Alejandre, R.; Lara-Padilla, H.; Rodriguez, C.A.; Dean, D. Three dimensional printing modality combining fused deposition modeling and electrospinning 2018.

43. Vaezi, M.; Seitz, H.; Yang, S. A review on 3D micro-additive manufacturing technologies. *The International Journal of Advanced Manufacturing Technology* 2013, *67*, 1721–1754.

44. Cipitria, A.; Skelton, A.; Dargaville, T.R.; Dalton, P.D.; Hutmacher, D.W. Design, fabrication and characterization of PCL electrospun scaffolds—a review. *Journal of Materials Chemistry* 2011, *21*, 9419.

45. Pensalfini, M.; Meneghello, S.; Lintas, V.; Bircher, K.; Ehret, A.E.; Mazza, E. The suture retention test, revisited and revised. *Journal of the Mechanical Behavior of Biomedical Materials* 2018, *77*, 711–717.

46. Drilling, S.; Gaumer, J.; Lannutti, J. Fabrication of burst pressure competent vascular grafts via electrospinning: Effects of microstructure. *Journal of Biomedical Materials Research - Part A* 2008, *88*, 923–934.

47. Billiar, K.; Murray, J.; Laude, D.; Abraham, G.; Bachrach, N. Effects of carbodiimide crosslinking conditions on the physical properties of laminated intestinal submucosa. *Journal of Biomedical Materials Research* 2001, *56*, 101–108.

48. Mangiavillano, B.; Pagano, N.; Baron, T.H.; Arena, M.; Iabichino, G.; Consolo, P.; Opocher, E.; Luigiano, C. Biliary and pancreatic stenting: Devices and insertion techniques in therapeutic endoscopic retrograde cholangiopancreatography and endoscopic ultrasonography. *World J Gastrointest Endosc* 2016, *8*, 143–156.

49. Yalcin, I.; Horakova, J.; Mikes, P.; Sadikoglu, T.G.; Domin, R.; Lukas, D. Design of Polycaprolactone Vascular Grafts. *Journal of Industrial Textiles* 2016, *45*, 813–833.

50. Radakovic, D.; Reboredo, J.; Helm, M.; Weigel, T.; Schürlein, S.; Kupczyk, E.; Leyh, R.G.; Walles, H.; Hansmann, J. A multilayered electrospun graft as vascular access for hemodialysis. *PLoS ONE* 2017, *12*, 1–22.

51. Roseti, L.; Parisi, V.; Petretta, M.; Cavallo, C.; Desando, G.; Bartolotti, I.; Grigolo, B. Scaffolds for Bone Tissue Engineering: State of the art and new perspectives. *Materials Science and Engineering: C* 2017, *78*, 1246–1262.

52. Rodriguez, C.A.; Lara-Padilla, H.; Dean, D. Bioceramics for Musculoskeletal Regenerative Medicine: Materials and Manufacturing Process Compatibility for Synthetic Bone Grafts and Medical Devices. In *3D Printing and Biofabrication*; Ovsianikov, A., Yoo, J., Mironov, V., Eds.; Springer International Publishing: Cham, 2018; pp. 161–193 ISBN 978-3-319-45443-6.

53. Chartrain, N.A.; Vratsanos, M.; Han, D.T.; Sirrine, J.M.; Pekkanen, A.; Long, T.E.; Whittington, A.R.; Williams, C.B. Microstereolithography of Tissue Scaffolds Using a Biodegradable Photocurable Polyester.; 2016; p. 17.

54. Thavornyutikarn, B.; Chantarapanich, N.; Sitthiseripratip, K.; Thouas, G.A.; Chen, Q. Bone tissue engineering scaffolding: computer-aided scaffolding techniques. *Prog Biomater* 2014, *3*, 61–102.

55. Wallace, J.; Wang, M.O.; Thompson, P.; Busso, M.; Belle, V.; Mammoser, N.; Kim, K.; Fisher, J.P.; Siblani, A.; Xu, Y.; et al. Validating continuous digital light processing (cDLP) additive manufacturing accuracy and tissue engineering utility of a dye-initiator package. *Biofabrication* 2014, *6*, 015003.

56. Dean, D.; Wallace, J.; Siblani, A.; Wang, M.O.; Kim, K.; Mikos, A.G.; Fisher, J.P. Continuous Digital Light Processing (cDLP): Highly Accurate Additive Manufacturing of Tissue Engineered Bone Scaffolds. *Virtual Phys Prototyp* 2012, *7*, 13–24.

57. Russmueller, G.; Liska, R.; Stampfl, J.; Heller, C.; Mautner, A.; Macfelda, K.; Kapeller, B.; Lieber, R.; Haider, A.; Mika, K.; et al. 3D Printable Biophotopolymers for in Vivo Bone Regeneration. *Materials* 2015, *8*, 3685–3700.

58. Castro, N.J.; O'Brien, J.; Zhang, L.G. Integrating biologically inspired nanomaterials and table-top stereolithography for 3D printed biomimetic osteochondral scaffolds. *Nanoscale* 2015, *7*, 14010–14022.

59. Shie, M.-Y.; Chang, W.-C.; Wei, L.-J.; Huang, Y.-H.; Chen, C.-H.; Shih, C.-T.; Chen, Y.-W.; Shen, Y.-F. 3D Printing of Cytocompatible Water-Based Light-Cured Polyurethane with Hyaluronic Acid for Cartilage Tissue Engineering Applications. *Materials (Basel)* 2017, *10*.

60. Seol, Y.-J.; Park, D.Y.; Park, J.Y.; Kim, S.W.; Park, S.J.; Cho, D.-W. A new method of fabricating robust freeform 3D ceramic scaffolds for bone tissue regeneration. *Biotechnology and Bioengineering* 2013, *110*, 1444–1455.

61. Lee, S.-J.; Kang, H.-W.; Park, J.K.; Rhie, J.-W.; Hahn, S.K.; Cho, D.-W. Application of microstereolithography in the development of three-dimensional cartilage regeneration scaffolds. *Biomed Microdevices* 2008, *10*, 233–241.

62. Lee, J.W.; Lan, P.X.; Kim, B.; Lim, G.; Cho, D.-W. 3D scaffold fabrication with PPF/DEF using micro-stereolithography. *Microelectronic Engineering* 2007, *84*, 1702–1705.

63. Xing, J.-F.; Zheng, M.-L.; Duan, X.-M. Two-photon polymerization microfabrication of hydrogels: an advanced 3D printing technology for tissue engineering and drug delivery. *Chem. Soc. Rev.* 2015, *44*, 5031–5039.

64. Lammel-Lindemann, J.; Dourado, I.A.; Shanklin, J.; Rodriguez, C.A.; Catalani, L.H.; Dean, D. Photocrosslinking-based 3D printing of unsaturated polyesters from isosorbide: A new material for resorbable medical devices. *Bioprinting* 2019, e00062.

# Appendix 1. Design of two degree of freedom positioning mechanism

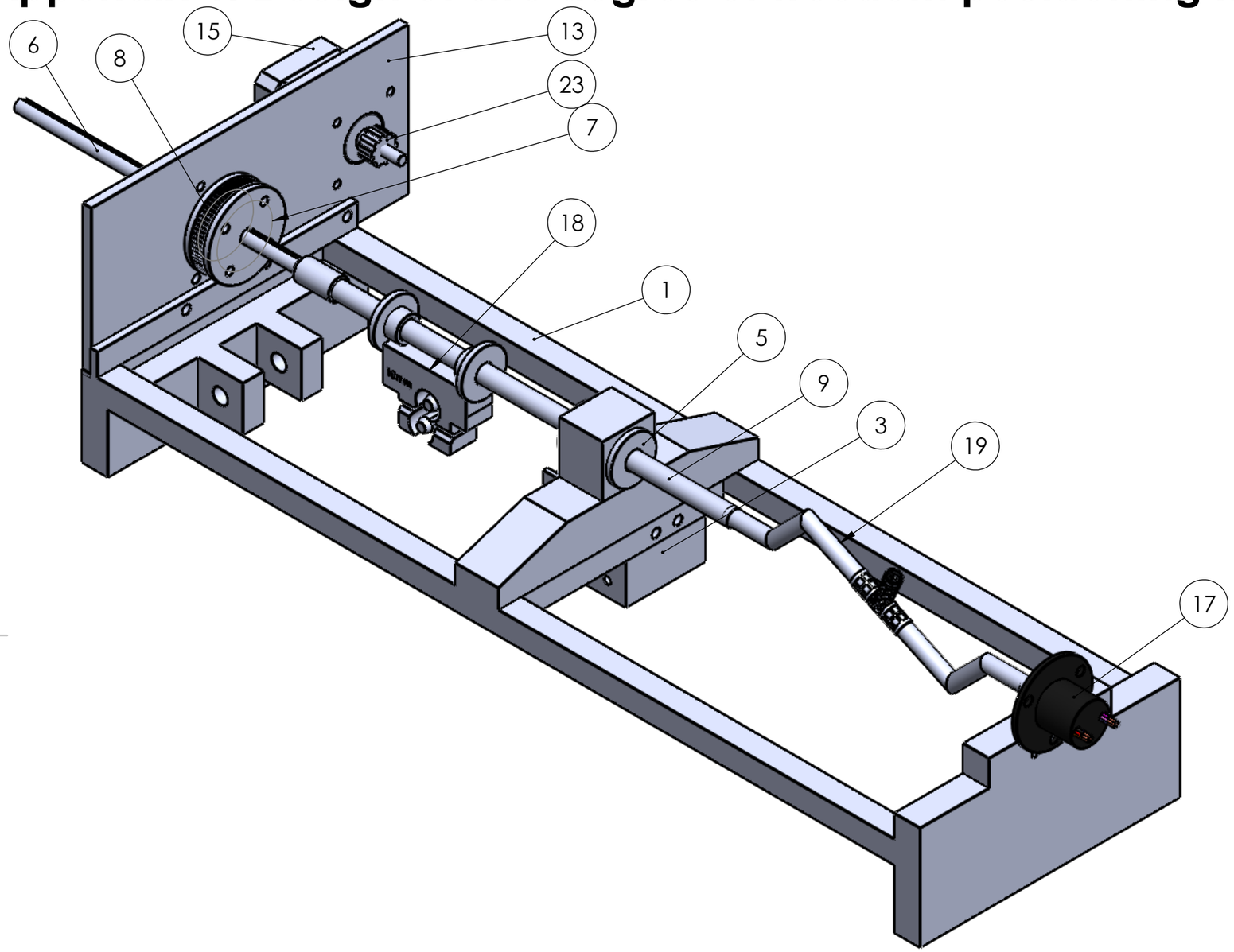


| N.º DE ELEMENTO | N.º DE PIEZA | CANTIDAD |
|---|---|---|
| 1 | Bed | 1 |
| 2 | Axis_support_1 | 1 |
| 3 | soporte_modif_v4_231017 | 1 |
| 4 | bushing | 1 |
| 5 | bushing2 | 1 |
| 6 | shaft_v2 | 2 |
| 7 | tapa1_impresion_v2 | 4 |
| 8 | pulley | 2 |
| 9 | shaft_axial | 2 |
| 10 | bushing3 | 1 |
| 11 | soporte_pulley_v5_2 | 1 |
| 12 | bushing4 | 1 |
| 13 | Axis_support_2_nema17_191017 | 1 |
| 14 | MotorMount_NEMA | 1 |
| 15 | Motor_NEMA | 1 |
| 16 | Motor_NEMA_2 | 1 |
| 17 | slip ring | 1 |
| 18 | y belt holder_201017_10mm | 1 |
| 19 | Flexible | 1 |
| 20 | bifurcated mandrel_arm1_291118 | 1 |
| 21 | bifurcated mandrel_arm2_291118 | 1 |
| 22 | bifurcated mandrel_center_291118 | 1 |
| 23 | Chain_pinion | 1 |
| 24 | Chain_pinion2 | 1 |
| 25 | Fiber | 1 |

| | | | | | | | |
|---|---|---|---|---|---|---|---|
| SI NO SE INDICA LO CONTRARIO: LAS COTAS SE EXPRESAN EN MM ACABADO SUPERFICIAL: TOLERANCIAS: LINEAL: ANGULAR: | ACABADO: | | REBARBAR Y ROMPER ARISTAS VIVAS | NO CAMBIE LA ESCALA | REVISIÓN | | |
| | NOMBRE | FIRMA | FECHA | | | | TÍTULO: |
| DIBUJ. | | | | | | | |
| VERIF. | | | | | | | |
| APROB. | | | | | | | |
| FABR. | | | | | | | |
| CALID. | | | | MATERIAL: | | | N.º DE DIBUJO |
| | | | | | | | mecanismo_2020-02-20_ |
| | | | | PESO: | | ESCALA:1:5 | HOJA 1 DE 1 |

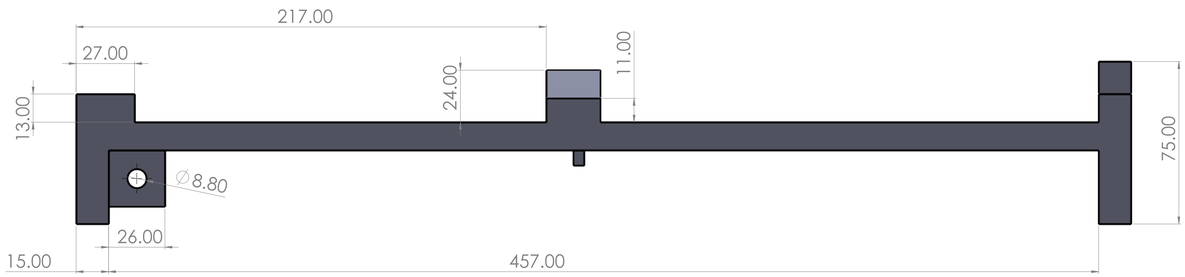


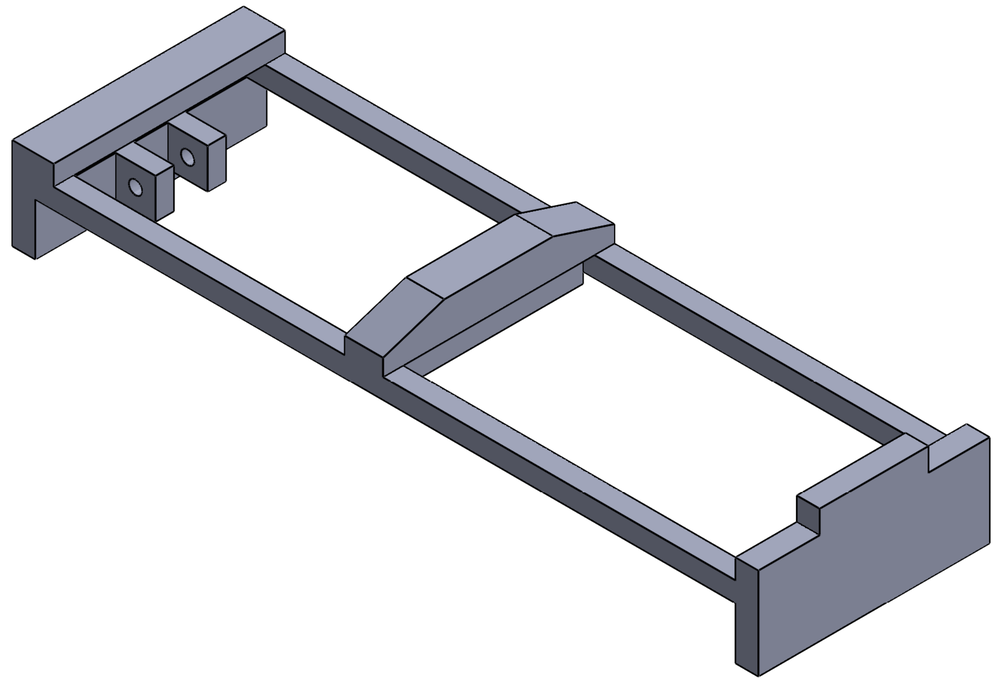

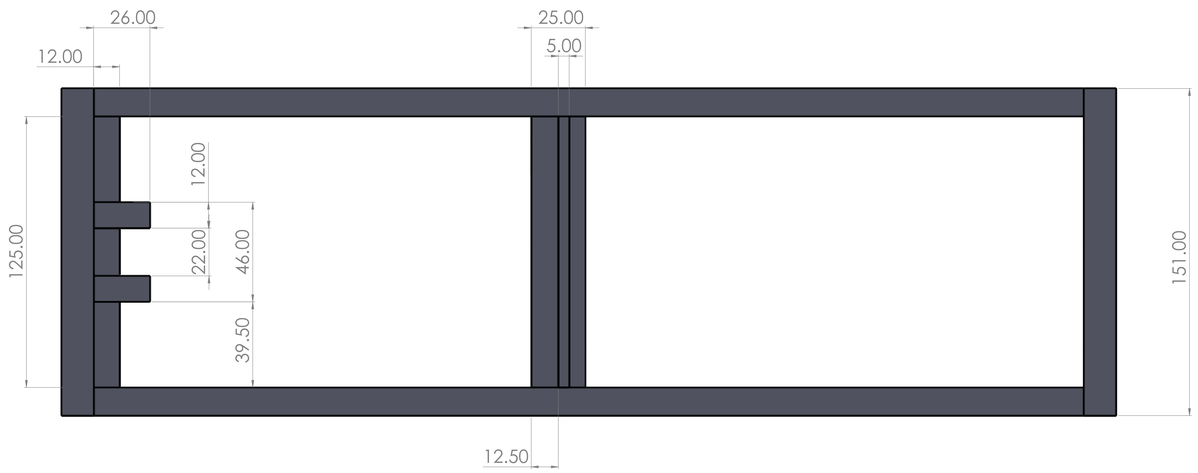


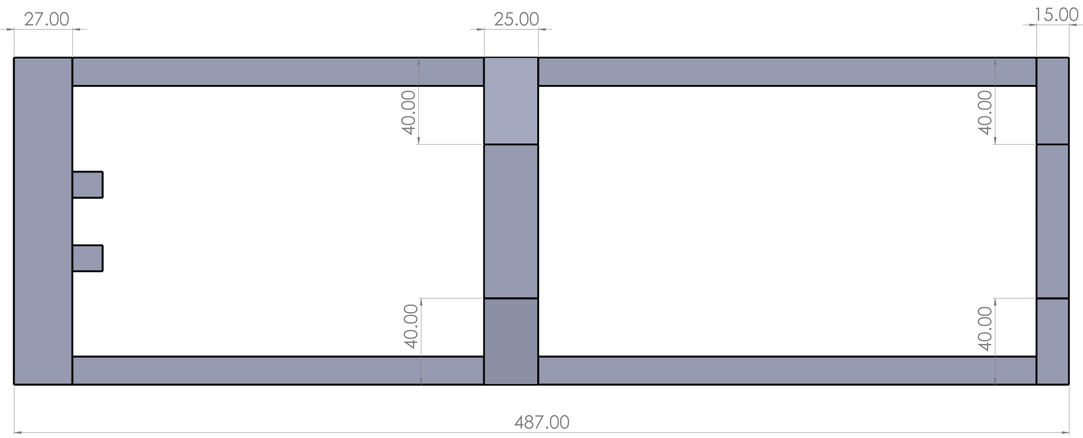


| | | | | | |
|---|---|---|---|---|---|
| SI NO SE INDICA LO CONTRARIO: LAS COTAS SE EXPRESAN EN MM. TOLERANCIA DIMENSIONAL: ESTÁNDAR DE LA INDUSTRIA. LINEAL: ANGULAR: | ACABADO: | REBARBAR Y ROMPER ARISTAS VIVAS. | NO CAMBIE LA ESCALA | REVISIÓN | |
| | NOMBRE | FIRMA | FECHA | TÍTULO: | |
| DIBUJ. | | | | | |
| VERIF. | | | | | |
| APROB. | | | | | |
| PABR. | | | | | |
| CALID. | | MATERIAL: | | Nº DE DIBUJO: Bed | A0 |
| | | PESO: | | ESCALA:1:1 | HOJA 1 DE 1 |

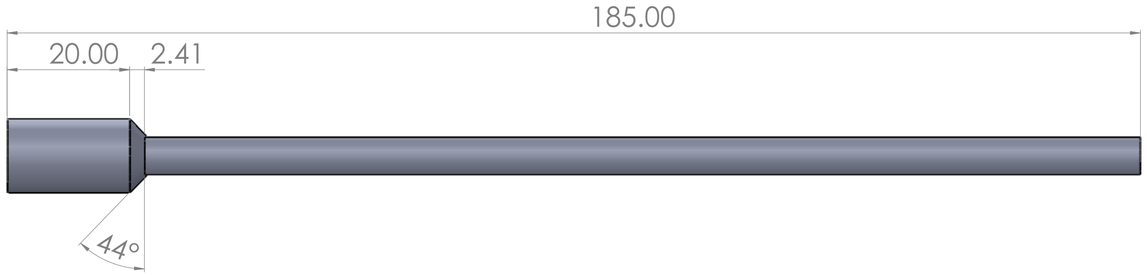


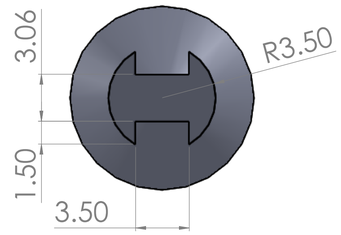


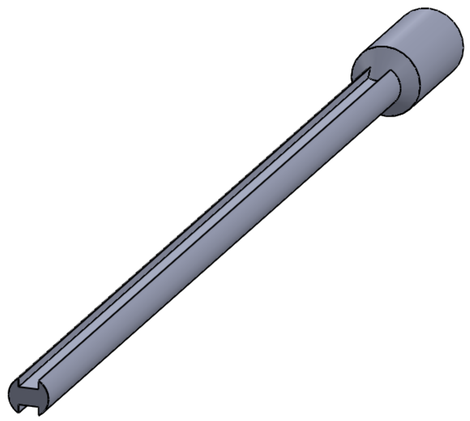

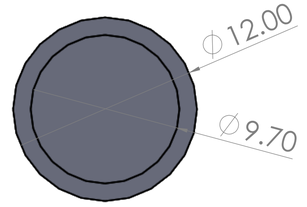


| | | | | | | | |
|---|---|---|---|---|---|---|---|
| SI NO SE INDICA LO CONTRARIO: LAS COTAS SE EXPRESAN EN MM. ACABADO SUPERFICIAL: TOLERANCIAS: LINEAL: ANGULAR: | ACABADO: | | REBARBAR Y ROMPER ARISTAS VIVAS | | NO CAMBIE LA ESCALA | REVISIÓN | |
| | NOMBRE | FIRMA | FECHA | | | TÍTULO: | |
| DIBUJ. | | | | | | | |
| VERIF. | | | | | | | |
| APROB. | | | | | | | |
| FABR. | | | | | | | |
| CALID. | | | | MATERIAL: | | N.º DE DIBUJO | A1 |
| | | | | | | shaft_v2 | |
| | | | | PESO: | | ESCALA:1:2 | HOJA 1 DE 1 |

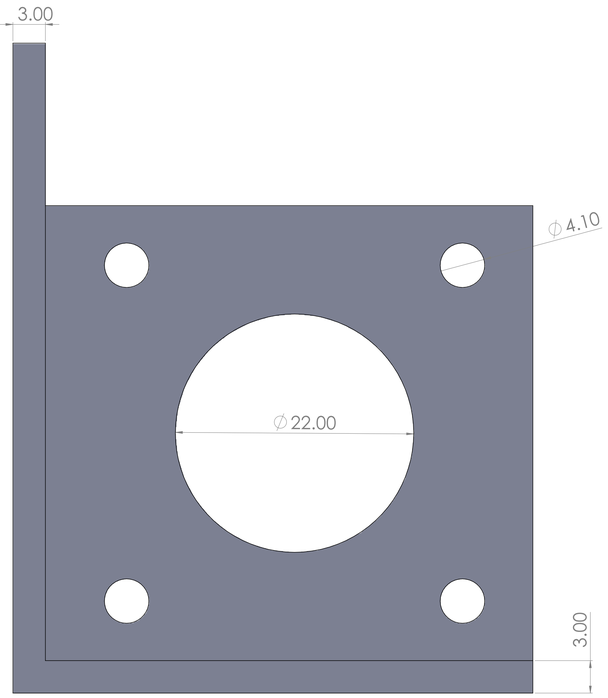


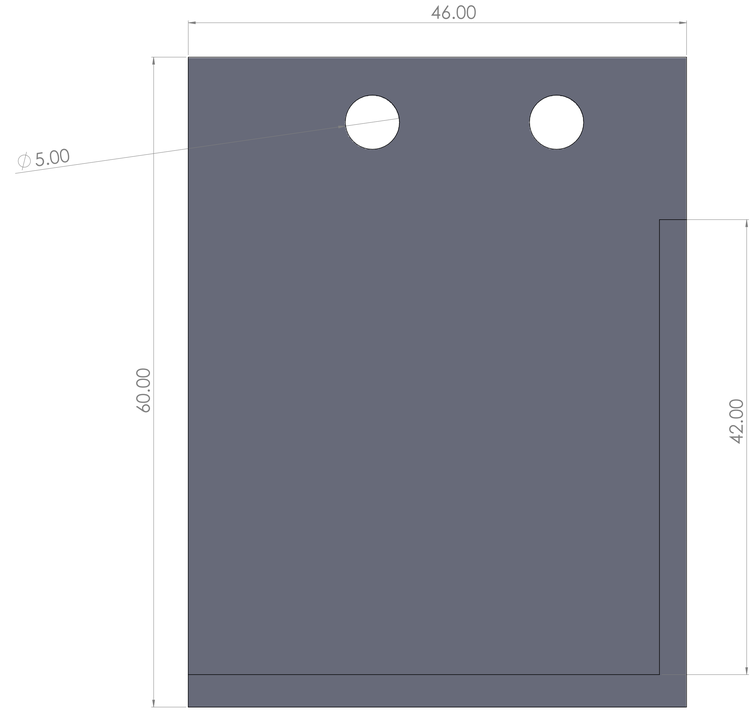



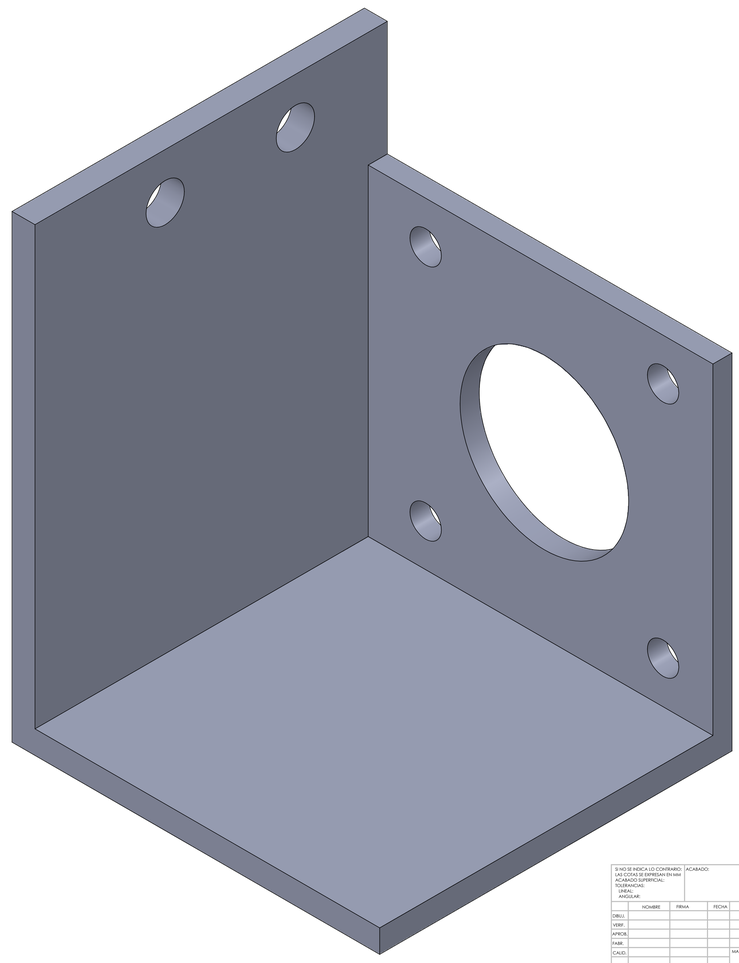

| | | | | | | | |
|---|---|---|---|---|---|---|---|
| SI NO SE INDICA LO CONTRARIO, LAS COTAS SE EXPRESAN EN MM | ACABADO: | | | REBARBAR Y ROMPER ARISTAS VIVAS | NO CAMBIE LA ESCALA | | REVISIÓN |
| ACABADO SUPERFICIAL: | | | | | | | |
| TOLERANCIAS: | | | | | | | |
| LINEAL: | | | | | | | |
| ANGULAR: | | | | | | | |
| | NOMBRE | FIRMA | FECHA | | | TÍTULO: | |
| DIBUJ. | | | | | | | |
| VERIF. | | | | | | | |
| APROB. | | | | | | | |
| FABR. | | | | | | | |
| CALID. | | | | | | | |
| | | | | MATERIAL: | | Nº DE DIBUJO | |
| | | | | PESO: | | ESCALA 2:1 | HOJA 1 DE 1 |

soporte_modif_v4_231017

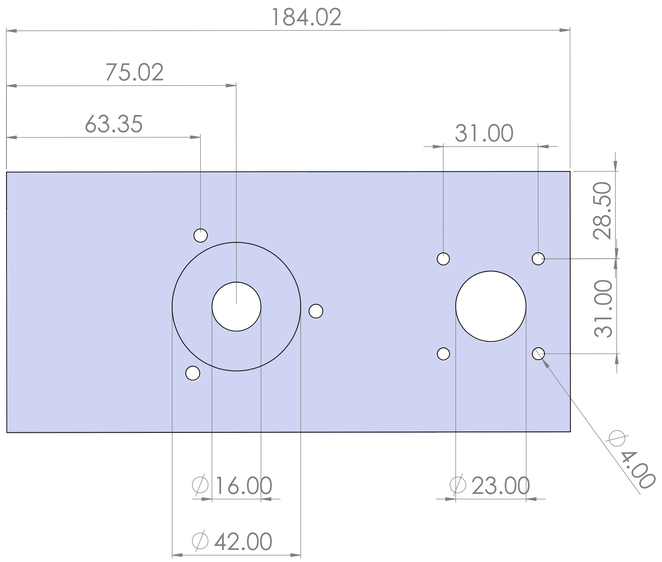


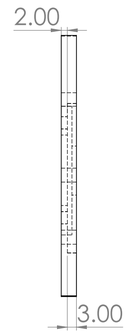


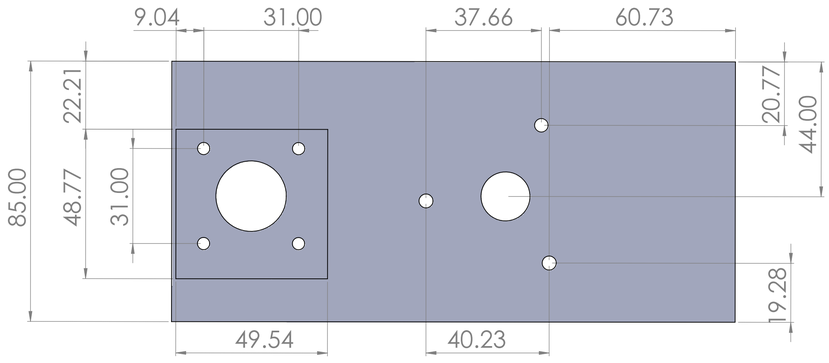


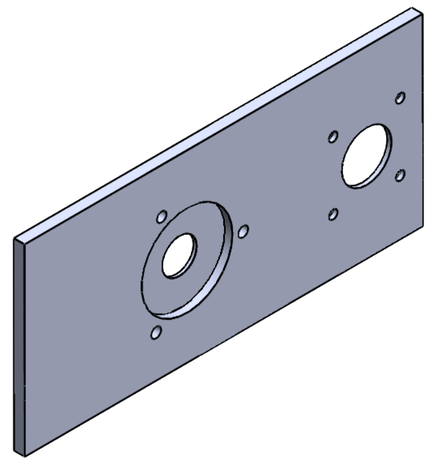

| | | | | | | |
|---|---|---|---|---|---|---|
| SI NO SE INDICA LO CONTRARIO: LAS COTAS SE EXPRESAN EN MM. ACABADO SUPERFICIAL: TOLERANCIAS: LINEAL: ANGULAR: | ACABADO: | | REBARBAR Y ROMPER ARISTAS VIVAS | NO CAMBIE LA ESCALA | REVISIÓN | |
| | NOMBRE | FIRMA | FECHA | TÍTULO: | | |
| DIBUJ. | | | | | | |
| VERIF. | | | | | | |
| APROB. | | | | | | |
| FABR. | | | | | | |
| CALID. | | | | MATERIAL: | N.º DE DIBUJO | A1 |
| | | | | PESO: | ESCALA:1:1 | HOJA 1 DE 1 |

soporte_mov-rotacional

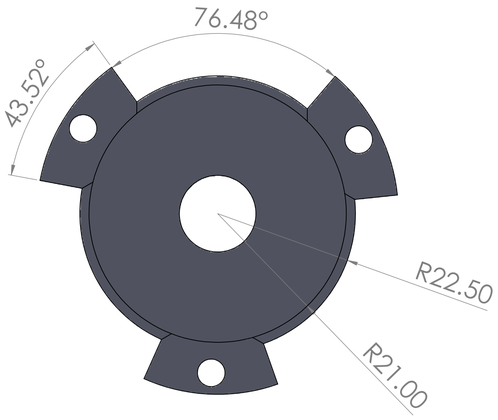


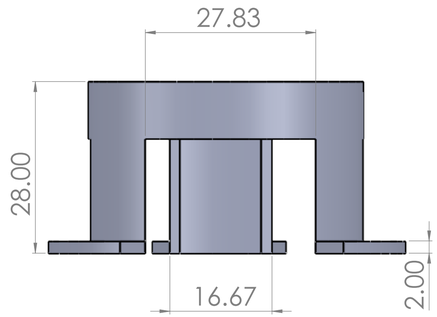


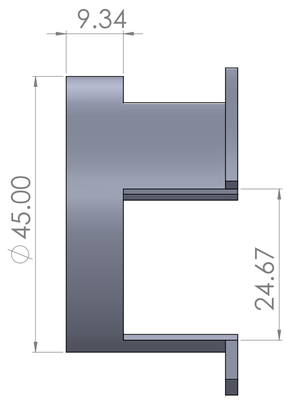


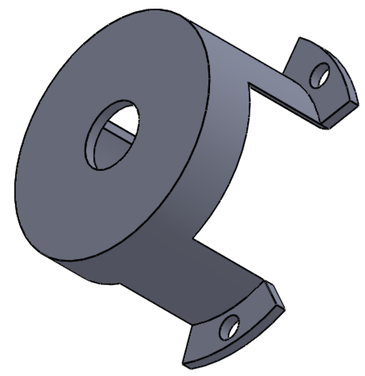

| | | | | | | | |
|---|---|---|---|---|---|---|---|
| SI NO SE INDICA LO CONTRARIO: LAS COTAS SE EXPRESAN EN MM. ACABADO SUPERFICIAL: TOLERANCIAS: LINEAL: ANGULAR: | | ACABADO: | | REBARBAR Y ROMPER ARISTAS VIVAS | | NO CAMBIE LA ESCALA | REVISIÓN |
| | NOMBRE | FIRMA | FECHA | | | TÍTULO: | |
| DIBUJ. | | | | | | | |
| VERIF. | | | | | | | |
| APROB. | | | | | | | |
| FABR. | | | | | | | |
| CALID. | | | | | | | |
| | | | | MATERIAL: | | N.º DE DIBUJO | |
| | | | | | | soporte_pulley_v5_2 | |
| | | | | PESO: | | ESCALA:2:1 | HOJA 1 DE 1 |

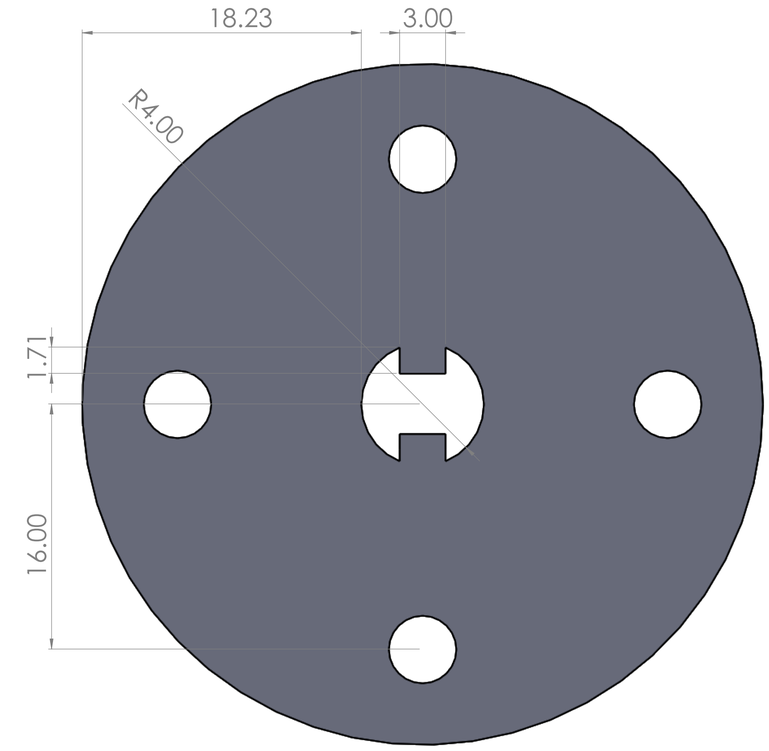


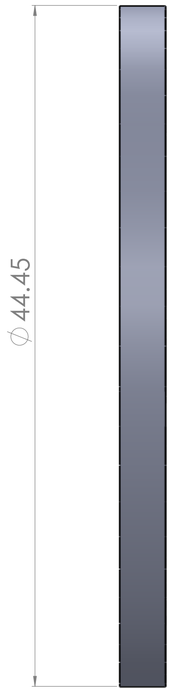



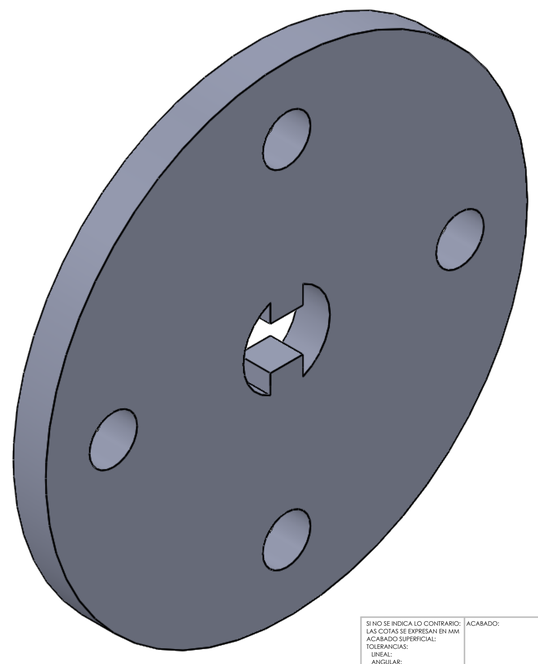

| | | | | | | | | |
|---|---|---|---|---|---|---|---|---|
| SI NO SE INDICA LO CONTRARIO: LAS COTAS SE EXPRESAN EN MM. ACABADO SUPERFICIAL: TOLERANCIAS: LINEAL: ANGULAR: | | ACABADO: | | REBARBAR Y ROMPER ARISTAS VIVAS | | NO CAMBIE LA ESCALA | | REVISIÓN |
| | NOMBRE | FIRMA | FECHA | | | TÍTULO: | | |
| DIBUJ. | | | | | | | | |
| VERIF. | | | | | | | | |
| APROB. | | | | | | | | |
| FABR. | | | | | | | | |
| CALID. | | | | | | | | |
| | | | | MATERIAL: | | N.º DE DIBUJO | | |
| | | | | | | tapa1_impresion_v2 | | |
| | | | | PESO: | | ESCALA:5:1 | | HOJA 1 DE 1 |

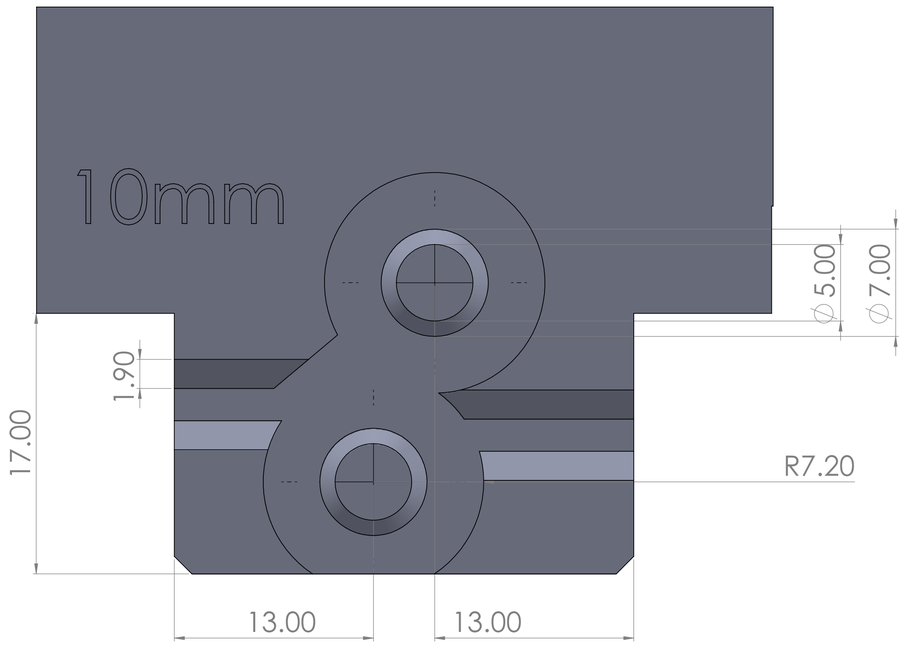


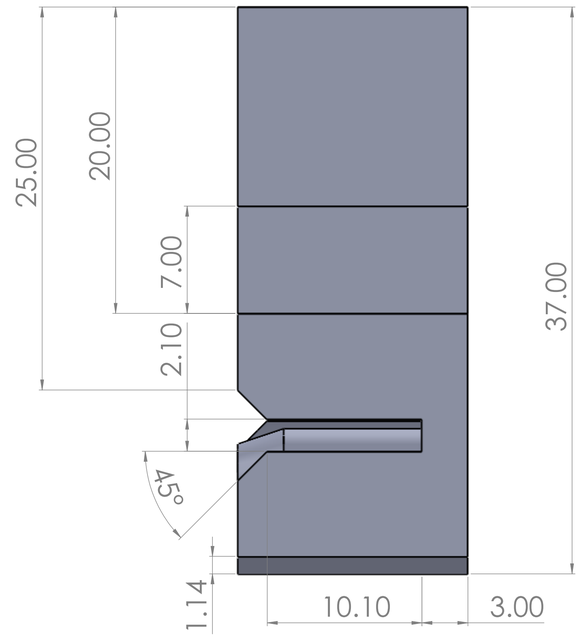


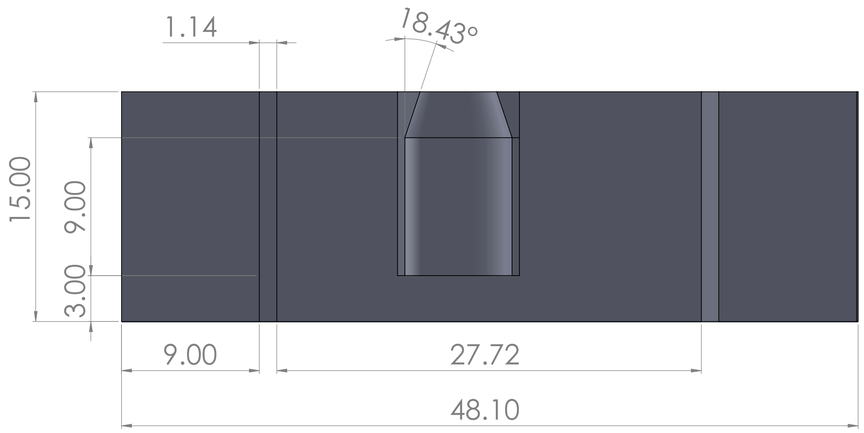


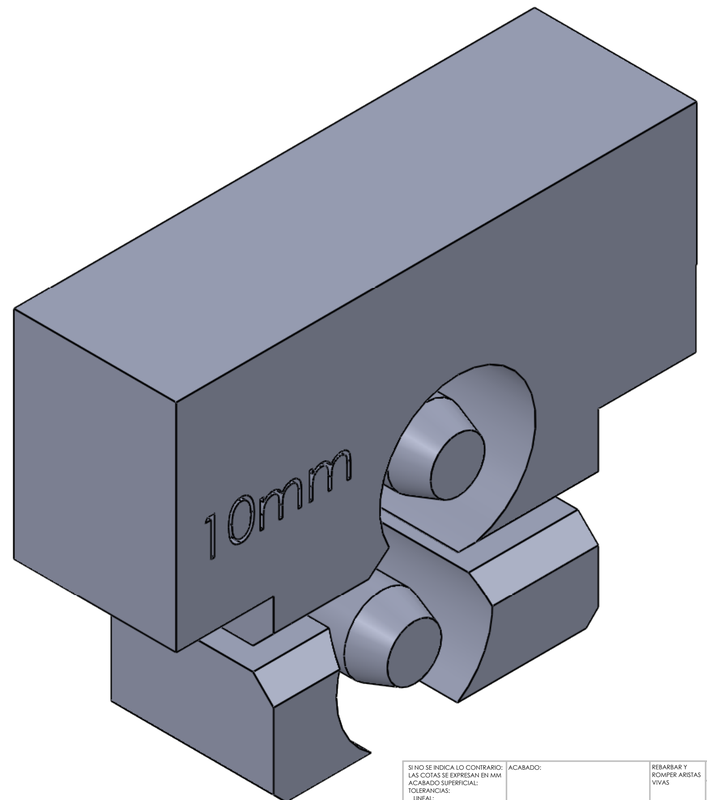


| | | | | | | |
|---|---|---|---|---|---|---|
| SI NO SE INDICA LO CONTRARIO: LAS COTAS SE EXPRESAN EN MM. ACABADO SUPERFICIAL: TOLERANCIAS: LINEAL: ANGULAR: | ACABADO: | | REBARBAR Y ROMPER ARISTAS VIVAS | NO CAMBIE LA ESCALA | REVISIÓN | |
| | NOMBRE | FIRMA | FECHA | TÍTULO: | | |
| DIBUJ. | | | | | | |
| VERIF. | | | | | | |
| APROB. | | | | | | |
| FABR. | | | | | | |
| CALID. | | | | | | |
| MATERIAL: | | | | N.º DE DIBUJO | | A1 |
| PESO: | | | | ESCALA:5:1 | | HOJA 1 DE 1 |

y belt holder_201017_10mm

## Appendix 2. Bifurcated vascular graft construction and characterization

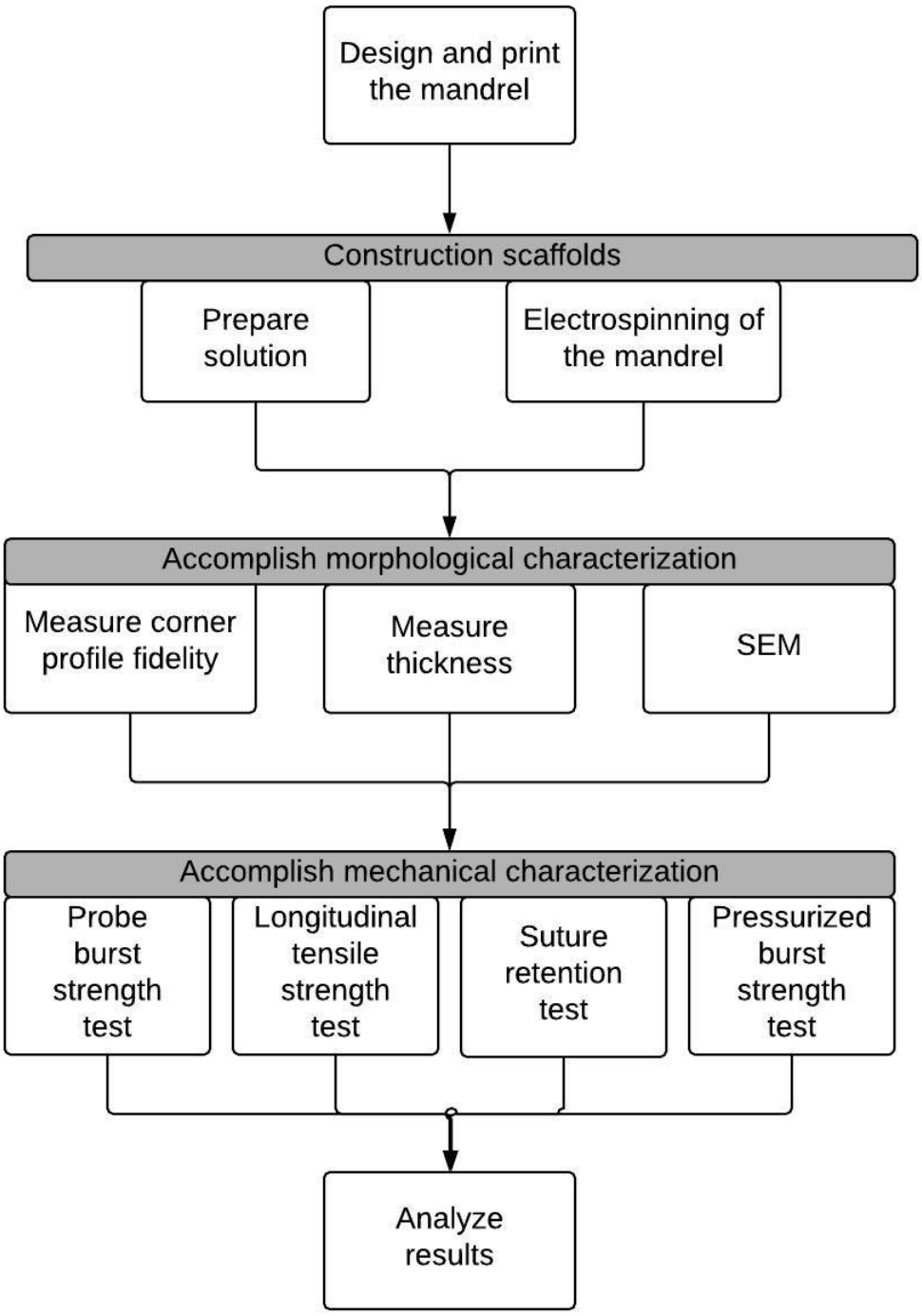

# A. Method for bifurcated tubular vascular graft construction

## A.1 Scope

This document describes the factors, elements and processes involved in the preparation of the bifurcated tubular vascular grafts using the combination of the electrospinning technique, additive manufacturing and a positioning mechanism.

## A.2 Materials

- Biocompatible resin (e.g E-Shell 200, E-Shell 300, E- Guard, E-Dent 400 EnvisionTec)
- PCL (pellets)
- Acetone
- Isopropanol

## A.3 Apparatus

a. The container in which the mix to be electrospun will be prepared must have a capacity of at least 50 ml (E.g. Beaker).
b. A magnetic stirring hot plate to help with temperature and mechanical stirring of the solution.
c. A mandrel for the scaffold, generated using a 3d printing machine based on DLP technology, with a 200µm resolution.
d. The chamber for electrospinning, which must be constructed of an electrically insulating material and the capacity for the positioning mechanism and its electronic control.
e. A syringe pump system with a minimally required flow rate of 10 ml/h.
f. A power supply with a minimum capacity of 20kV.

## A.4 Sampling

### *A.4.1 Test specimens*

All the samples must be handled with gloves.

#### *A.4.1.1. Tubular specimens*

The specimens will be a mandrel with 30mm of length, 7.5mm for inner diameter and 1mm of thickness. The size of each square cell is 1.5mm by side. 3D printed mandrel will be covered on the top with a mat of fibers.

#### *A.4.1.2. Bifurcated specimens*

The specimens will be a mandrel with 30mm of length, 7.5mm for inner diameter and 1mm of thickness. In the middle of the structure, there will be a 3$^{rd}$ cylinder with 20mm of length, 7.5mm for inner diameter and 1mm of thickness. The size of each square cell is 1.5mm by side. 3D printed mandrel will be covered on the top with a mat of fibers.

*A.4.2 Test conditions*

The mandrel will be inserted in a flexible mechanism, which is covered with aluminum foil and will subsequently be covered by fibers. The electrospinning chamber must be sealed to maintain stable the temperature and humidity.

*A.4.3 Measurements*

The measurements of viscosity will be taken and recorded by the operator, with the help of a capillary viscometer.

The measurements of temperature and humidity while the electrospinning is being done, will be taken and recorded by the operator, using a commercially available probe.

## A.5 Procedure

*A.5.1 3D printing process*

a. Generating the file of the piece to be constructed, must be in *.stl* format
b. The printer must be cleaned and calibrated previously.
c. Once constructed, the piece will be cleaned with isopropanol and dried.
d. The piece must be cured in Otoflash® UV cure box at 3000 cycles.
e. The supports must be then removed from the final desired part.

*A.5.2 Electrospinning process*

### A.5.2.1 Pre-electrospinning phase

a. To test each speed profile (low, medium and high speed), a batch of 12 specimens is required, to be divided into 2 groups (tubular and bifurcated) for a total of 6 specimens per group. The 6 samples corresponding to a specific group of the batch of each speed profile (low, medium and high speed).
b. Every batch will be prepared with the same solution, consisting of 3.5gr PCL and 40ml Acetone.
c. The solution is prepared by heating it to 35-40°C and magnetic stirring in a hot plate on a cycle between 6 and 8, for approximately 6-12hrs.
d. At this point, the viscosity will be measured and documented.
e. The flexible mechanism will be prepared by being covered in aluminum foil.

### A.5.2.2 Electrospinning phase

a. The mandrel must be set on the flexible mechanism to be electrospun, as can be seen on the Fig. 1. The T-arm must be refilled with aluminum.
b. The flexible mechanism must be set on the positioning mechanism.
c. The syringe pump must be set on 0.5mL/h.
d. The power supply must be set on 18kV.
e. The parameters of the electrospinning will be documented in Table 1.

### A.5.2.3 Post-electrospinning phase

a. The specimens will be stored and labeled according to the batch and group it belongs, HSP (high-speed profile), MSP (medium-speed profile) and LSP (low-speed profile), respectively, adding the prefix B (Bifurcated) or T (Tubular), according to the geometry (see Table A.1).
b. The thickness of the resultant mat will be measured. (See Secc 3. Thickness measurement)

Table A.1 Labeling method

| | **Speed profile** | | |
|---|---|---|---|
| **Geometry** | LSP | MSP | HSP |
| ***B*ifurcated** | ***B*LSP_#** | ***B*MSP_#** | ***B*HSP_#** |
| ***T*ubular** | ***T*LSP_#** | ***T*MSP_#** | ***T*HSP_#** |

Table A.2 Data collection of the process

| | | Electrospinning solution | | | | | | | Electrospinning process | | | | | | |
|---|---|---|---|---|---|---|---|---|---|---|---|---|---|---|---|
| | | Preparation parameters | | | | | Environment parameters | | Parameters | | | | | | Results |
| Shape | Name | PCL | Acetone | Preparation temperature | Stirring | Time | Humidity | Room temperature | Voltage | Rate | Speed profile | Humidity | Electrospinninn temperature | Viscosity | Thickness |
| | | [gr] | [ml] | [°C] | | [hr] | [%] | [°C] | [kV] | [ml/h] | [rad/s] | [%] | [°C] | [cp] | [µm] |
| Bifurcated | BLSP_1 | | | | | | | | | | 0.45 | | | | |
| | : | | | | | | | | | | 0.45 | | | | |
| Bifurcated | BLSP_6 | | | | | | | | | | 0.45 | | | | |
| Tubular | TLSP_1 | | | | | | | | | | 0.45 | | | | |
| | : | | | | | | | | | | 0.45 | | | | |
| Tubular | TLSP_6 | | | | | | | | | | 0.45 | | | | |
| Bifurcated | BMSP_1 | | | | | | | | | | 0.45 | | | | |
| | : | | | | | | | | | | 0.45 | | | | |
| Bifurcated | BMSP_2 | | | | | | | | | | 2.2 | | | | |
| Tubular | TMSP_2 | | | | | | | | | | 2.2 | | | | |
| | : | | | | | | | | | | 2.2 | | | | |
| Tubular | TMSP_6 | | | | | | | | | | 2.2 | | | | |
| Bifurcated | BHSP_1 | | | | | | | | | | 3.7 | | | | |
| | : | | | | | | | | | | 3.7 | | | | |
| Bifurcated | BHSP_6 | | | | | | | | | | 3.7 | | | | |
| Tubular | THSP_1 | | | | | | | | | | 3.7 | | | | |
| | : | | | | | | | | | | 3.7 | | | | |
| Tubular | THSP_6 | | | | | | | | | | 3.7 | | | | |

## B. Corner Profile Fidelity [$F_{CP}$]

### B.1 Scope

The purpose of this measurement is to determine the area recovered by the electrospinning process on each sample on both points M5 and M6 (see Figure B.1)

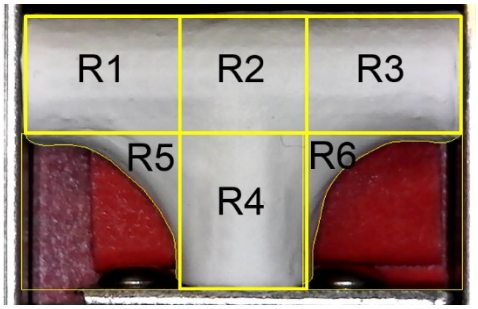


Figure B.1 The order of different points measured on the resultant mat of fibers

### B.2 Materials

- ImageJ software
- Ehe software

### B.3 Apparatus

- Microscope (camera)
- PC

### B.4 Sampling

*B.4.1 Test specimens*

- The samples must be measured with the same coordinate system.
- All the samples must be handled with gloves.

*B.4.2 Test conditions*

- All the samples must be measured in the same position in which they were electrospun. As shown in Figure B.1
- The samples must be measured by the system, in the same position they were extracted from the mechanism. As shown in Figure B.1
- The samples will be measured in dry conditions.

*B.4.3 Measurements*

- The measurements will be taken with *ImageJ* software and saved as *.txt* file.
- The images will be saved as *.bmp* file, with the marks made during the measuring.

## B.5 Procedure

a. First, it must be stablished the ideal measurements to which accomplish. In this case, the square areas to measure are 115.5mm$^2$.
b. It is necessary to set the scale for each image. For this step, we suggest taking the same pixel on each sample, with the objective to obtain the points in the same position, for all the images. When the points are drawn to reproduce the shape of the recovered area, there is a better matching between all the samples.
c. Once set the scale, it is necessary drawing a line under the T-arm of the mandrel just to define a reference for the square area to measure. This line must match with the initial and end of the scale line, just to be sure that this reference is 30mm length.
d. The next step is drawing the square area on M5 (see Figure B.1) and record the measurement. It must match to the target area ~115.5mm$^2$.
e. With the polygon section tool, it can be delimited the electrospun area and record the measurement. The first point will be the left down corner of the drawn square. The measurement will be done on clockwise since the first point.
f. With the recovered area delimited, we use the multi-point tool, and mark points on the drawn line with the polygon section tool and save the points.
g. It will be repeated steps 4-6, on M6 point.
h. With the multi-point tool again, it can be marked the points of the mandrel. It can be set a point on each corner, to draw the complete image later, reconstruct it and match all the samples to observe the differences between the recovered areas.

# C. Thickness measurement

## C.1 Scope

The purpose of this measurement is to determine the thickness obtained by the electrospinning process on each sample.

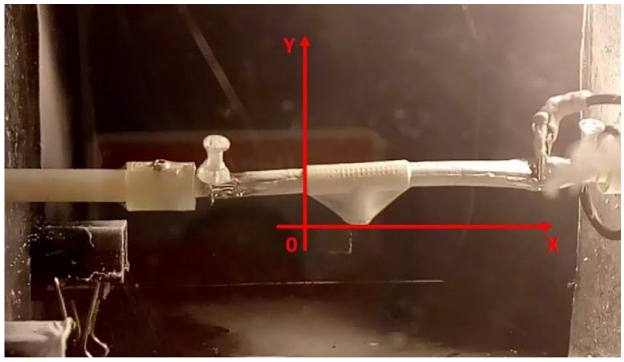


Figure C.1 The scaffold will be measured in the same position it was extracted from the mechanism.

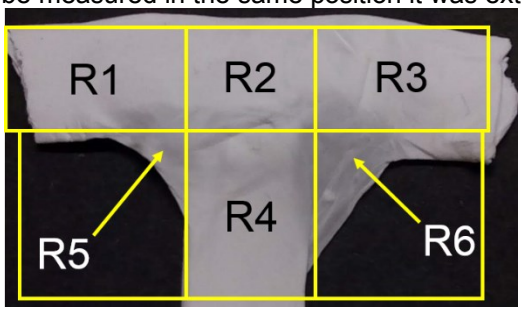


Figure C.2 The scaffold will be divided into 6 different regions to accomplish the characterization.

## C.2 Materials

- ImageJ software
- Ehe software
- Fixture to hold the micrometer (picture)

## C.3 Apparatus

- Digital micrometer (IP65 coolant proof, Mitutoyo, U.S.A.)
- Microscope (camera)
- PC

## C.4 Sampling

### *C.4.1 Test specimens*

- The samples must be measured with the same coordinate system (see Figure C.1)
- All the samples must be handled with gloves.

*C.4.2 Test conditions*

- All the samples must be measured in the same position in which they were electrospun. As shown in Figure C.1
- The samples must be measured by the system, in the same position they were extracted from the mechanism. As shown in Figure C.1.
- The samples must be hydrated before the measuring process, and extract the mandrel.

*C.4.3 Measurements*

- The measurements will be taken with micrometer and registered, region by region

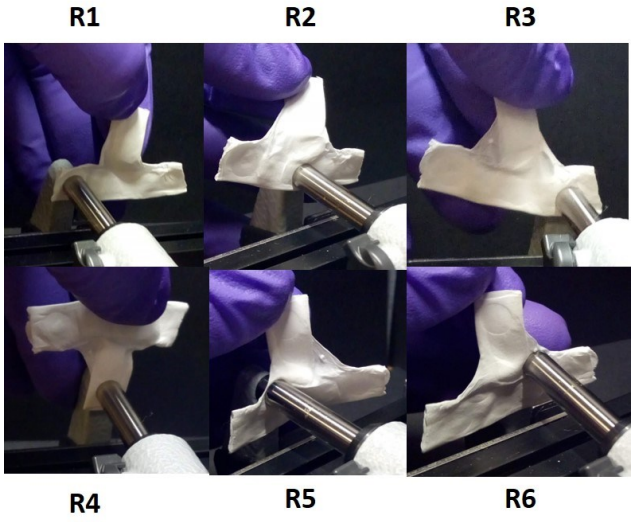


Figure C.3 Regions considered to measure the thickness.

## C.5 Procedure

a. The regions must be stablished to measure the thickness.
b. The scaffold must be flattened to accomplish the measurements (see Figure C.2)
c. A measurement must be accomplished on each region (see Figure C.3)
d. The measurements will be registered to calculate the final thickness by the expression:

$$t = \frac{1}{2}\left(\frac{1}{n}\sum_{i=1}^{n} R_i\right)$$

where:

t = thickness
R = region
n = 6

## D. Probe burst strength test

### D.1 Scope

The purpose of this test is to determine the strength of an area of the sample prosthesis that is clamped over an orifice while a cylindrical probe is traversed through the specimen until it ruptures.

### D.2 Materials

a. PBS solution
b. Indenter of ¼”

### D.3 Apparatus

a. A universal compression test machine, having a constant rate of traverse and capable of operation in the compression mode or fitted with a suitable compression cage, with measurement of the compressive load should be of an accuracy of ±5 % of the reported value;
b. A length measuring device accurate to ±0,5 mm.
c. An indenter to traverse the specimen. The traversing probe should have a hemispherical radius with a diameter of 6.35 mm (1/4in).

### D.4 Sampling

*D.4.1 Test specimen*

a. At least 6 specimens should be used to this test.
b. All the specimens will be a mandrel with 30mm of length, 7.5mm for inner diameter and 1mm of thickness. In the middle of the structure, there will be a 3rd cylinder with 20mm of length, 7.5mm for inner diameter and 1mm of thickness. The size of each square cell is 1.5mm by side. This 3D printed mandrel will be covered on the top with a mat of fibers.
c. All the samples must be handled with gloves.

*D.4.1.1 Tubular specimens*

The specimens will be a mandrel with 30mm of length, 7.5mm for inner diameter and 1mm of thickness. The size of each square cell is 1.5mm by side. 3D printed mandrel will be covered on the top with a mat of fibers. See *Secc A.4.1*

*D.4.1.2 Bifurcated specimens*

The specimens will be a mandrel with 30mm of length, 7.5mm for inner diameter and 1mm of thickness. In the middle of the structure, there will be a 3rd cylinder with 20mm of length, 7.5mm for inner diameter and 1mm of thickness. The size of each square cell is 1.5mm by side. 3D printed mandrel will be covered on the top with a mat of fibers. See *Secc A.4.1*

*D.4.2 Test conditions*

The specimen will be taken out of the media of PBS solution and immediately tested at room temperature.

*D.4.3 Measurements*

The measurements will be taken and recorded by the software of the testing machine. In this case, INSTRON 3365.

## D.5 Acceptance criteria

The measurements will be accepted as long as they show a minimum strength into 2-3 MPa, according to [1].

## D.6 Test method

*D.6.1 Pre-probe burst strength test*

a. To test each speed profile, a batch of 18 specimens is required. Each batch is divided into 3 groups (Low, Medium and High-Speed Profile), each having 6 specimens, labeled as HSP (high-speed profile), MSP (medium speed profile) and LSP (low-speed profile), respectively.
b. Each specimen will be hydrated, with the mandrel inside, with PBS solution during 6hrs before the test at room temperature.
c. The specimen will be taken out of the media and immediately tested, for each sample.

*D.6.2 Probe burst strength test*

a. The sample must be placed with the T-arm upwards, concentrically matching the internal diameter of the T-arm with the indenter.
b. The indenter must be placed over the mat of fibers in this diameter.
c. The speed of the test must be set on 0.6mm/min (0.01mm/s), to obtain a defined curve of the max low supported and deformation.

*D.6.3 Post probe burst strength phase*

After the test, the specimen must be dried and kept at room temperature, for the next test. The collected data is processed to give a maximum strength for each speed profile.

## D.7 Calculation and presentation of the results

The probe diameter shall be expressed in millimeters, the rate of traverse millimeters per minute, and the bursting load in Newtons [N]. The test report shall include the mean and standard deviations of the bursting load, the probe diameter, and the rate of traverse.

# E. Longitudinal tensile strength test

## E.1 Scope

This document describes the factors involved in the determination of the longitudinal tensile strength of the sample prosthesis in its bifurcated tubular form when loaded longitudinally along its centerline. The sample is stretched at a uniform rate until the yield and/or breakpoint is reached.

## E.2 Materials

a. PBS solution
b. Adhesive tape
c. 1L beaker

## E.3 Apparatus

a. A universal machine able to practice tensile tests, having a constant rate of traverse and suitable jaws to hold the sample prosthesis firmly without damaging its structure (i.e. because such damage might cause the break to occur prematurely at the jaw margins)
b. A temperature controlled bath
c. A length measuring device accurate to ±0,5 mm.

## E.4 Sampling

### *E.4.1. Test specimens*

a. At least 6 specimens should be used to this test.
b. All the specimens will be a rectangle approx. 10 x 30mm.
c. All the samples must be handled with gloves.

### *E.4.2. Test conditions*

Each specimen will be immersed in PBS solution during the test, with the temperature set on 37°C.

The media must be replaced with a new batch, while the test is running.

### *E.4.3. Measurements*

The measurements will be taken and recorded by the software of the testing machine. In this case, INSTRON 3365.

## E.5 Acceptance criteria

The measurements will be accepted while it shows a minimum strength into 3-4 MPa, according to [2], [3]

## E.6 Test method

### *E.6.1. Pre longitudinal tensile strength test*

a. Every mandrel with the mat of fibers must be cut in the middle to obtain 2 rectangular samples, with 10mm of width and 20-30mm of length.
b. To test each speed profile, a batch of 18 specimens is required. Each batch is divided into 3 groups (Low, Medium and High-Speed Profile), each having 6 specimens, labeled as HSP (high-speed profile), MSP (medium speed profile) and LSP (low-speed profile), respectively.
c. To ensure a firm but delicate retention of the membrane within the metal tensile system clamps, each specimen will be mounted using a sandwich of thin adhesive tape by both sides.

### *E.6.2. Longitudinal tensile strength phase*

a. Preparation of immersion solution.
   The media to be used as immersion solution is prepared according to the set parameters and conditions.

b. The speed of the test must be set on 5mm/min, to obtain a defined curve of the max strength and deformation.

### *E.6.3. Post longitudinal tensile strength phase*

The collected data is processed to give a maximum strength for each speed profile.

## E.7 Calculation and presentation of the results

The longitudinal tensile strength of each sample is expressed in Newtons [N] as Maximum load = Tmax. The test report shall include the mean and standard deviations of the longitudinal tensile strength of the sample prostheses and the rate of extension and the test sample gauge length (with rationale, if not within the specified range).

# F. Suture retention strength test

## F.1 Scope

The purpose of this test is to determine the force necessary to pull a suture from the prosthesis or cause the wall of the prosthesis to fail while pulling a suture inserted through the wall.

## F.2 Materials

a. PBS solution
b. Adhesive tape
c. Suture Prolene 5-0

## F.3 Apparatus

a. A universal machine able to practice tensile tests, having a constant rate of traverse and suitable jaws to hold the sample prosthesis firmly without damaging its structure (i.e. because such damage might cause the break to occur prematurely at the jaw margins)
b. A temperature controlled bath
c. A temperature controller
d. A length measuring device accurate to ±0,5 mm.

## F.4 Sampling

### *F.4.1 Test specimen*

a. At least 6 specimens should be used to this test.
b. All the specimens will be a rectangle approx. 10 x 30mm.
c. All the samples must be handled with gloves.

### *F.4.2 Test conditions*

Each specimen will be immersed in PBS solution during the test, with the temperature set on 37°C.

The media must be replaced with a new batch, while the test is running.

### *F.4.3 Measurements*

The measurements will be taken and recorded by the software of the testing machine.

### F.5 Acceptance criteria

The measurements will be accepted while it shows a minimum strength of approx. 2N, according to [4].

### F.6 Test method

*F.6.1 Pre suture retention strength test*

a. To test each speed profile, a batch of 18 specimens is required. Each batch is divided into 3 groups (Low, Medium and High-Speed Profile), each having 6 specimens, labeled as HSP (high-speed profile), MSP (medium speed profile) and LSP (low-speed profile), respectively.
b. To ensure a firm but delicate retention of the membrane within the metal tensile system clamps, each specimen will be mounted using a sandwich of thin adhesive tape by one side. In the other, the suture will be passed through the material by means of the provided needle, at 2mm from the edge [4], then into the hole of a suture holder connected to one of the clamps, and finally closed into a loop.

*F.6.2 Suture retention strength test*

a. Preparation of immersion solution.
   The media to be used as immersion solution is prepared according to the set parameters and conditions. The solution is composed by 5 tablets of Phosphate Buffered Saline (PBS) dissolved in 1L of distilled water at room temperature. It will be necessary 2 beakers to refill the temperature controlled bath.
b. Connect the temperature controller and place the thermocouple into the bath, with the PBS solution.
c. After placing the specimen, place the bath to cover the jaws with the PBS solution.
d. The speed of the test must be set on 5mm/min, to obtain a defined curve of the max strength and deformation.

*F.6.3 Post suture retention strength phase*

The collected data is processed to give a maximum strength for each speed profile.

### F.7 Calculation and presentation of the results

The force is measured in grams. The test report shall include details of the measurement method used, mean and standard deviations of the suture retention strength of the sample prostheses, and the type and size of suture used.

# G. Pressurized burst strength test

## G.1. Scope

The purpose of this test is to determine the pressurized burst strength by either

a) filling the prosthesis directly with fluid or gas at a measured rate of pressure change until bursting of the sample prosthesis takes place, or

b) Placing an elastic, non-permeable liner inside the prosthesis and filling the liner with fluid or gas at a measured rate of pressure change until bursting of the sample prosthesis takes place.

## G.2. Materials

a. Distilled water
b. Balloon dilatation catheter
c. Pipes
d. Hose clamps
e. RS232 connector

## G.3. Apparatus

a. A system capable of measuring and recording pressure to greater than the bursting pressure to an accuracy of ±5 % of the reported value
b. An apparatus capable of applying a steadily increasing at a controlled rate fluid or gas pressure to the inside of the sample prosthesis extended, and
c. If applicable, an elastic, non-permeable liner distension apparatus with a diameter notably greater than the nominal pressurized diameter of the sample at 16 kPa (120 mmHg).

## G.4. Sampling

### *G.4.1. Test specimen*

a. At least 6 specimens should be used to this test.
b. All the specimens will be 8.5mm of internal diameter and 30mm of length
c. All the samples must be handled with gloves.

### *G.4.2. Test conditions*

Each specimen will be pressurized with an inflator and distilled water into an angioplasty balloon at room temperature.

The media must be replaced for each sample.

### *G.4.3. Measurements*

The measurements will be taken and recorded by the software of the testing machine.

## G.5. Acceptance criteria

The measurements will be accepted while it shows a minimum pressure of 4000mmHg, according to [5].

## G.6. Test method

### *G.6.1. Pre-pressurized burst strength test*

a. To test each speed profile, a batch of 18 specimens is required. Each batch is divided into 3 groups (Low, Medium and High-Speed Profile), each having 6 specimens, labeled as HSP (high-speed profile), MSP (medium speed profile) and LSP (low-speed profile), respectively.
b. The specimen, without the mandrel will be inserted on the balloon with the help of tweezers.
c. The pressure sensor and the catheter of the balloon must be connected to the setup.

### *G.6.2. Pressurized burst strength test*

a. The inflator will be filled in with distilled water at room temperature.
b. While the LabView routine and the pressure sensors are recording the pressure of the test, the balloon will be refilled with the help of the inflator.
c. Once the balloon achieved the Max Pressure, the water must be extracted from the balloon inside and then, observe resultant scaffold.

### *G.6.3. Post pressurized burst strength phase*

The collected data is processed to give a maximum pressure for each speed profile.

## G.7. Calculation and presentation of the results

The rate of pressure rise shall be expressed in kilopascals per second and the bursting pressure in kilopascals. The test report shall include the mean and standard deviation of the bursting pressure of the sample prostheses.

## H. References


[1] S. Kim and M. W. King, “The Mechanical Performance of Weft- knitted / Electrospun Bilayer Small Diameter Vascular Prostheses,” *J. Mech. Behav. Biomed. Mater.*, vol. 61, no. April, pp. 410–418, 2016.

[2] S. de Valence *et al.*, “Long term performance of polycaprolactone vascular grafts in a rat abdominal aorta replacement model,” *Biomaterials*, vol. 33, no. 1, pp. 38–47, 2012.

[3] B. Nottelet *et al.*, “Factorial design optimization and in vivo feasibility of poly(\epsilon -caprolactone)-micro- and nanofiber-based small diameter vascular grafts,” *J. Biomed. Mater. Res. - Part A*, vol. 89, no. 4, pp. 865–875, 2009.

[4] M. Pensalfini, S. Meneghello, V. Lintas, K. Bircher, A. E. Ehret, and E. Mazza, “The suture retention test, revisited and revised,” *J. Mech. Behav. Biomed. Mater.*, vol. 77, no. August, pp. 711–717, 2018.

[5] S. Drilling, J. Gaumer, and J. Lannutti, “Fabrication of burst pressure competent vascular grafts via electrospinning: Effects of microstructure,” *J. Biomed. Mater. Res. - Part A*, vol. 88, no. 4, pp. 923–934, 2009.

## Appendix 3. Design of set up for mechanical test

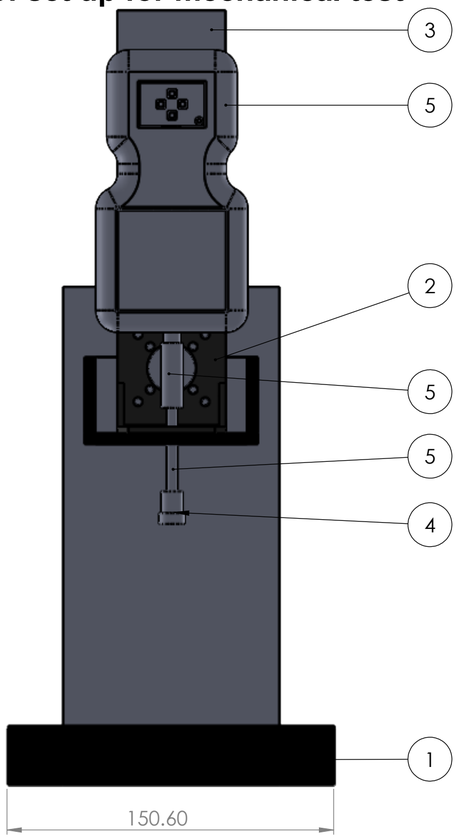


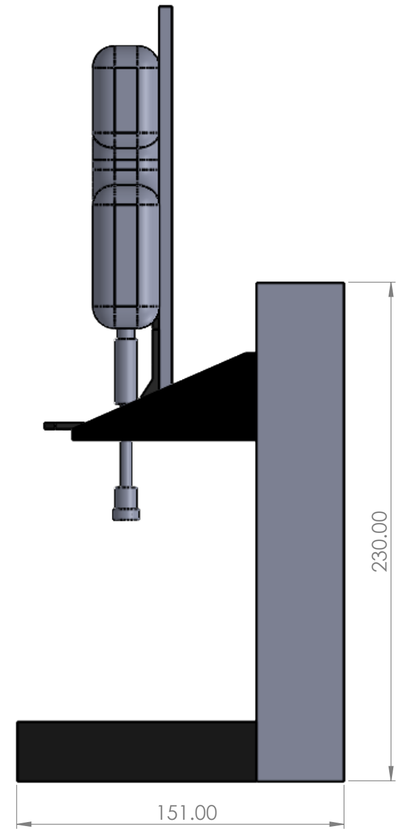


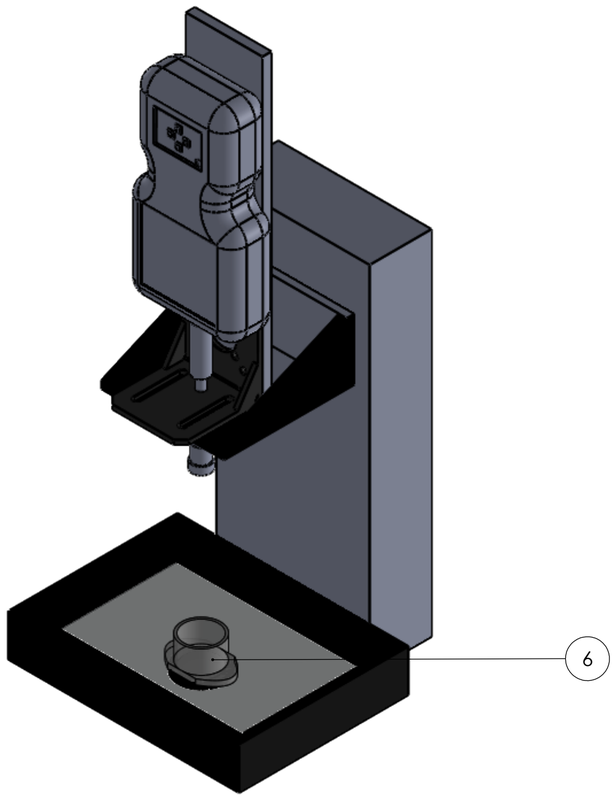


| N.º DE ELEMENTO | N.º DE PIEZA | DESCRIPCIÓN | CANTIDAD |
|---|---|---|---|
| 1 | basement | | 1 |
| 2 | MotorMount_NEMA | | 1 |
| 3 | sensor_holder | | 1 |
| 4 | platform | | 1 |
| 5 | sensor | | 1 |
| 6 | syringe | | 1 |

SI NO SE INDICA LO CONTRARIO: LAS COTAS SE EXPRESAN EN MM
ACABADO SUPERFICIAL:
TOLERANCIAS:
LINEAL:
ANGULAR:

ACABADO:

REBARBAR Y ROMPER ARISTAS VIVAS

NO CAMBIE LA ESCALA

REVISIÓN

| | NOMBRE | FIRMA | FECHA |
|---|---|---|---|
| DIBUJ. | | | |
| VERIF. | | | |
| APROB. | | | |
| FABR. | | | |
| CALID. | | | |

TÍTULO:

ensamble 2_ok_plano tesis

MATERIAL:

N.º DE DIBUJO

A2

PESO:

ESCALA:1:5

HOJA 1 DE 1

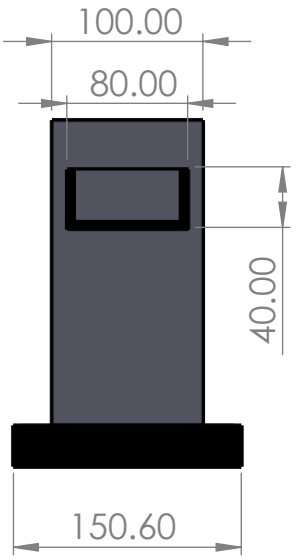


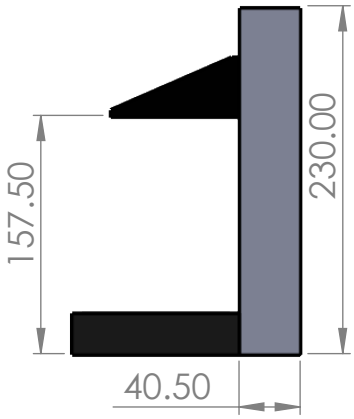


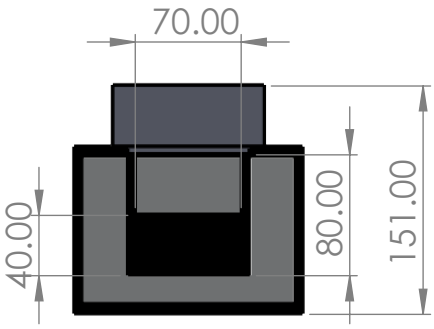


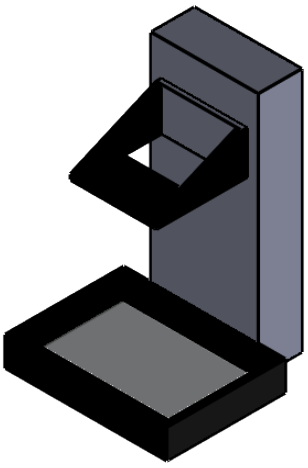

| | | | | | | | |
|---|---|---|---|---|---|---|---|
| SI NO SE INDICA LO CONTRARIO: LAS COTAS SE EXPRESAN EN MM ACABADO SUPERFICIAL: TOLERANCIAS: LINEAL: ANGULAR: | | ACABADO: | | REBARBAR Y ROMPER ARISTAS VIVAS | | NO CAMBIE LA ESCALA | REVISIÓN |
| | NOMBRE | FIRMA | FECHA | | | TÍTULO: | |
| DIBUJ. | | | | | | | |
| VERIF. | | | | | | | |
| APROB. | | | | | | | |
| FABR. | | | | | | | |
| CALID. | | | | MATERIAL: | | N.º DE DIBUJO basement | A4 |
| | | | | PESO: | | ESCALA:1:5 | HOJA 1 DE 1 |

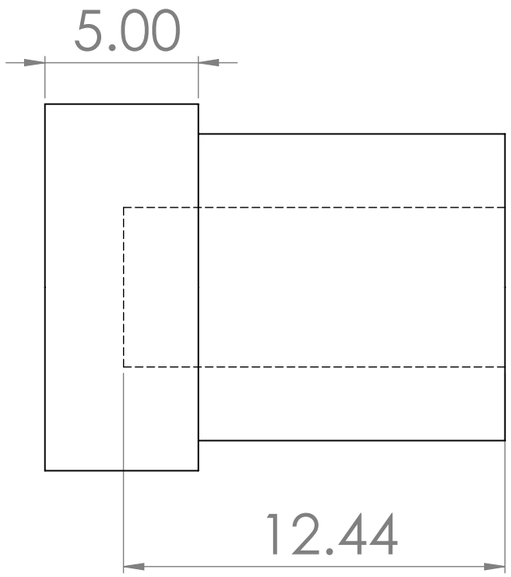


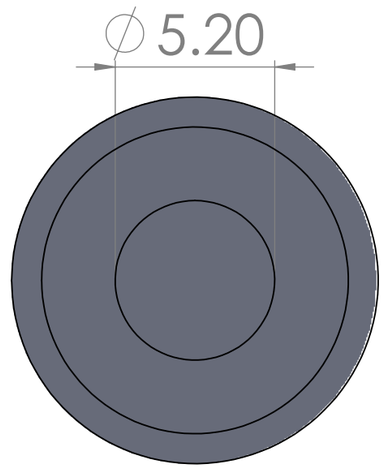


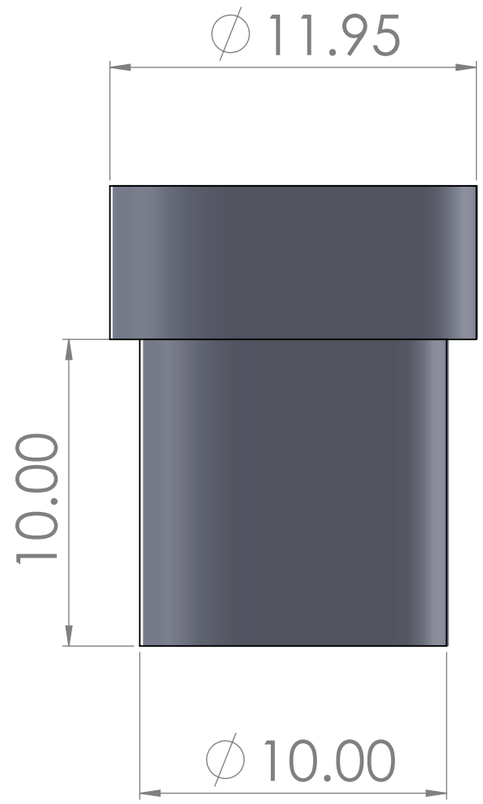


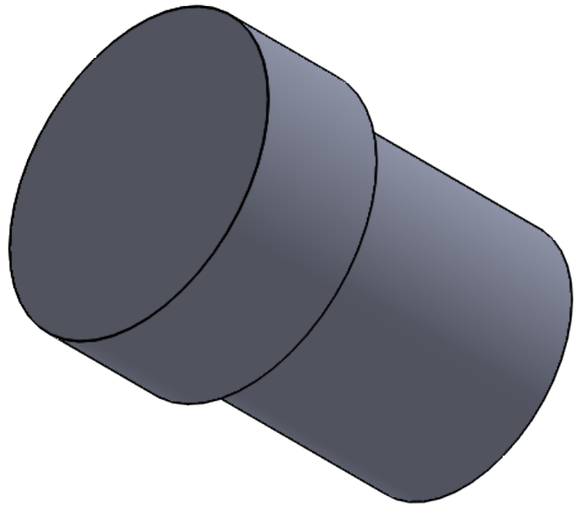

| | | | | | | | |
|---|---|---|---|---|---|---|---|
| SI NO SE INDICA LO CONTRARIO: LAS COTAS SE EXPRESAN EN MM<br>ACABADO SUPERFICIAL:<br>TOLERANCIAS:<br>LINEAL:<br>ANGULAR: | | ACABADO: | | REBARBAR Y ROMPER ARISTAS VIVAS | NO CAMBIE LA ESCALA | REVISIÓN | |
| | NOMBRE | FIRMA | FECHA | | | | TÍTULO: |
| DIBUJ. | | | | | | | |
| VERIF. | | | | | | | |
| APROB. | | | | | | | |
| FABR. | | | | | | | |
| CALID. | | | | MATERIAL: | | N.º DE DIBUJO | A3 |
| | | | | | | platform | |
| | | | | PESO: | ESCALA:5:1 | HOJA 1 DE 1 | |

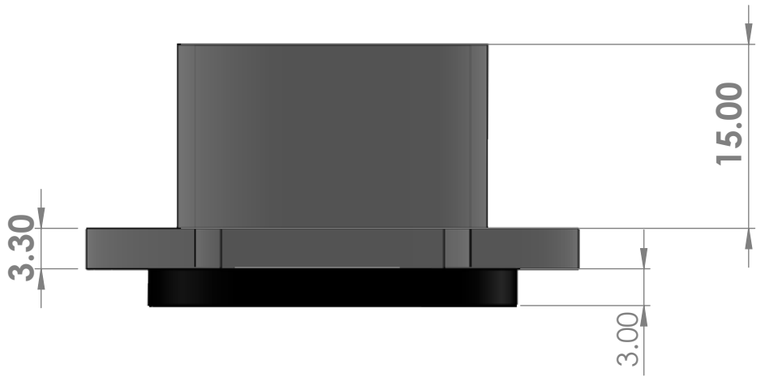


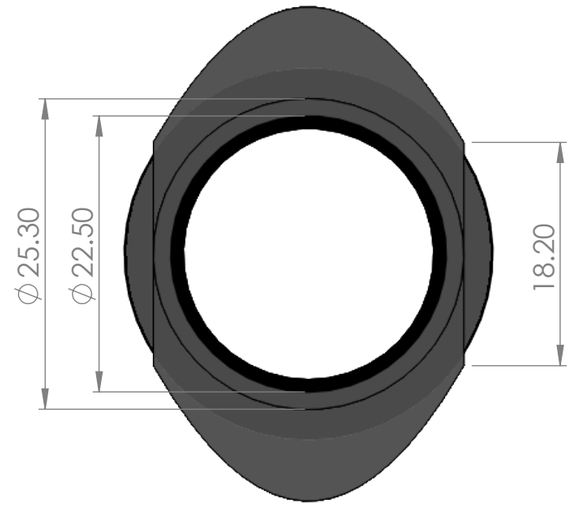


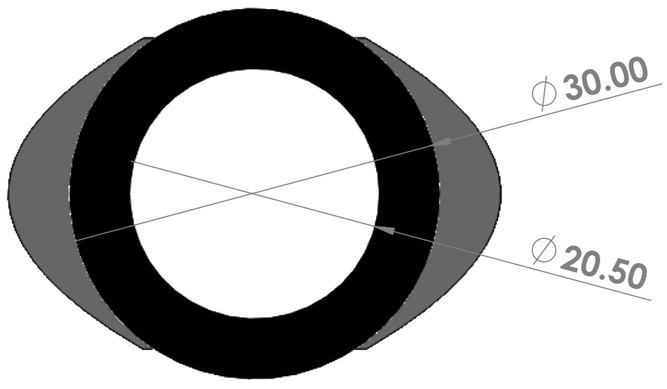


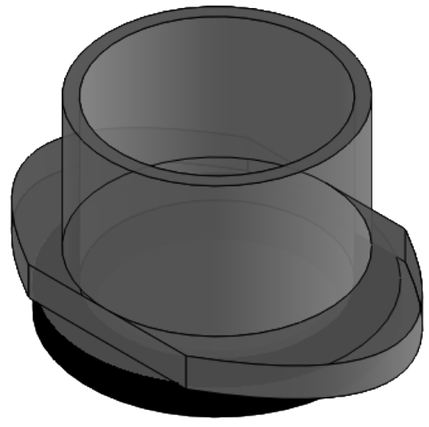

| | | | | | | | |
|---|---|---|---|---|---|---|---|
| SI NO SE INDICA LO CONTRARIO: LAS COTAS SE EXPRESAN EN MM<br>ACABADO SUPERFICIAL:<br>TOLERANCIAS:<br>LINEAL:<br>ANGULAR: | | ACABADO: | | | REBARBAR Y ROMPER ARISTAS VIVAS | NO CAMBIE LA ESCALA | REVISIÓN |
| | NOMBRE | FIRMA | FECHA | | | TÍTULO: | |
| DIBUJ. | | | | | | | |
| VERIF. | | | | | | | |
| APROB. | | | | | | | |
| FABR. | | | | | | | |
| CALID. | | | | MATERIAL: | | N.º DE DIBUJO | A3 |
| | | | | | | resin container | |
| | | | | PESO: | | ESCALA:2:1 | HOJA 1 DE 1 |

# Appendix 4. Resin formulation for Isosorbide

**Purpose**

To prepare Isosorbide resin to print scaffolds.

**Equipment and Materials**

*Equipment:*

- Stirring hot plate
- Stir bar
- Scale
- Transfer pipet
- Weight boats

*Materials:*

- Isosorbide (stored in the fridge).
- 1-vinylimidazole (VIM)
- Irgacure 819 (BAPO)
- Oxybenzophenone (HMB)
- Ethyl Acetate (EA).

*Storage:*

- Isosorbide polymer is stored in the refrigerator.

**Preparation**

1. Prepare the Isosorbide resin (see Resin Calculator.xls) or grab prepared resin from the refrigerator.
2. Place magnetic stirrer in beaker of Isosorbide resin, place on stirring plate at 6-8 level of stirring.
3. Let the resin stirring before use it (~2hrs).

**RESIN CALCULATOR.xls -** Sample 2019

INPUTS

| PERCENTAGES | ISO 1 | ISO 2 | ISO 3 | ISO 4 |
|---|---|---|---|---|
| VIM (1-Vinylimidazole) | 32.00 | 32.00 | 33.50 | 33.50 |
| ISOSORBIDE | 54.90 | 52.50 | 54.90 | 53.00 |
| BAPO | 4.000 | 5.000 | 4.000 | 5.000 |
| E.A. | 7.000 | 7.000 | 6.900 | 6.900 |
| HMB | 2.100 | 3.500 | 0.700 | 1.600 |
| TOTAL | 100.0 | 100.0 | 100.0 | 100.0 |

OUTPUTS

| WEIGHTS | ISO 1 | ISO 2 | ISO 3 | ISO 4 |
|---|---|---|---|---|
| BEAKER | | | | |
| BEAKER WITH Isosorbide | | | | |
| ISOSORBIDE | 0.000 | 0.000 | 0.000 | 0.000 |
| TOTAL MASS | 0.00 | 0.00 | 0.00 | 0.00 |
| VIM | 0.000 | 0.00 | 0.00 | 0.00 |
| BAPO | 0.0000 | 0.00 | 0.00 | 0.00 |
| HMB | 0.0000 | 0.00 | 0.00 | 0.00 |
| E.A. | 0.0000 | 0.00 | 0.00 | 0.00 |
| TOTAL | 0.000 | 0.000 | 0.000 | 0.000 |

# Appendix 5. Mechanical Reliability approach tests

**Cure depth test protocol**

**Purpose**

To accomplish cure depth test on resin formulations using the Perfactory Micro (Perfactory μicro EnvisionTEC®, Inc., Dearborn, MI, USA)

**Equipment and Materials**

*Equipment:*

- Perfactory μicro EnvisionTEC®

*Materials:*

- Slides
- Digital caliper.
- Cotton wipes

*Storage:*

- The resin is stored in the refrigerator.
- Store the thin films in a previously labeled petri dish.

**Preparation**

1. Prepare the resin (see PPF or Isosorbide resin protocol) or grab prepared resin from the refrigerator.
2. Measure 4 slides to use them for the test. Label the slides from A-D and register the measurements on the "Printed slide" column in the "Cure test calculator" file. Do the same for each exposure time.

3. Measure 4 slides to use them for the test. Label the slides from 1-4 and register the measurements on the “Top slide” column in the “Cure test calculator” file. Do the same for each exposure time.

## Procedure

1. Open software “Micro-Printer 300”

2. Connect the 3D printer by clicking the button ‘Connect’. Go to ‘Main Menu’, ‘Motion controller’. The status will be from ‘n/a’ to ‘Online’.

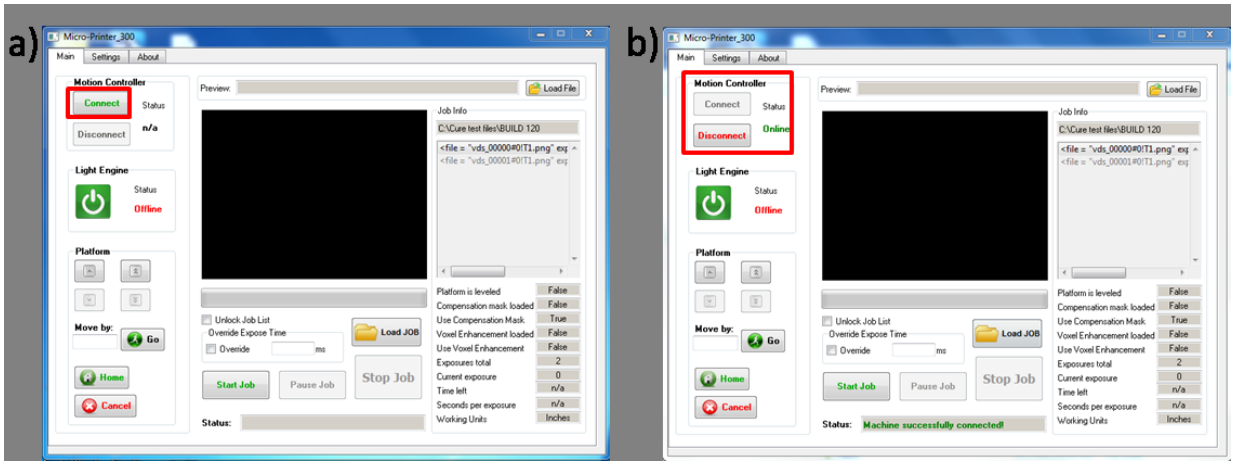


3. Turn on the light by clicking the green button. Go to ‘Main Menu’, ‘Light Engine’. The status will be from ‘Offline’ to ‘Running’.

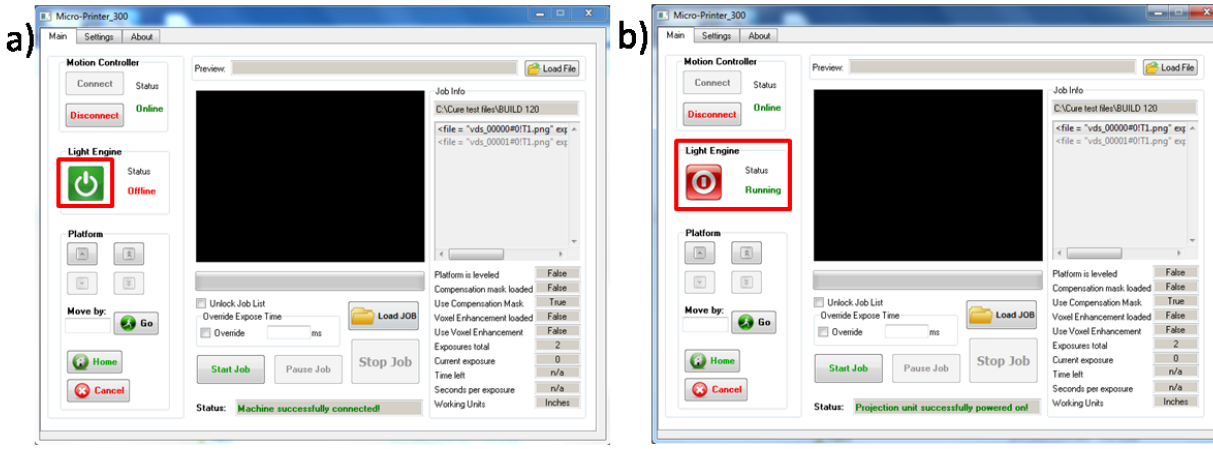

4. Load build job. Go to ‘Main menu’, click on ‘Load JOB’ button. The ‘Job Info’ section (right side of the window) will show the location of the selected folder and the content of the JOB. The status will be from ‘Projection unit successfully powered on!’ to ‘New Job is loaded’

a)

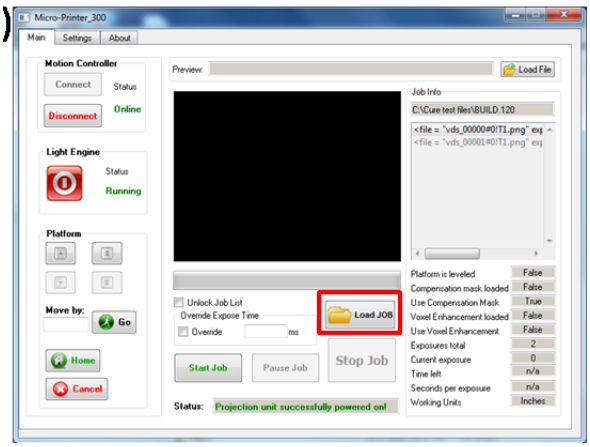


b)

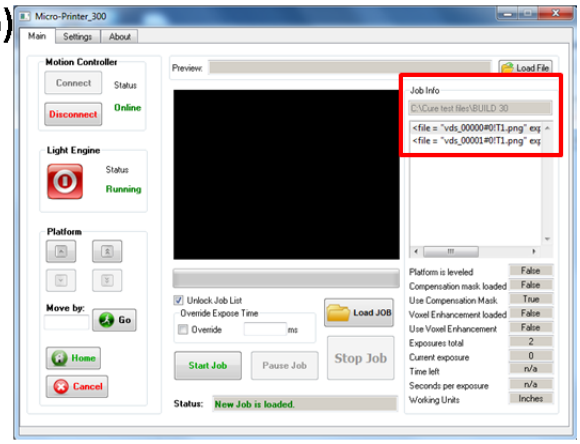


5. Aided by a transfer pipette, pour enough resin for each square over the slide.

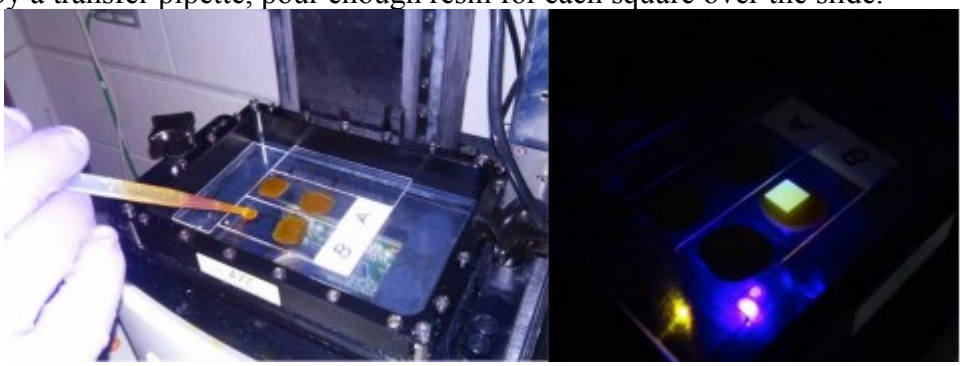

6. Go to the software window and click on ‘Start Job’ button. It will ask you if you already did homing, click on ‘Yes’.

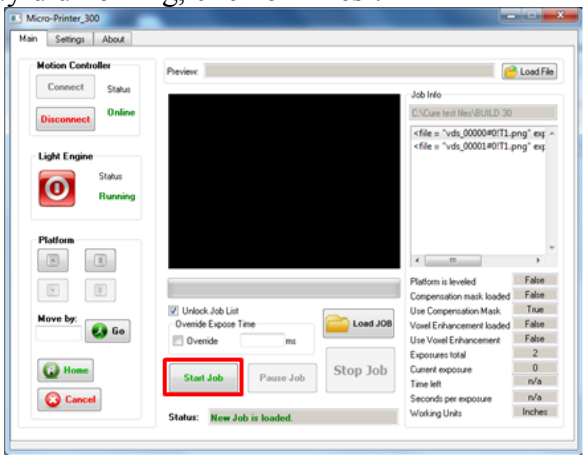


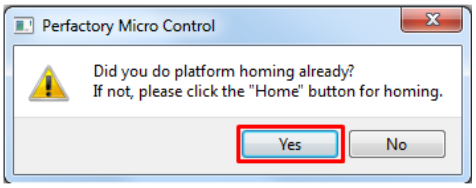

7. After the Job is done, clean the slide very carefully with a cotton wipe to remove excess resin.
8. Place the slide over the printed slide and measure each square with the caliper. Register the measurements on the “Stack” column in the “Cure test calculator” file.
9. Repeat Step 2 through 8, as many times as exposure times you want to test.

**Clean-up**

1. Note where to dispose of any solutions.
2. Or where to store any solutions.

## Green strength test protocol

### Purpose

To accomplish green strength test on resin formulations using the Perfactory Micro (Perfactory μicro EnvisionTEC®, Inc., Dearbon, MI, USA)

### Equipment and Materials

*Equipment:*

- Perfactory μicro EnvisionTEC®
- Load sensor

*Materials:*

- 3ml syringe

*Storage:*

- Resin is stored in the refrigerator.
- Store the thin films in a previously labeled petri dish.

### Preparation

1. Prepare the resin (see PPF or Isosorbide resin protocol) or grab prepared resin from the refrigerator.

2. Turn on the load sensor.


Figure 1. Setup with load sensor

3. Open the load sensor software (EDMS). Make sure the bottom part of the window shows ‘Connected #port’, ‘Ready’ and buttons in the ‘control area’ are available.

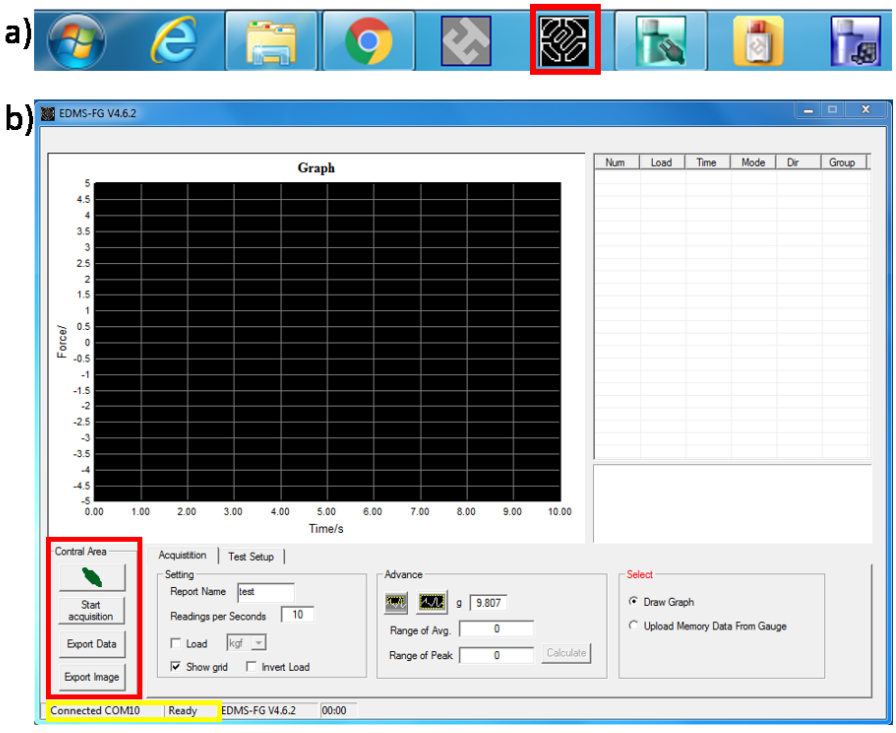


Figure 2. Load sensor software

4. Set the time to collect the data by clicking on ‘Test Setup’ tab, writing the time as ‘Stop condition’.

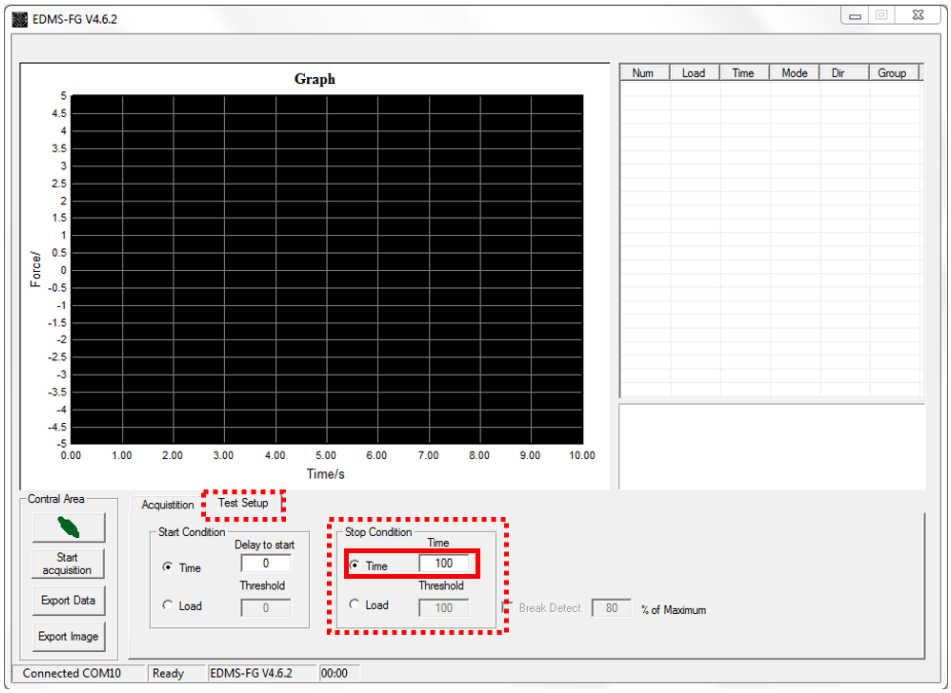


Figure 3. Load sensor configuration.

## Procedure

1. Open software “Micro-Printer 300”

Figure 4.

2. Connect the 3D printer by clicking the button ‘Connect’. Go to ‘Main Menu’, ‘Motion controller’. The status will be from ‘n/a’ to ‘Online’.

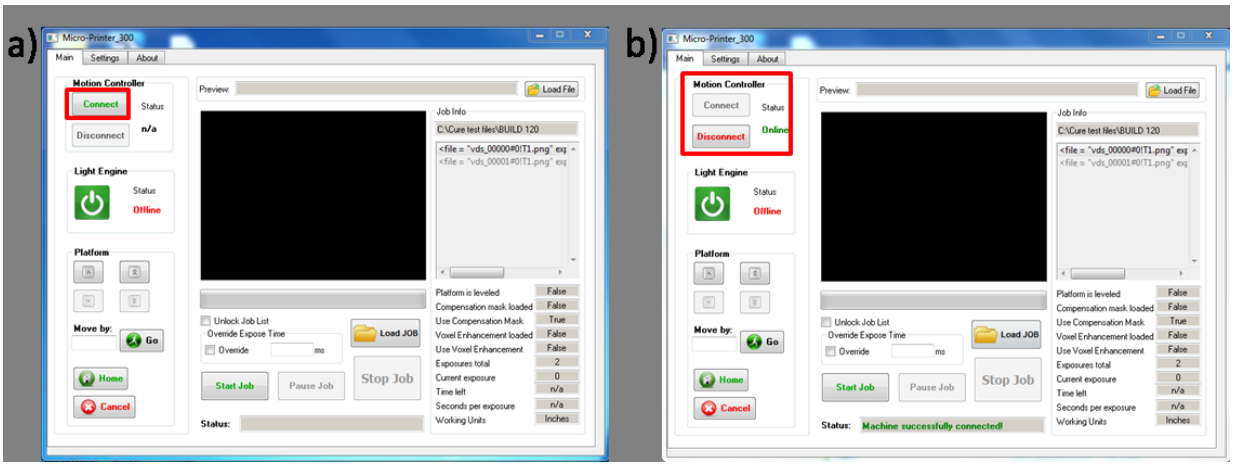


Figure 5. Micro-printer connection

3. Center the resin container on the basement below the platform. You should use carefully the option “Move by & Go” in the main window of Micro-Printer. Positive distance goes up, negative distance goes down.

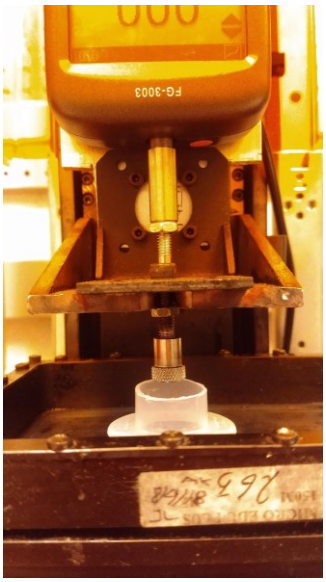

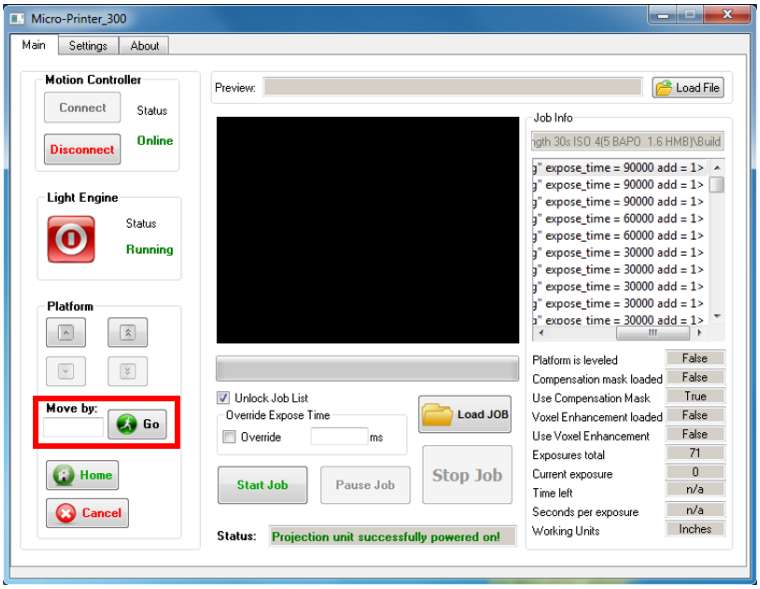


Figure 6. Micro-printer configuration

4. After center correctly the resin container, click on ‘Home’

5. Turn on the light by clicking the green button. Go to ‘Main Menu’, ‘Light Engine’. The status will be from ‘Offline’ to ‘Running’.

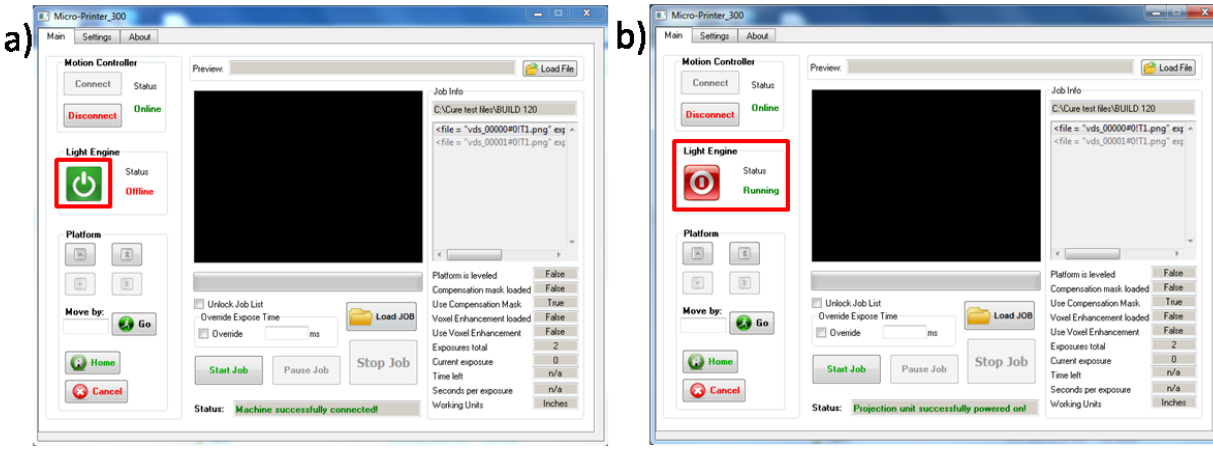


Figure 7.

6. Load build job. Go to ‘Main menu’, click on ‘Load JOB’ button. The ‘Job Info’ section (right side of the window) will show the location of the selected folder and the content of the JOB. The status will be from ‘Projection unit successfully powered on!’ to ‘New Job is loaded’.

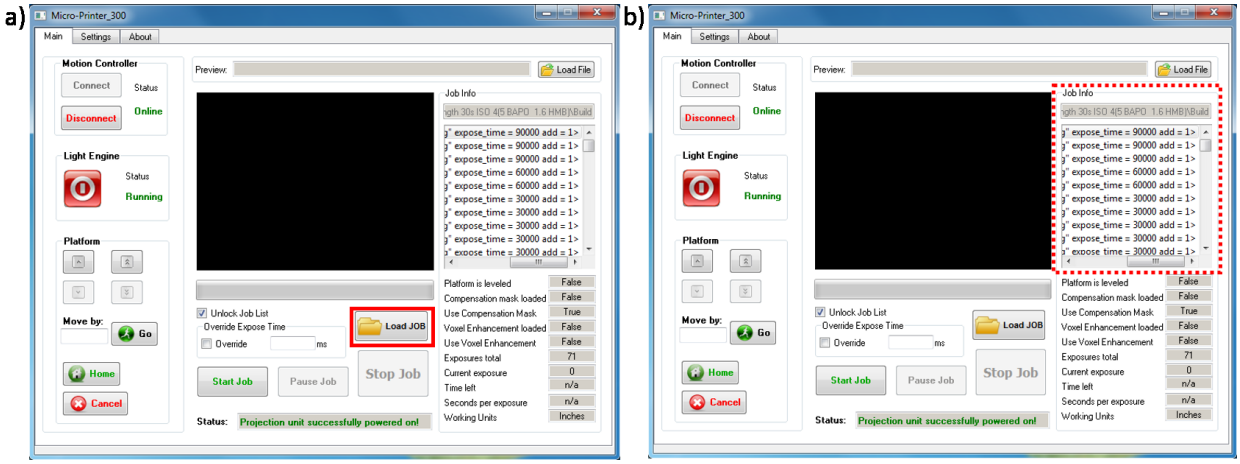


Figure 8.

7. Aided by a syringe, pour enough resin for the gyroid printing and set “Home” in the software.

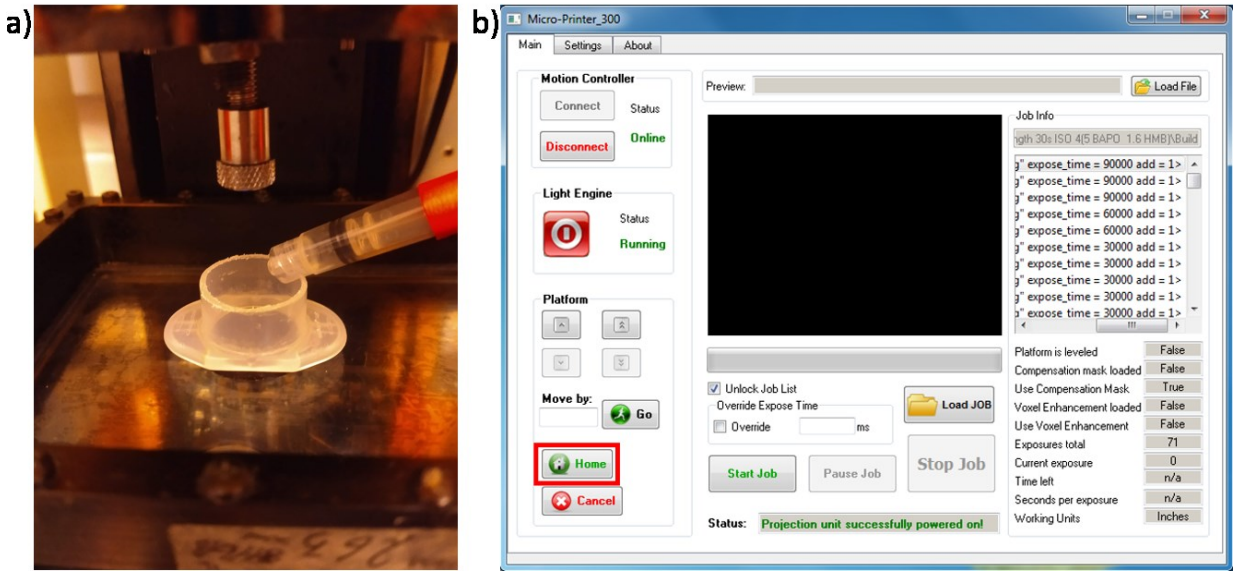


Figure 9.

8. Go to the EDMS software window and click on “Start Acquisition”, and immediately ‘Start Job’ button. It will ask you if you already did homing, click on ‘Yes’.

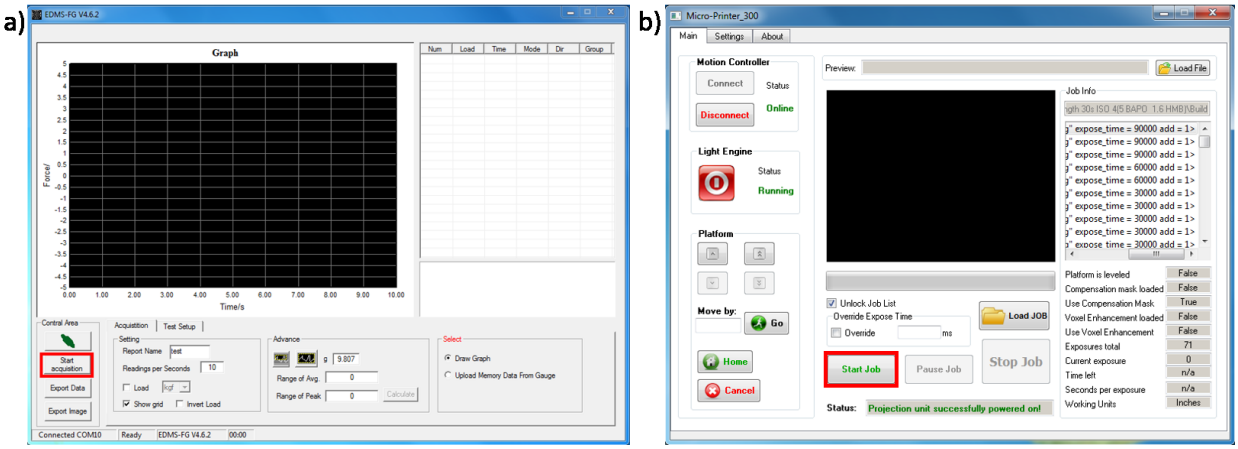


Figure 10.

9. After the Job is done, select “Export Data” and save the file with the measurements.

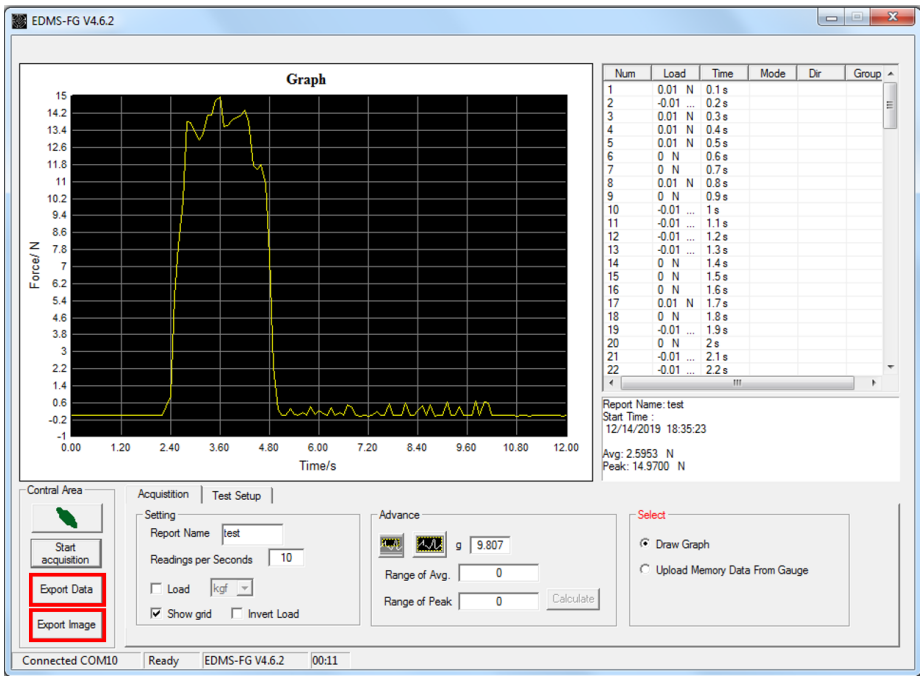


Figure 11.

## Clean-up

1. Note where to dispose of any solutions.
2. Or where to store any solutions.